Theses and Dissertations   Graduate School

2022

Towards the Systematic Evaluation of Variable Modes of Mechanical Conditioning on the Compositional, Microstructural and Mechanical Properties of Engineered Tissue Vascular Grafts.

Sarah Saunders

TOWARDS THE SYSTEMATIC EVALUATION OF VARIABLE MODES OF

MECHANICAL CONDITIONING ON THE COMPOSITIONAL, MICROSTRUCTURAL

AND MECHANICAL PROPERTIES OF ENGINEERED TISSUE VASCULAR GRAFTS.

A Dissertation submitted in partial fulfillment of the requirements for the degree of

Doctor of Philosophy at Virginia Commonwealth University.

By

Sarah K. Saunders

Bachelor of Science, Virginia Commonwealth University, May 2017

Advisor: Dr. Joao S. Soares, Ph.D.,

Assistant Professor, Mechanical and Nuclear Engineering

Virginia Commonwealth University

Richmond, Virginia

June 2022

Acknowledgement

I would like to thank the many members that the Engineering Multiscale Mechanics and Modeling Lab has seen over the years. In particular, my dear friend and colleague Johane Bracamonte, who has been generous in dispensing his sage advice. Thank you for teaching me what you could, always being a sounding board for my ideas or a repository for what troubled me and making the PCL solution since I could never get mine to come out right. Thank you even more for the backyard cookouts, concerts and camping trips that kept me sane through it all. To Madhura, Shivani, and Katie, thank you for being my first mentees and going through the growing pains with me. To Sam Cole, thank you for staying late with me when I was assembling bioreactors. I already miss our sporadic chess games and brainstorming sessions. To Madeline, Kathryn, Valeria, Federica, and Emily, it was a pleasure to work with you all and teach some of you what I could. I know each one of you are following your dreams and finding success and nothing could make me happier or more optimistic about the future of women in STEM. To Keenan, Isabelle, Taylor, and Marissa, thank you for being the latest and greatest of my mentees and all your help collecting data for this project. I would also like to thank all the work-study electro-spinners who contributed in making scaffolds for this project, as well as Caleb Wells, John Spota and Luke Dague, whose special projects in the lab also contributed to the progress of this work. I would also like to thank the colleagues who served on the Graduate Student Association Executive Board with me. Serving my community as the Events Chair and then as President the following year was an extremely rewarding experience for me, and the enthusiasm of my team helped to carry me through the pandemic without losing heart.

I would like to thank my mentor, Dr. Joao Soares, whose support and guidance has molded me into the confident, independent researcher I am today. Starting a new lab and learning new techniques has been an extremely rewarding experience, and I am indebted to you for the patience that you have afforded me as we tackled each new challenge together. Additionally, I would like to thank the members of my dissertation

committee, Dr. Gary Tepper, Dr. Stefano Toldo, Dr. Michael McClure and Dr. Laleh Golshahi and my graduate program director, Dr. Karla Mossi, for the encouragement and input they have given me over the years to help me navigate through my research. I would also like to thank the numerous faculty, staff, and fellow students among the Mechanical and Nuclear Engineering Department, Biomedical Engineering Department, Department of Internal Medicine, Institute for Engineering and Medicine, Nanomaterials Core Characterization Facility and Center for Life Sciences for letting me use their equipment and offering guidance on the wide variety of technical aspects associated with this project and assorted words of encouragement.

Finally, I would like to thank the family and friends who have been there for me since the beginning. Thank you Devin for introducing me to research and giving me my first lab experience. Thank you Nathan for introducing me to Dr. Soares and setting me on this path. I especially want to thank my parents, John and Kim Saunders, for their unwavering support throughout this undertaking. I have been lucky enough to have their love and encouragement my entire life and their faith in me inspires me to me to have faith in myself. I am so happy I can make them proud. And most importantly, I would like to thank my partner, Alex Belt, for everything. Thank you for being a constant reminder that I should not be so hard on myself. Thank you for your wide-eyed love of science and how things work, which kindles my own enthusiasm. Thank you for your unconditional love and support while we struggled through a pandemic, and for always doing the dishes. He encourages me to be better every day, and I truly could not have done this without him

Table of Contents

List of Figures

Abstract

Towards the systematic evaluation of variable modes of mechanical conditioning on the compositional, microstructural, and mechanical properties of engineered tissue vascular grafts.

By: Sarah Kaye Saunders, Ph.D.

A Dissertation submitted in partial fulfillment of the requirements for

the degree of Doctor of Philosophy at Virginia Commonwealth University, 2022.

Advisor: Dr. Joao de Silva Soares, Ph.D. Assistant Professor,

Department of Mechanical and Nuclear Engineering

Coronary artery bypass surgery (CABG) remains one of the most common cardiac surgical procedures performed worldwide, frequently involving multiple bypasses, and commonly employing the patient's internal mammary artery, radial artery, or saphenous vein. CABG is often not possible because native vessels were already employed in previous interventions or are diseased themselves. Synthetic vascular grafts are currently integral tools of vascular surgery and have had relative success in large-caliber applications providing substantial benefit to aortic or iliac grafting; however, small diameter (< 6 mm) arterial grafts have not yet translated into clinical effectiveness due to thrombosis and anastomotic intimal hyperplasia. ETVGs present an exciting potential alternative in vascular grafting by offering a blood vessel substitute that could exhibit all the functional characteristics of native vasculature. In addition to relieving supply limitations associated with coronary artery bypass surgery ETVGs are especially ideal for pediatric patients with congenital heart disease who require grafts that grow as they do, eliminating the need for reoccurring invasive surgeries.

Though the role of biomechanics in regulating cellular behavior promoting non-thrombogenicity, vasoactivity, and ECM synthesis and maintenance is well established, scientists have yet to find the

optimum culture conditions to obtain viable small diameter ETVGs suitable for clinical application. Mechanical conditioning is widely recognized as one of the most relevant methods to enhance tissue accretion and microstructure, leading to engineered tissues with improved mechanical behaviors. However, determining optimal conditioning protocols for ETVGs is rather empirical and based on extensive trial-and-error iterations. We are unable to predict this cause-and-effect relationship accurately, and thus unable to reliably produce ETVGs with targeted properties. This is only magnified when considering the phase after deployment where the understanding of the in vivo performance of the grafts until it is fully absorbed is crucial to improve patency.

This dissertation documents the development of protocols for the systematic study of ETVGs cultured under biaxial mechanical stress. Firstly, we define our chosen ETVG development model and surgical techniques for in vivo deployment. Tissue engineering scaffolds 2mm in diameter are manufactured from electrospun PCL and perfusion seeded via bioreactor with rat vascular smooth muscle cells (VSMCs). Seeded ETVGs cultured in the same bioreactor environment are then implanted into the abdominal aorta of mature Sprague Dawley rats for a period of up to 2 weeks to observe the acute immune response to the implant. Histology revealed ETVGs with fully confluent circumferential cell coverage after in vitro culture. Grafts were able to maintain patency for the short deployment period, and fibrotic tissue formation was observed around the implant at harvest. Secondly, we refine our bioreactor design and seeding method to improve consistency between the 4 ETVGs being cultured, a key feature to increase the statistical significance of each experiment and speed progress in the field. The modifications resulted in ETVG with 60% surface coverage of viable cells 24 hours after seeding, a significant improvement over traditionally employed static methods. Finally, we develop protocols to standardize the use of the bioreactor system for the study of the effects of biaxial mechanical strain on ETVG development. The development of this vital tool not only marks the transition of vascular tissue engineering from a field of empirical discovery to one of systematic characterization but contributes significantly towards progress in the field.

Chapter 1

Background and Significance

1.1 Clinical Need

Cardiovascular disease (CVD) is the principal cause of death worldwide and includes disorders such as peripheral arterial disease, coronary artery disease, cerebrovascular disease and rheumatic heart disease. A common treatment for a variety of CVD related pathologies is revascularization, where blood flow is restored to an area previously blocked by injured or pathological vasculature via a vessel like conduit. Specifically, coronary artery bypass grafting (CABG) remains one of the most common cardiac surgical procedures performed worldwide, with an estimated 400,000 procedures performed annually in the US alone[1]. CABG also represents a unique problem considering revascularization given its classification as a small diameter (<5mm) vessel. For vessels of a larger diameter, the use of synthetic vessels constructed from polymers like PTFE or Dacron for revascularization has been met with great success[2,3]. However as the size of the vessel decreases, issues with thrombogenicity and fibrotic immune response become more pronounced and long term patency becomes increasingly difficult to achieve[4].

Autologous grafts represent the current gold standard in vascular bypass with a 10 year patency rate of 61% and 81% for venous and arterial grafts respectively[5]. The most commonly employed vessel for autologous grafting is the saphenous vein, but arterial candidates such as the internal thoracic arteries, internal mammary artery, radial artery and the gastroepiploic arteries have also been used[6] (Fig 1). The obvious advantages of autologous grafting include the lack of immune response and instant remodeling potential, but the risk associated with vessel harvesting and the limited supply of available candidates raise concerns. In fact, for over 30% of patients in need of revascularization the procedure is deemed too

dangerous, the necessary vasculature was already employed in previous grafting, or the cardiovascular pathology has spread to the graft candidates[7]. These considerations delineate the need for small diameter vascular grafting alternatives to compensate for the limited supply of autografts and account for patients in which autografting proves too unsafe to pursue.
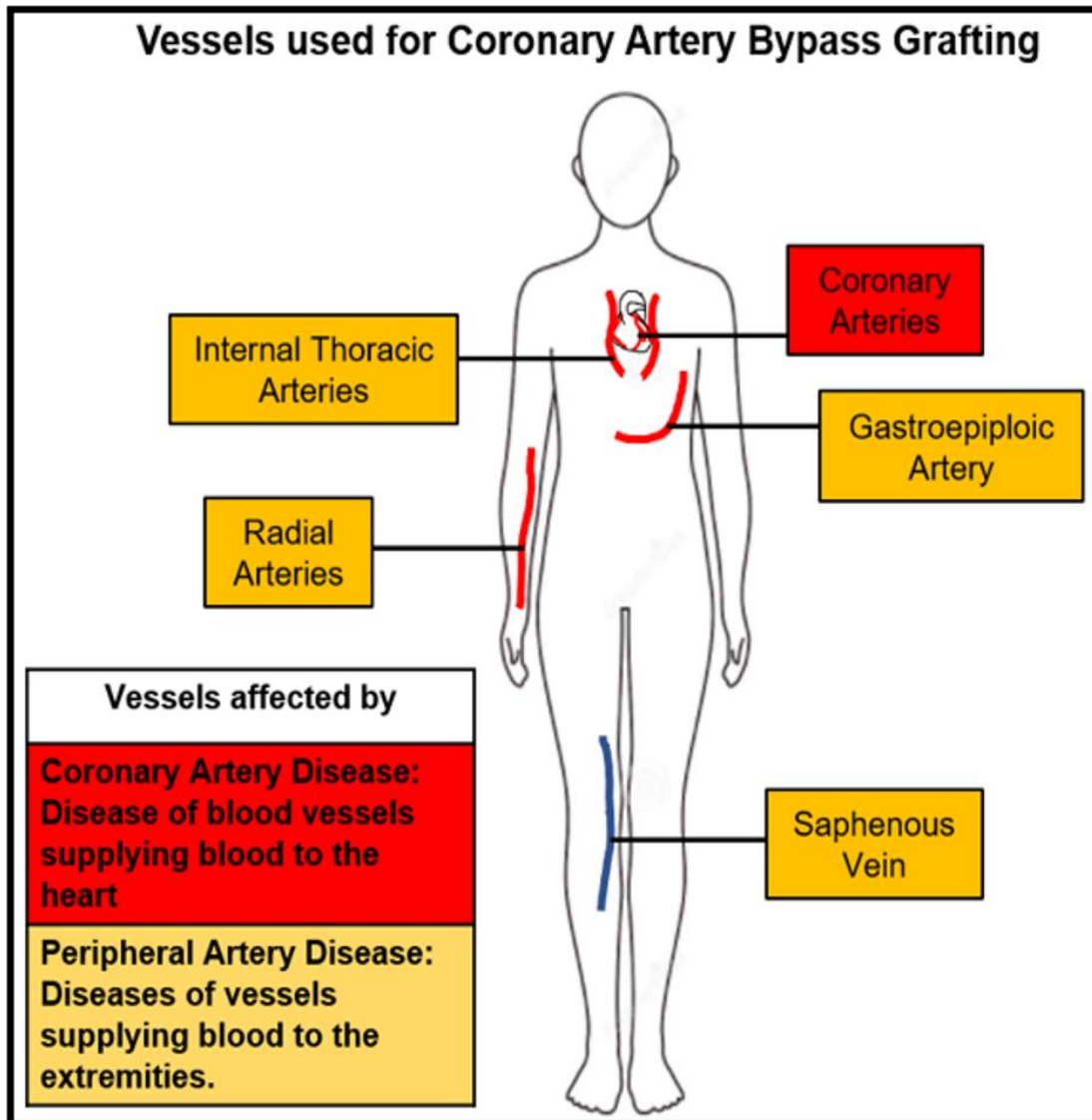
Figure 1. Diagram of the physiological locations of common vessels utilized for CABG.

Cases of pediatric vascular reconstruction (PVR) would also benefit from small diameter vascular grafts that emulate autologous grafts. PVR is rare and the operation is technically difficult given the small size of the patient and associated considerations like smaller total blood volume, and underdeveloped tissue

supporting the structural integrity of the vasculature leading to persistent vasospasms following injury[8]. In children, vascular injury is also typically accompanied by bone, nerve, and soft tissue injuries, meaning that there is increased risk of stunted development or even loss of limb when complications arise during vascular surgery[9]. Additionally, as a pediatric patient grows the implanted graft needs to accommodate for this development. If an autologous graft is not used, the patient will eventually require additional surgeries to replace the undersized synthetic graft[10]. The technical difficulty, lack of procedural resources and high risk of potentially devastating outcomes associated with PVR are all aspects that could partially be alleviated by the discovery of a suitable manufacturable bioactive vessel alternative.

Vascular reconstructive surgery of medium sized vessels (> 5 mm) also encounters issues with patency, though not as severe as small diameter grafts. Medium sized vascular reconstruction is related to repair of peripheral artery disease or vascular injury, restoring blood flow to the extremities. It is very common to use synthetic grafts in these applications, but the risk of thrombosis is higher and autologous vessels are still preferred[11,12]. Some of the first functional modifications made to synthetic vascular grafts were anti-thrombotic linings, including a fully developed endothelial cell monolayer[13]. Another common application of vascular grafting are arteriovenous fistulas for hemodialysis access. In this application, a graft is used to connect a vein to an artery in the patients arm so blood can be accessed and circulated through a hemodialysis machine for filtration. This application comes with additional complications, as it is constantly punctured for treatment, and consequently prone to developing infection[14]. Testing new vascular graft conduits in these applications is common prior to attempting smaller diameter, high risk reconstruction trials like CABG.

1.2 Vascular Structure

The cardiovascular system consists of two blood flow circuits connected and driven by the muscular pump that is the heart[15]. The pulmonary circuit circulates blood through the lungs for oxygenation then returns the blood to the heart. The newly oxygenated blood enters the left atrium and travels through the mitral valve into the left ventricle. Blood is then pumped through the aorta to deliver oxygen and other

nutrients throughout the second circuit, the systemic circulatory system. The vessels that carry blood away from the heart are referred to as arteries. The aorta is the largest artery averaging about 30 mm in diameter, and as blood travels away from the heart the aorta branches into several smaller arteries that facilitate the delivery of blood to and from the extremities[15]. The smallest arteries, called arterioles are the last defined vessels blood travels through on its way to the capillary beds that facilitate nutrient transfer to tissues, and they can be as small as 10 µm. Deoxygenated blood then makes its way back to the heart, carrying CO_2 and other cellular waste products through the veins.

1.2.1 The Vessel Wall

Blood vessels consist of three layers, the tunica intima, the tunica media and the tunica adventitia[15] (Fig 2). The intima is located on the luminal surface of blood vessels and consists of a monolayer of vascular endothelial cells (EC). The ECs are spindle shaped and aligned in the direction of blood flow[16]. The purpose of this layer is to form a protective barrier between blood and tissues by facilitating the passage of certain molecules and cells from blood to tissues, regulating vascular disease, preventing thrombus formation and maintaining vascular tone through extracellular signaling[17]. The intima is supported by and connected to the media by a thin basement membrane called the internal elastic laminae, a fenestrated membrane of elastic fibers that contribute to the physical and mass transfer properties of blood vessels. The media layer is primarily made of vascular smooth muscle cells (VSMCs) and is the thickest layer of the arterial wall. This layer is a dynamic environment, constantly remodeling to better accommodate changes in blood flow and pressure[18]. VSMCs play a major role in maintaining this environment in response to external chemical and mechanical stimuli. The ECM secreted by VSMCs is primarily made up of collagen to provide structural support and strength, and elastin to provide compliance and elasticity[19]. VSMCs orient themselves into circumferentially aligned concentric rings of lamellar units, in which elastin forms the dominate compartmental structures housing the VSMCs and collagen is present as circumferentially aligned parallel bundles weaving through the entire mesh[20,21]. The media is connected to the adventitia by another elastic boundary called the external elastic lamina. In venous blood vessels this is the thickest layer, and it

4

is primarily composed of fibroblast which synthesize a thick layer of collagen[16]. This layer is viewed as connective tissue and anchors blood vessels to the surrounding connective tissue in the environment.
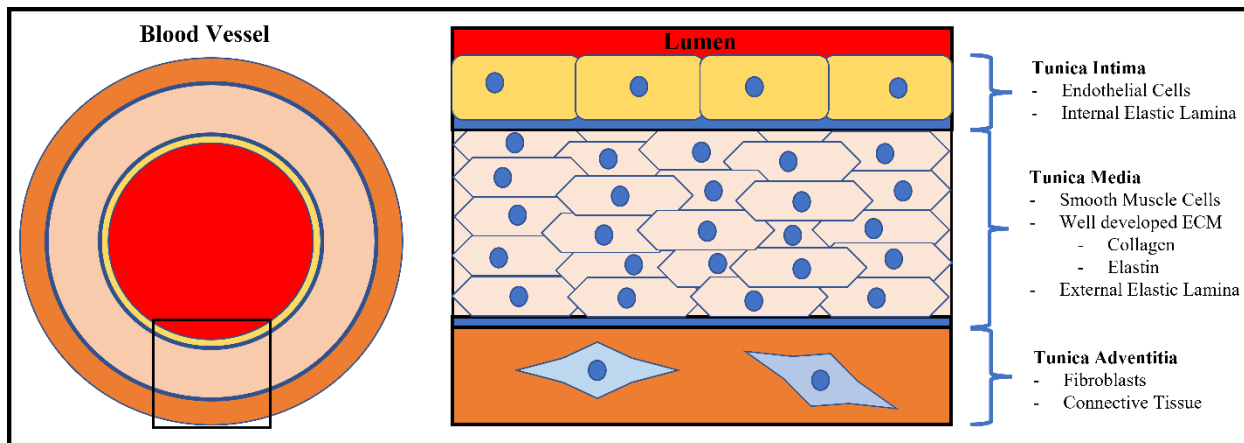
Figure 2. Gross anatomy of the blood vessel wall.

The mechanical properties of the vascular wall are directly related to the composition and structure of these components. As such the gross morphology between arteries and veins is different. Arteries can be further divided into two subclasses called elastic and muscular arteries[22]. Elastic arteries are typically found near the heart and experience high pressures associate with blood being ejected from the right ventricle. These vessels contain a higher proportion of elastin in their lamellar units, contributing to a high compliance and strain capacity. This is essential for regulating blood flow in more distal regions of the vasculature by providing volume control in response to the pressure gradient. As the size of arteries decrease, the relative amount of elastin decreases and the number of VSMCs increases, contributing to a stiffer structure. In these arteries, called the muscular arteries, blood flow is facilitated more by the viscoelastic contractile properties of VSMCs, which modulates the diameter of the vasculature in response to changes in blood pressure and flow rate. The ratio of collagen to elastin continues to increase in veins as blood pressure continues to decrease, while vein diameters are consistently larger than their arterial counterparts[23]. The tunica media of veins is much thinner than that of arteries, and there is little contribution to the flow of blood from the structure itself. Veins contain most of the blood in the circulatory system and are some of the most distensible vessels in the body, able to accommodate changes in volume without a detrimental increase in

blood pressure[24,25]. An additional feature found in veins, not present in arteries, are valves intermittently spaced to prevent blood regurgitation.

The composition, structure and mechanical properties of the arterial wall are significantly different from those in veins, and when used in arterial revascularization venous vascular smooth muscle cells attempt to remodel the vessel structure to accommodate new arterial stresses. The required remodeling is typically too extensive, which contributes to the lower patency of venous autografts. Even though decades of research has demonstrated the use of arteries in vascular reconstruction significantly enhances both short term and long term mortality in CABG patients, the use of vein grafts still dominates the field[26]. Concerns regarding arterial harvest, such as deep sternal wound infection associated with internal thoracic arteries, limits widespread adoption of the technique. This coupled with the extensive data collected in regard to saphenous vein grafts showing their reliability and safety contribute to low arterial utilization (< 10%) within the society of thoracic surgeons' databases. However, more recent studies regarding utilization of radial arteries offer lower morbidity associated with harvesting with additional benefits including increased length and infection resistance, suggesting arterial grafting could eventually increase in popularity.

1.2.2   Vascular Biomechanics

Blood vessels are dynamic structures, constantly remodeling in response to external cues. There are three main forms of mechanical force constantly acting on a blood vessel: (1) shear stress of blood flow, (2) circumferential distension by the blood pressure gradient, and (3) axial stretch mediated by connective tissue anchoring[27] (Fig 3). When evaluated as a biomaterial, blood vessels have unique properties that allow them to respond appropriately to changes in these factors in both immediate and long-term ways. For example, vascular walls can withstand large levels of deformation, however as additional pressure is applied and the vessel is distended the vascular wall becomes rigid and stiff[28]. Most materials that exhibit strain hardening properties are resistant to deformation, however, the unique undulation of collagen fibers oriented in the circumferential

6

direction facilitate this interesting characteristic[29]. In low pressure situations, arteries maintain

compliance and the circumferentially aligned collagen is in a crimped state. With an increase in

pressure and circumferential strain, the collagen fibers straighten out and experience tensile strain,

greatly reducing the vessel elasticity and increasing stiffness.
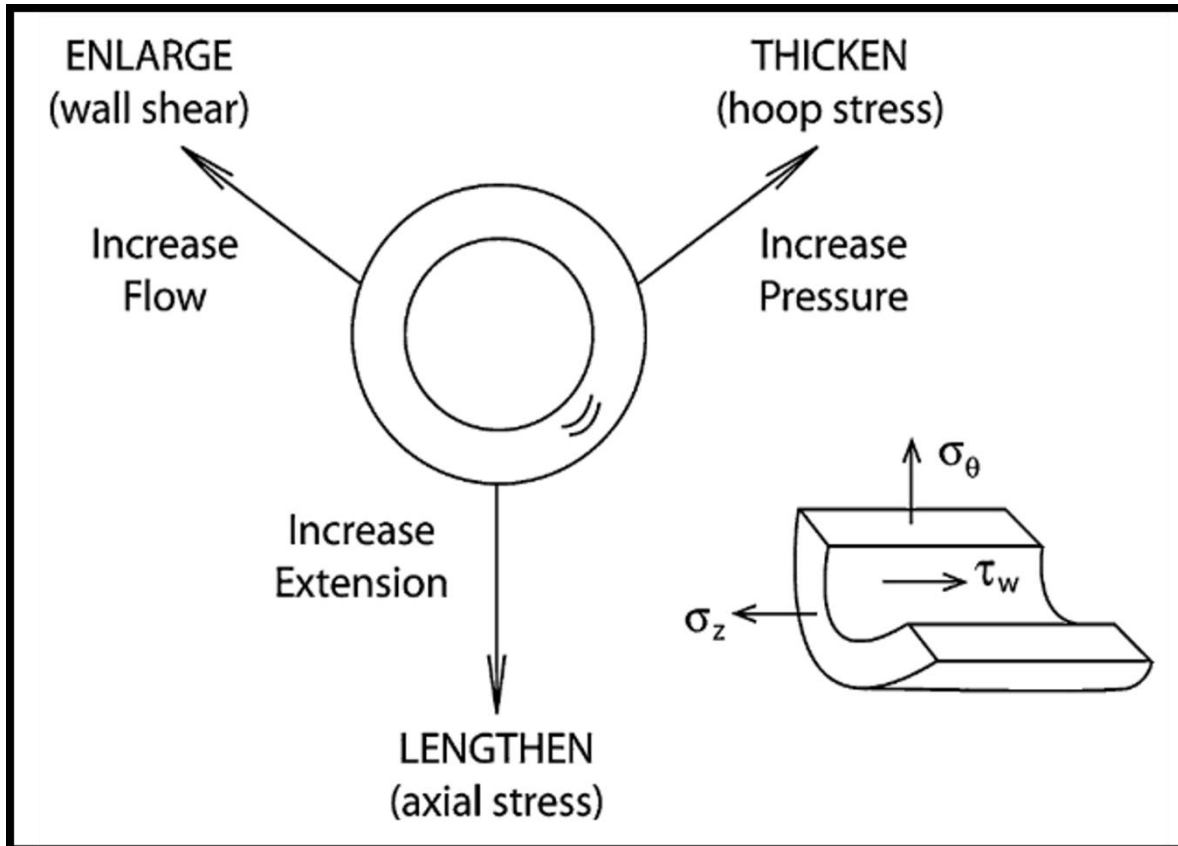
Figure 3. Diagram of vascular wall dynamics. The 3 primary forms of loading experienced by native
vasculature are flow-induced wall shear stress (τw) , pressure-induced circumferential wall stress ($\sigma\theta$), and
axial load-induced axial wall stress (σz). Copied with permission from [27].

1.2.3   VSMCs and Strain

VSMCs exert direct control over the mechanical properties of blood vessels by modulation of their

contractile state. When activated the Young's modulus of VSMCs jumps from 10 kPa to 100 kPa, and the

diameter of the vessel constricts. However, as VMSC are consistently exposed to cyclic stress it is important

to take into account other characteristics they have that are not observable in the immediate sense but occur

over time. VSMCs are viscoelastic, meaning they exhibit time dependent strain. This can be majorly

7

attributed to mechanical adaptation of the VSMCs in response to the mechanical cues of their environment[30]. Cyclic stretch modulates proliferation, differentiation, and ECM synthesis by VSMCs. It has been observed that cells respond in equal measure to being over-stressed and under-stressed, while physiological levels of stress maintain homeostasis and a contractile phenotype[31]. In response to injury, VSMC will switch from the contractile phenotype to the synthetic phenotype, to facilitate proliferation and wound repair. However, if the VSMCs are unable to switch back into the contractile phenotype after repair is complete, they tend to over proliferate and invade the intimal layer[32]. This is called intimal hyperplasia, one of the 6 classifications of atherosclerotic plaques which causes narrowing and occlusion of blood vessels. In this section what is known about VSMC response to mechanical stimulation is reviewed.

When vascular smooth muscle cells undergo stretch they produce increased levels of h-CaD, a molecule that helps regulate contractile function. This effect is doubled when VSMCs are cultured on laminin, suggesting laminin plays an important role in maintaining cell contractility and regulating blood flow[33]. Laminin has also been reported to inhibit VSMC proliferation, preventing neointimal hyperplasia[34]. Culturing VSMCs on different substrates typically found in the ECM is a method used to study cell-matrix interactions. Culturing VSMCs on fibronectin followed by the application of a gradient of mechanical stretch resulted in the migration of smooth muscle cells to stiffer regions, however the same treatment applied to VSMCs coated on laminin resulted in random migration patterns[35,36]. This suggests that cell motility is a response of mechanical stimulation regardless, but migration can be directed by modulating surface coatings and substrate stiffness. Furthermore, it has been reported that stretch increases DNA synthesis in VSMCs cultured on fibronectin or vitronectin, but not in VSMCs cultured on elastin, collagen or laminin[37,38]. This provides evidence that the mechanism for the upregulation of cell proliferation by mechano-transduction is dependent on specific integrin-ECM interactions unrelated to the cyclin-dependent kinase complexes that fill that role in response to growth factors. Cyclic strain has also been demonstrated to induce TGFb signaling through SMAD pathways, which upregulates ECM synthesis in vascular smooth muscle cells[39].

More macroscopic observations from ETVGs can be tied to these cellular interactions, such as the preference of VSMC to align in the direction of the force being applied and subsequent matrix deposition at the same orientation[33]. Also, macrophages recruited for wound healing secrete fibronectin, which has been proven to increase DNA synthesis and directed migration in VSMCs[34]. By combining the knowledge of the countless empirical efforts applying mechanical strain to ETVGs and general VSMC biomechanics, the creation of logical progressive experiments geared toward consistent and reliable manipulation of graft properties can be achieved.

1.2.4   ECs and Shear Stress

Hemodynamic shear stress on ECs is essential in mediating VSMC contractile state. In response to changes in shear force acting on the vessel wall, ECs can produce endothelin-1, a vasoconstrictor, or NO, a vasodilator[40]. Overall shear stress on ECs aid in maintaining VSMCs in a quiescent state, preventing neointimal hyperplasia and luminal narrowing. If ECs experience high strain and low levels of oscillatory shear stress, they begin to secret inflammatory molecules like TGFβ, which promotes the synthetic proliferative state. It has been suggested that induction of NO by ECs contributes to the negative regulation of PDGF, a biomolecule that triggers the synthetic phenotype in VSMCs[41]. Additionally, NO release by endothelium also inhibits MMP9 induction in VSMCs. MMP-9 is a gelatinase that acts directly on elastin, a primary structural protein of the vascular ECM, suggesting that shear stress directly affects elastin remodeling in the presence of both VSMCs and ECs. Investigating the wide variety of responses to biomechanical cues in vasculature highlights the importance of a dynamic environment to maintaining proper blood flow. If the cells of a blood vessel have limited ability to respond to such cues, they will eventually become diseased.

1.3   Available Alternatives

Additional methods for revascularization consist of percutaneous coronary interventions (PCI). In 1977, percutaneous transluminal coronary angioplasty was developed[42]. This method utilized the inflation of balloons to widen narrowing vessels, however the procedure was relatively complicated and had a high

failure rate. The next generation of PCIs featured stents, small stiff tubular structures inserted into the vessel lumen and expanded to open the passage. These have evolved from simple bare metal stents to drug eluting stents, which are functionalized to reduce thrombogenicity and the potential of restenosis[43]. Stents are now the preferred treatment method for minor coronary lesions, however the criteria for determining if PCI or revascularization surgery is necessary requires further elucidation[7,43].

Due to the superior patency of autologous vein grafts, researchers started investigating allogenic vein grafts for patients who lack suitable autologous vessels[44,45]. Early clinical experience exhibited patency rates of <50% after 4 years, suggesting un-altered allografts were unsuitable for use as arterial replacements[46]. Fixed human umbilical veins (hUV) had experienced some success in animal trials in the mid 1970's[47–49]. The fixative, glutaraldehyde, made the grafts exceptionally resilient to infection and assisted in retaining their structure in vivo. Unfortunately, the grafts no longer retained their ability to remodel in vivo, excluding them from use with pediatric patients. Clinical results with commercially available hUV vascular grafts (Dardik Biograft, Meadox Laboratories, Oakland, NJ) were promising, with stabilized hUVs demonstrating patency rates nearly comparable to SV interventions in femoral popliteal bypass (70% after 6 years) and 100% patency after 16 months in coronary artery bypass[50,51]. Still, complications associated with this graft like the fragility of the intima makes the surgical procedure difficult[52].

Decellularized bovine and human cadaver grafts were also extensively researched and made up some of the first commercially available acellular ETVGs in the 1970s such as Artegraft (North Brunswick, NJ), Procol (Hancock Jaffe Laboratories Inc., Irvine, CA), and Cryovein (CryoLife, Kennesaw, GA)[53]. While these vessels are approved for use in most revascularization procedures, it is with an understanding that no autologous candidate is available. In addition to cadaveric grafts, decellularized small intestinal submucosa (SIS) functionalized with heparin and vascular endothelial growth factor were studied in the vasculature of lambs. Interestingly, when deployed in neonatal lambs the SIS grafts exhibited increased elastin production and diameter dilation accommodating for growth, suggesting that this method may hold potential for the

treatment of congenital heart defects[54]. Unfortunately, this study was never progressed towards clinical trials.

1.4 Engineered Tissue Vascular Grafts (ETVGs)

These initial attempts to find small diameter vascular replacements signaled the beginning of a new era of cardiovascular medicine: the engineered tissue vascular graft. ETVGs are an enigma which promise to be a manufacturable blood vessel substitute that exhibit all the functional characteristics of native vasculature. In addition to relieving supply limitations associated with autologous grafts, ETVGs would be especially ideal for pediatric patients with congenital heart disease who require grafts that grow with them, eliminating the need for reoccurring invasive surgeries. When planning how to construct an ETVG it is important to consider the functional requirements of the tissue being replaced. The basic functional requirements for vascular tissue engineering include non-immunogenicity, sufficient mechanical properties like burst pressure and fatigue strengths as well as a stable and non-thrombogenic lumen[55]. From early research it was evident that the vessel needed sufficient elasticity in order to avoid developing neointimal hyperplasia at the anastomotic sites. From an end-user perspective, the feasibility of the design must also be considered. The time and effort needed to create a fully mature ETVG, the ability to maintain sterile conditions throughout production, the method used to store and transfer the ETVG to the intended recipient, and the ease with which the scaffold can be manipulated during surgery are all of the utmost importance. There are a wide variety of methodologies currently employed for the creation of ETVGs which can be delineated into 4 major categories: synthetic functionalized scaffold approaches, biological matrix approaches, and cellularized scaffold based approaches[56].

1.4.1   Synthetic Functionalized Scaffolds
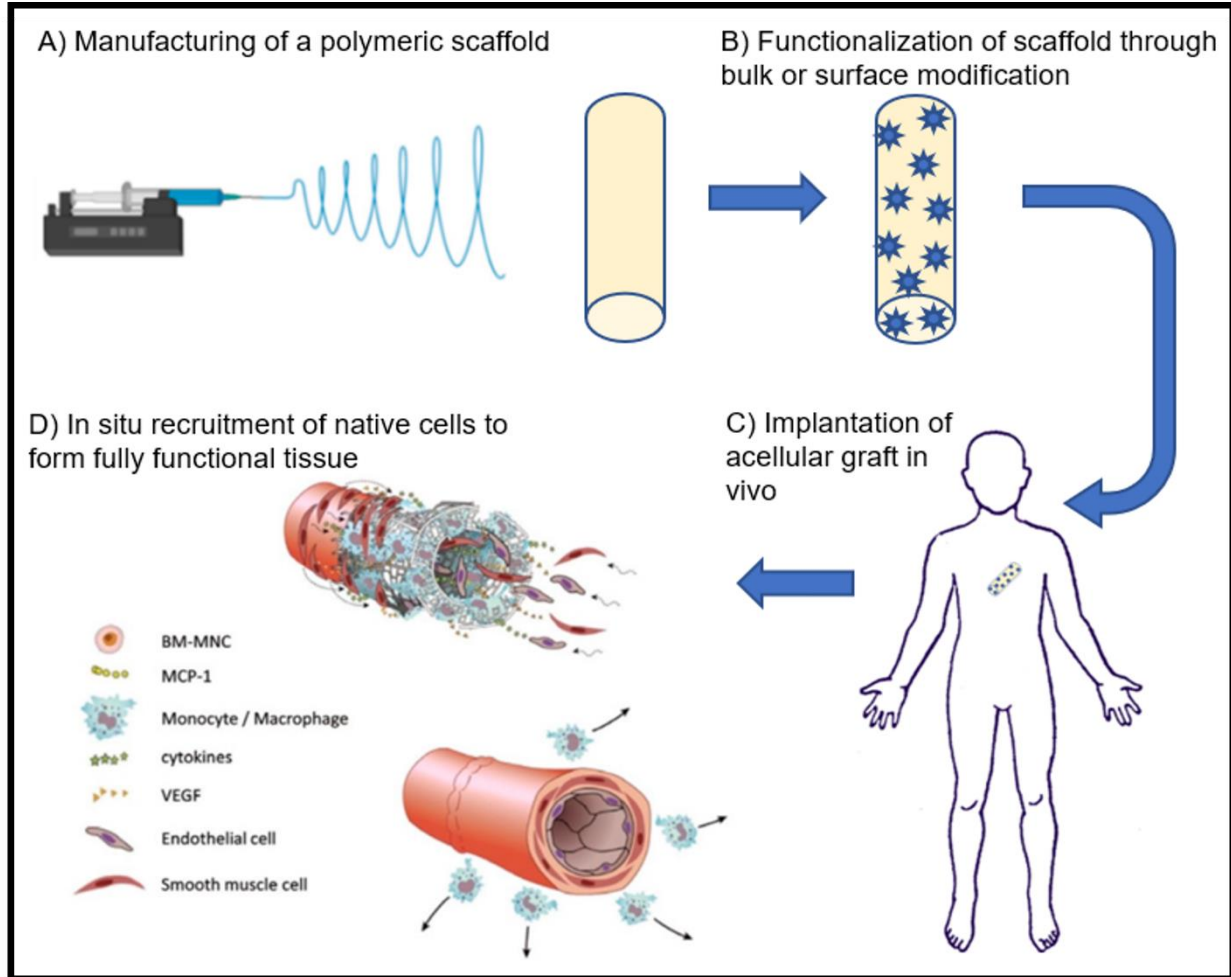
Figure 4. Flow chart of the in situ vascular engineering technique. Modified with permission from [56].

In recent years, the trend has been to create "off the shelf" ETVGs from synthetic polymers that have been functionalized to encourage host cell migration in situ and non-thrombogenic properties[57] (Fig 4). While the concept of an acellular ready to use graft seems like the holy grail of vascular tissue engineering, one major failure in researching this method is acknowledging the mode of healing experienced at the intended implant site. In humans, transanastomatic endothelial outgrowth is limited to a few millimeters away from the anastomosis and comes to a complete halt just under a year[58]. This reveals that the only available modes of endothelial cell (EC) recruitment in humans are either facilitated fall out healing or transmural endothelialization, yet the majority of the studies investigating in situ regeneration

methods use short graft lengths in animal models that exhibit rapid transanastomatic endothelialization, which limits the clinical relevance of the studies in question[59]. Experimental models that exclude transanastomatic outgrowth as well as both transanastomatic and transmural endothelialization for examining fall out healing specifically have emerged in the last 40 years, but their use has been limited[60,61]. From these studies it can be surmised that transmural endothelialization should be the focus of in situ vascular engineering efforts going forward, and those studying this method should take extra care to use in vivo models that give meaningful results.

The in situ approach is also limited by the mechanical properties of the materials the ETVGs are made from, as the most common driver of failure in current studies is compliance mismatch[62]. This is applicable to the stiff polymers typically used for this application, however, it also holds true for in situ methods featuring fast degrading polymers. In a study by Wei and colleagues testing rapidly degrading cell free grafts in the rat abdominal aorta, the resulting vasculature was compliant and achieved a patency of 80%[63]. However, translating to this to higher-pressure systems in large animal models is unfeasible.

1.4.2 Natural Matrices

Completely natural matrices, devoid of synthetic polymers, have been investigated since early attempts at ETVG development, starting with the decellularized allografts and xenografts attempted in the early 1970s. One of the earliest attempts was a form of autograft called the autoplastic cutis graft in 1958, which was made from the graft recipients own skin[64,65]. Some research groups operate under the assumption that scaffolds force cells to develop unnaturally rather than facilitating proper alignment. This line of thinking gave rise to self-assembling ETVGs, where cells placed in a 3-D environment with the right stimuli organize themselves into complex tissue structures, no scaffold necessary[66]. Three main strategies have been investigated, including cell-sheet assembly, micro-tissue aggregation and cell printing (Fig 5).
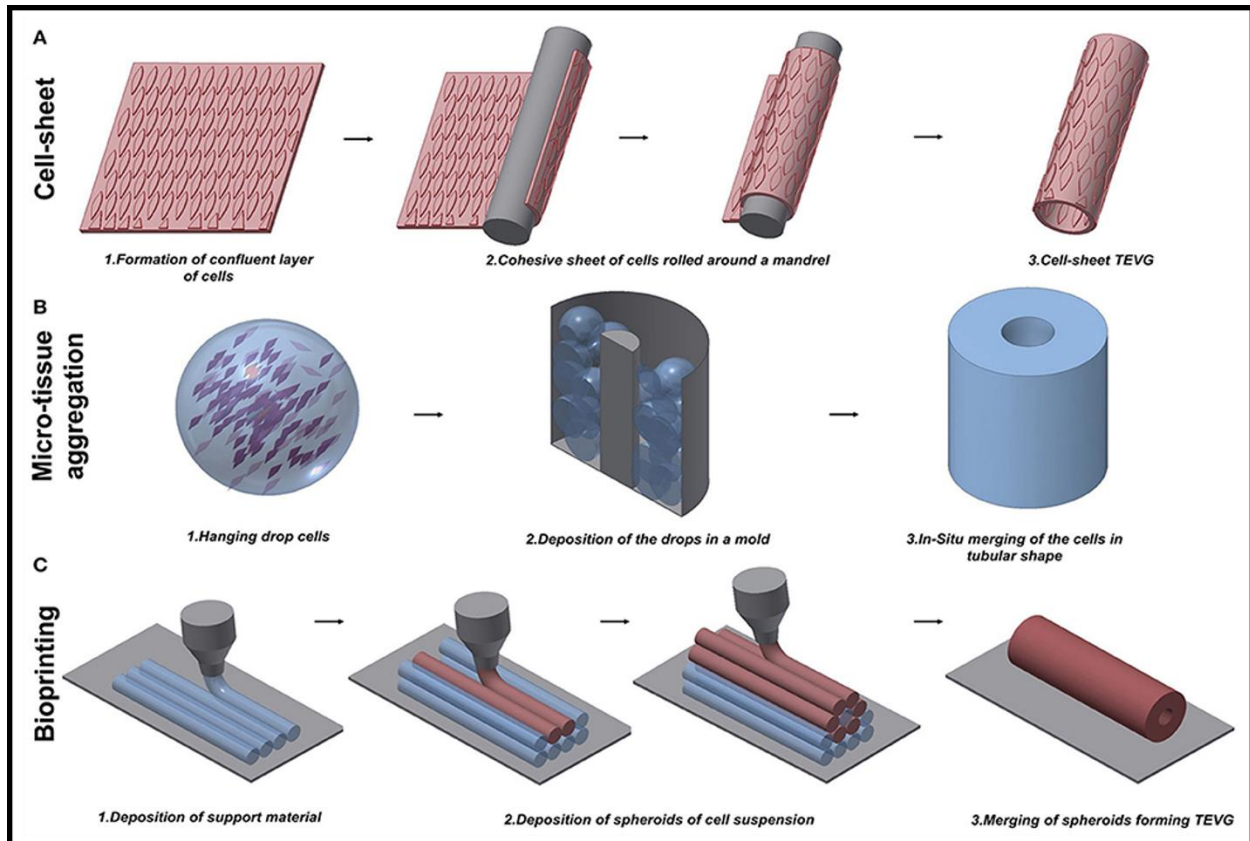
Figure 5. Methods for ETVG manufacturing using natural matrices. Copied with permission from [66].

Cell-sheet wrapping has been the most successful, making it all the way to clinical trials as hemodialysis access grafts, A-V shunts, lower limb revascularization and radial artery replacement[67,68]. The main drawback associated with cell sheet wrapping is the manufacturing time of over 30 weeks, which may be too long for someone in need of vascular bypass. Briefly, autologous cells are harvested from the patient and cultured until they form fully confluent tissue sheets with well-defined ECM, then they are gently lifted, wrapped around mandrels, and cultured for an additional 12 weeks while the concentric layers fuse to form the mature ETVG[69]. Microtissue aggregation involves culturing cells onto temperature responsive polymers[70]. Once the construct is completely confluent, the polymer is signaled and shrinks to release the formed ETVG. Bioprinting is one of the new methods being outfitted for ETVG manufacturing and offers more flexibility in terms of the shapes it can create[71]. Many materials can be utilized in bioprinting, from polymers to cells encapsulated in various protein based gels[72–74]. There is also preliminary research being

14

done on 4-D bioprinting using smart materials that can respond to environmental cues like temperature or pH, which opens up countless possibilities for advanced graft functionalization[75]. Current research is focused on printability of desired constructs, and more research needs to be done before we can tell if this method will produce viable ETVGs. Overall, natural matrices are one of the most promising approaches to ETVG development, but the long incubation periods required to meet mechanical function requirements still make them a less attractive option than autologous grafting.

1.4.3   Cellularized Scaffolds

Polymeric scaffold-based methods are the most researched and most variable form of ETVG development. Over the last 30 years many variables have been identified within this methodology including the materials, cell populations and culturing techniques applied[76–78] (Fig 6). They can be divided into two main categories: permanent and biodegradable. Permanent scaffolds are the easiest to manipulate, yet they suffer from the same potential issues as acellular grafts when it comes to mechanical property mismatch. It is easy to achieve the desired burst pressure and fatigue strengths, but this usually comes at the cost of compliance which leads to intimal hyperplasia formation at the anastomosis[79]. The synthetic materials also offer very few cell attachment sites, making it difficult to achieve a fully confluent endothelium, but both of these issues can be overcome with the appropriate choice of materials, coatings and manufacturing techniques[80].

However, synthetic ETVGs have very little remodeling potential, making them an unattractive option for pediatric patients. Synthetic permanent ETVGs have achieved clinical success with follow-up periods of up to 17 years when complemented with a confluent autologous endothelium, but researchers still admit that autologous grafting is the preferable option in regards to long term patency[81]. The lack of bioactivity in synthetic ETVGs led scientist to consider the addition of natural polymers that are typically found in the ECM. This provided more cell binding sites and a general improvement in biocompatibility of manufactured ETVGs[82,83]. Collagen, gelatin, elastin, fibrin, and silk-fibroin are the most extensively used

biopolymers in tissue engineering, and can be susceptible to degradation *in vivo*, which can lead to aneurysm formation and rupture.
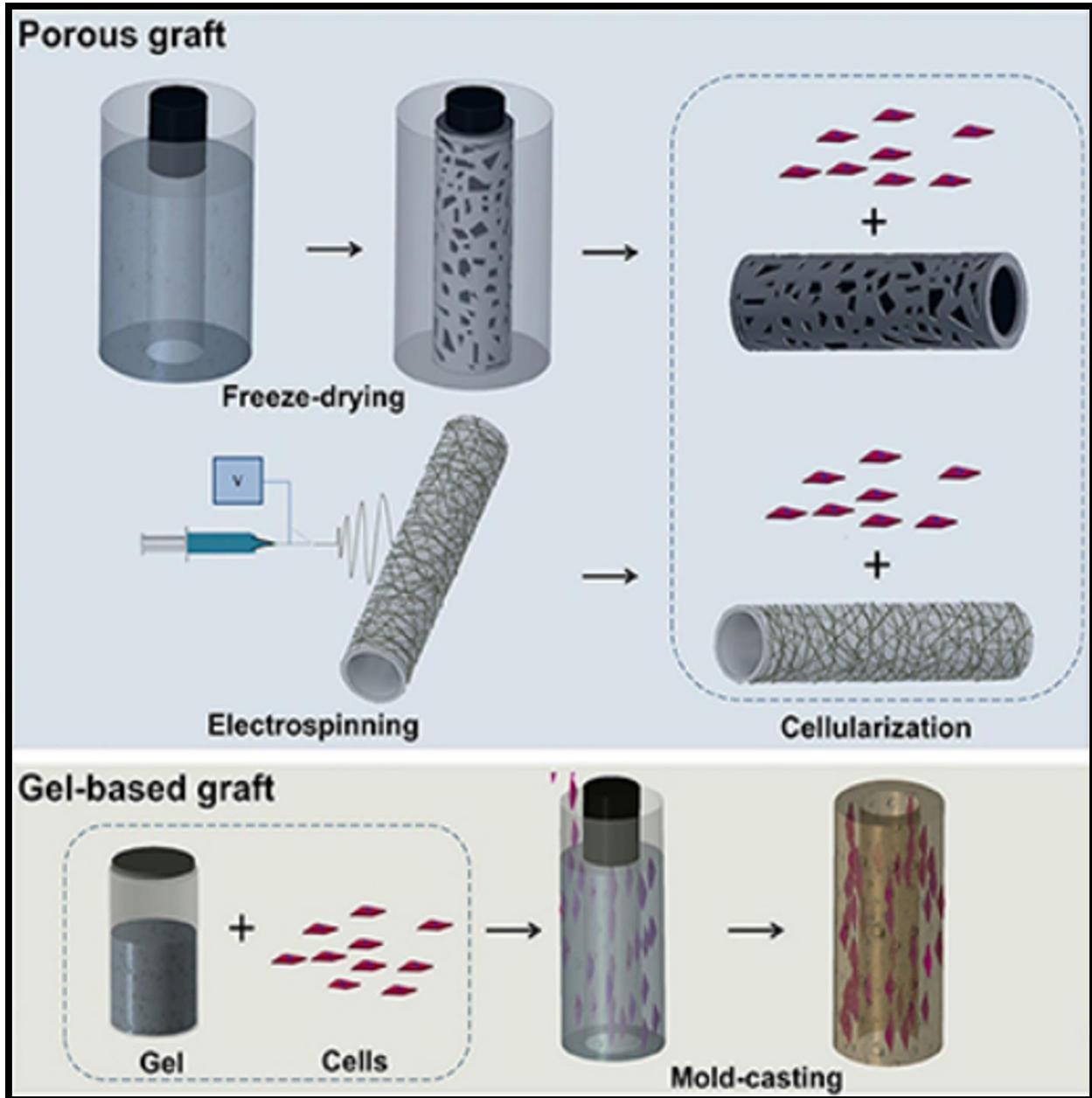
Figure 6. Examples of techniques for manufacturing cellularized scaffolds. Copied with permission from [66].

Biodegradable scaffolds are the middle ground between scaffold-based approaches and self-assembling ETVGs. Ideally this method would combine the speed and production ease of synthetic grafts

16

with the in vivo remodeling potential of natural matrices[84,85]. Keeping all the usual functional requirements in mind, biodegradable ETVGs must also consider degradation rate. Essentially, the polymer must degrade at a rate equal to or slightly slower than the rate of neo-vascularization to ensure that the resulting vessel maintains functional mechanical properties throughout development. Most of the attempts to investigate these methods have been isolated, disorganized, and generally unsatisfactory, leading to limited advancement in the field, but this is also the area that has been researched the most, contributing significant information for the development of systematic ETVG procedures.

1.4.4   Modes of ETVG Failure

ETVG failure can be classified into 3 categories dependent upon the timespan in which they fail after implantation. The first category is acute failure which occurs within 3 months after implantation and is typically attributed to infection and thrombosis[12]. Infection is a risk associated with any surgery, and risk mitigation techniques in this context are fairly conserved across surgical procedures. The risk for thrombosis is typically attributed to a coagulation reaction driven by platelet adhesion to a thrombogenic lumen[80]. We know that this can be avoided most readily and consistently avoided by a confluent layer of non-thrombogenic autologous endothelium, but primary cell isolation and expansion to achieve cell numbers relevant to ETVG manufacturing is a major detriment to manufacturing time[81]. *In situ* engineering techniques typically employ an anti-thrombogenic molecule coating, such as heparin, however as previously discussed rapid endothelialization of such grafts after deployment is unlikely. If the coating wears off before endothelialization occurs, it is likely that thrombosis will develop leading to graft failure.

Midterm failure occurs between 3 month and 2 years after graft deployment and is typically driven by a compliance mismatch between the implanted graft and native vasculature. The unique mechanical properties of vasculature are difficult to emulate, and typically when designing ETVGs, compliance is sacrificed to achieve adequate strength to withstand arterial pressures[86]. Unfortunately, the stiffness of the implanted graft induces VSMCs to shift into their synthetic state and proliferate, eventually leading to neointimal hyperplasia and eventual occlusion of the vessel at the distal anastomosis. The mechanism

behind the causality is poorly understood, but it has been speculated that the difference in compliance disrupts blood flow causing a loss of energy due to reflection of the pressure and flow pulse wave as it encounters the graft and propagates through it[87]. VSMCs in small diameter arteries facilitate the absorption of pulsatile energy during vasoconstriction and its subsequent release during vasodilation. This contribution to blood flow is sorely missed in synthetic vascular grafts, which can diminish the pulsatile energy by 60% due to their increased stiffness[88]. Recently, a study was conducted that isolated graft compliance as the single variable of interest in an ex vivo culture model, and the results strongly support this line of thought[89]. Thus, ensuring that graft materials demonstrate compliance values similar to native vasculature is the way to most readily avoid midterm failure, though several other factors may contribute to intimal hyperplasia development and graft failure.

Late term failure typically occurs after two years post implantation and involves a return of atherosclerosis in the effected area[12]. As previously mentioned, those suffering from CVD will likely need multiple revascularization surgeries in their lifetime, even if autologous grafts were used in the procedure. Late term failure can be attributed to deterioration of graft properties or a failure of the graft to fully integrate with host tissue and undergo remodeling.

1.4.5 Experimental Progress

Over the past 50 years, research in the field of small diameter ETVGs has been broad, but a few relevant discoveries have been made[90]. A meta-analysis of ETVG preclinical trials by Skovrind and coworkers[91] has shown that a living cell component in ETVGs typically results in better long term patency rates when compared to ETVGs without (Figure 7). The same study also recognizes functional coatings of the scaffold surface as a contributing factor. Both are often used in ETVG development to modulate the immune response to ETVGs and enhance in vivo integration with host tissue. As such it is assumed that great care must be taken with ETVG manufacturing to ensure the structure promotes cell seeding, proliferation and differentiation both in vitro and in vivo, encouraging continuous remodeling after implantation. According to recently collected data, the EC layer is the most important for achieving early

patency, but the average follow-up for these studies is only 56 days which is much too short to evaluate

effects on mid to long term patency[91]. Achieving a healthy and functional media equivalent may yet prove

vital for long term patency of ETVGs. Improved mechanical properties can be achieved by careful selection

of materials and manufacturing techniques, but another method of achieving stronger tissues with enhanced

compliance is preconditioning cellularized ETVGs in a bioreactor with the capability to apply mechanical

strain. When analyzed as a factor in ETVG development, Skovrind also found bioreactor preconditioning

to improve patency of implanted ETVGs (Fig 7). Given that the primary effect of conditioning is to enhance

ECM production by VSMCs, this also suggests the VSMC component is essential for promoting ETVG

patency.
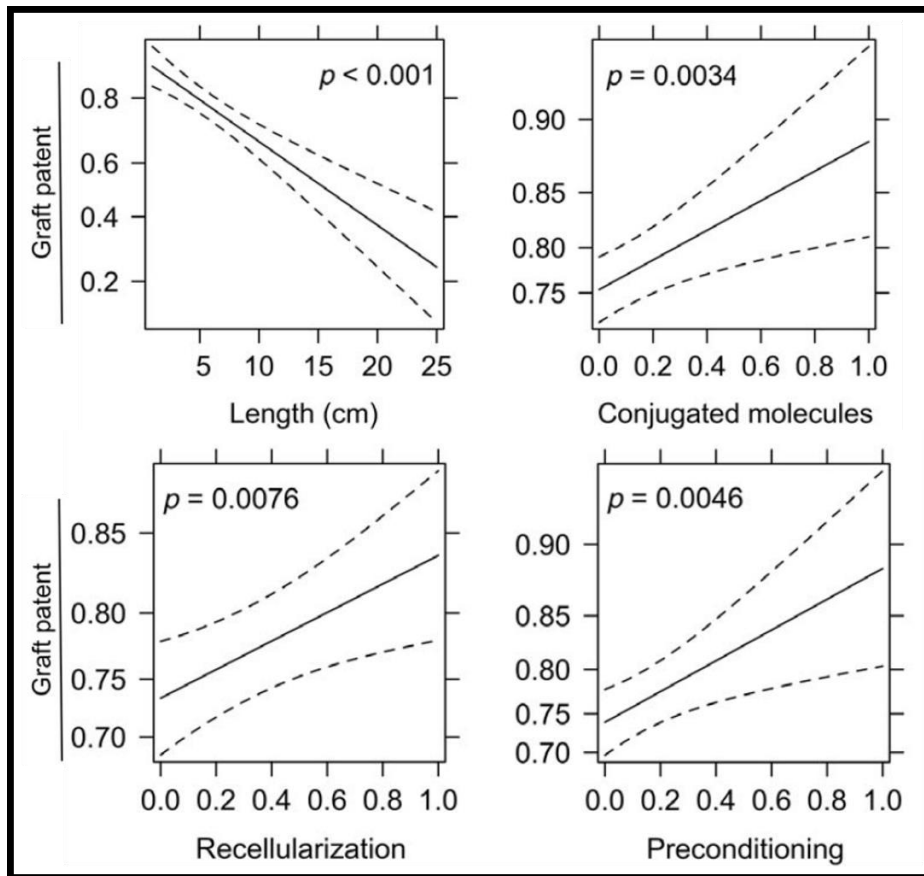
Figure 7. Select variables considered in ETVG development and their effect on graft patency. Dotted lines indicate standard error. As the length of ETVGs increase, their patency levels tend to decrease. By modifying scaffolds with conjugated molecules, seeding them with cells, and preconditioning assembled ETVGs in a bioreactor, graft patency improves significantly. Modified with permission from [91].

1.4.6 Seeding Techniques

The small diameter tubular geometry of ETVGs makes it difficult to efficiently deliver cells onto the luminal surface evenly. Optimizing seeding efficiency by promoting rapid cell attachment to the scaffold and mimicking tissue microstructure may contribute to relieving current constraints related to cell availability, prolonged culture protocols and mechanical and physiological performance[92]. Many seeding methods have been utilized in ETVG development. The first and most employed is drip seeding, in which cell suspension is deposited directly onto the scaffold material[93–96]. This is usually done along the outside of the scaffold as pipetting into the scaffold lumen can prove difficult and even cell seeding is not likely to be achieved. Other seeding techniques that have been investigated include magnetic cell labeling[97–99], rotational seeding[100–102], and perfusion based seeding[103–106]. In addition to seeding ETVGs, perfusion based cell seeding has been investigated in many applications such as tissue engineered bone grafts[107,108], heart valves[109], and other scaffolds of unique geometries[110]. Perfusion cell seeding has consistently been shown to improve cell adhesion to surfaces, increase cell proliferation, and encourage uniform cell distribution. Perfusion based cell seeding is typically bioreactor mediated, requiring a continuous or oscillating flow to facilitate the attachment of cells to the desired scaffold. In addition to being used as a seeding mechanism, bioreactors are often used to facilitate graft conditioning before implantation to enhance mechanical properties.

1.4.7 Mechanical Conditioning and Bioreactors

Mechanical conditioning is widely recognized as one of the most relevant methods to enhance tissue accretion and microstructure in engineered tissues. In most bioreactor conditioning models; uniaxial circumferential pressure is applied to mimic pulsatile conditions of the vascular system. Though these experiments have been largely disorganized, very rarely revealing relevant trends for manipulation, the universal effects of mechanical stimulation on ETVGs are apparent. Cyclic strain generally leads to increased cell numbers, higher collagen content, higher yield and ultimate stresses, higher elastic modulus, higher burst pressures and higher suture retention rates[111–113].

Niklason and colleagues pioneered the inclusion of cyclic circumferential stretch in ETVG development in the late 1990s. Cyclic distension was applied to cell seeded PGA scaffolds via a silicone catheter for a period of 8 weeks (Fig 8 A). The dynamic environment led to increased collagen production and superior mechanical properties such as higher suture retention rates, higher burst pressures, and higher strength. Niklason and colleagues further investigated biaxial stretching in 2016[114] (Fig 8 B). The same benefits gained from uniaxial stretch were present, but other more unique effects were also observed. While elastin deposition has been variable when investigating the effects of mechanical stimulation on ETVG development, biaxial stretching increased the level of elastin fiber maturation as well as increased fibrillin-1 formation and collagen III formation and undulation. This organization is similar to that seen in native vasculature, which had not been achieved via uniaxial stretch. This organization was most likely what contributed to the improved mechanical properties in biaxially treated grafts like increased distensibility and compliance. The effects this improved microstructure has on in vivo performance has not been investigated.

Though the list of studies utilizing circumferential strain in their procedure is lengthy, few truly sought to elucidate the role mechanical conditioning plays in ETVG development, and studies incorporating axial conditioning are extremely rare. In 2011, Tranquillo and coworkers published results regarding cyclic distension applied to fibrin gel grafts and effect on mechanical properties[115] (Fig 8 C). Over the course of the dynamic culture period the ETVG was allowed to naturally contract in response to the conditioning. The study found that mechanical conditioning encouraged the development of mature elastin fibers and enhanced mechanical properties. Additionally, ETVGs typically experienced an axial retraction of 60% and had a significant effect on collagen fiber alignment when compared to fixed end controls. Determining optimal conditioning protocols for ETVGs has been rather empirical, and progress has been slow without relevant in vivo models for confirmation of improvement. Though the role of biomechanics in regulating non-thrombogenicity, vasoactivity, ECM synthesis and regular maintenance is well established, harnessing these pathways to create ETVGs with targeted properties has not been sufficiently investigated. A

comprehensive perspective looking at the effects different levels of mechanical stimulation influence at the cellular level, in engineered tissues and in vivo could reveal the major modes of mechanical based remodeling and how best to manipulate them.
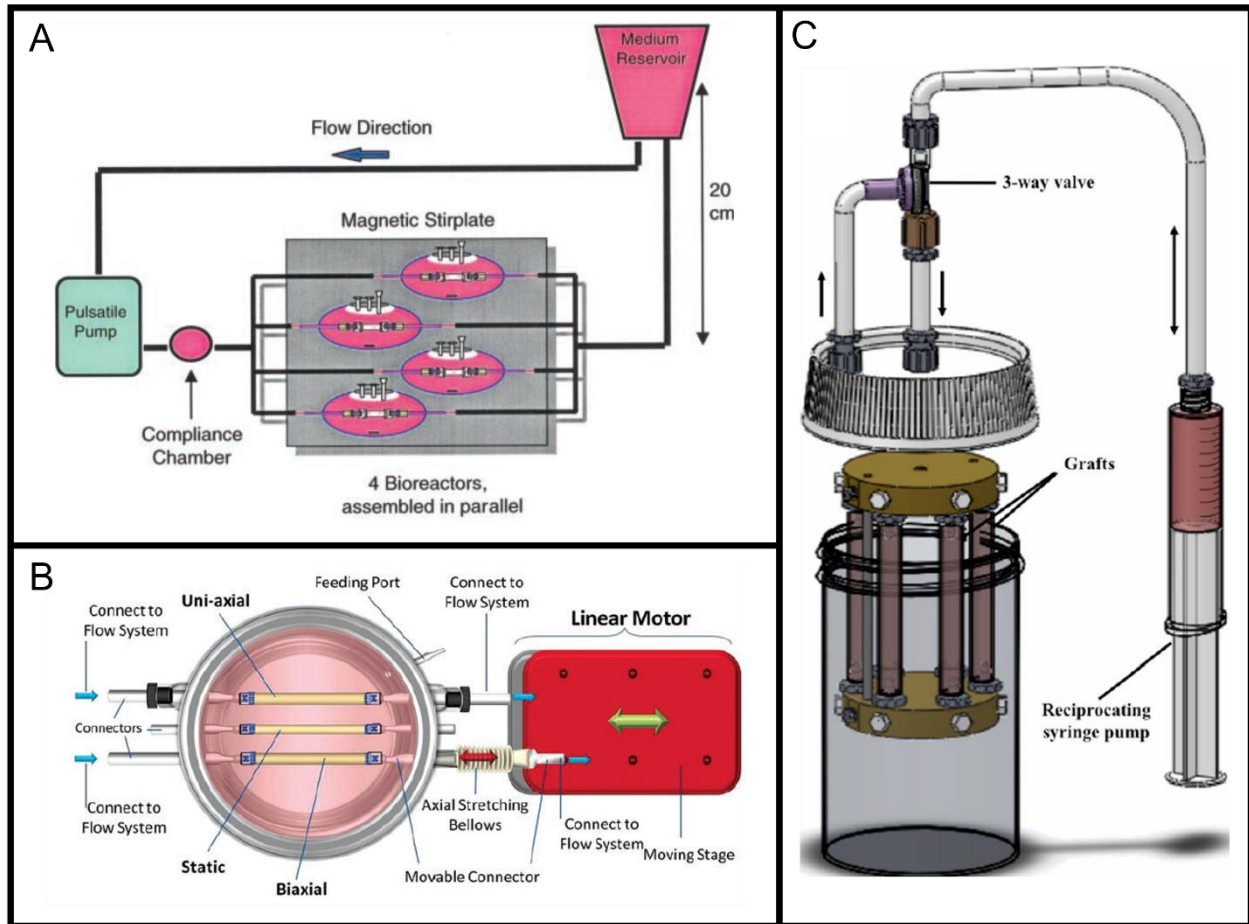
Figure 8. Examples of bioreactors capable of applying mechanical strain to cultured ETVGs. A) illustrates the pulsatile bioreactor developed by Niklason and coworkers. The pulsatile pump creates circumferential distension via PBS flow through balloons in the graft lumen. Copied with permission from [93]. B) depicts the biaxial stimulation bioreactor created by the Niklason group, modified from A with a linear motor to facilitate axial stretch for one of the cultured ETVGS. Copied with permission from [113] . C) is a schematic diagram of the pulsatile bioreactor created by Tranquillo. The syringe is mounted to a reciprocating pump which consistently pulses flow into the upper manifold, facilitating medium flow through the lumantransmurally through the tissue and through the lumens collecting on the ablumenal side of the grafts and reinjected into the upper manifold. Copied with permission from [115].

1.4.8 Limited Clinical Progress

Very few ETVGs have progressed all the way to clinical trials, despite over 50 years of dedicated research in the field. Major considerations to take into account include the consistency of the manufactured

product, the simplicity of employing the device, the suitability of the animal models employed for in vivo testing, the design of the preclinical proof of concept studies, and adequate safety testing. However, these benchmarks are not specified in the case of ETVGs and the level and quality of in vivo testing varies widely between studies. It has been found that the majority of in vivo studies evaluate graft performance of the course of 6 months, but many studies only evaluate performance for a month or less[91]. These time periods are not long enough to be clinically relevant, as neointimal hyperplasia can take up to 2 years to develop.

Early on, attempts at improving that patency on ePTFE grafts in femoral popliteal bypass applications was carried out by Zilla and colleagues[81]. A large-scale clinical study was conducted on the effects of seeded a autologous EC monolayer into ePTFE conduits affected graft patency in vivo. The study characterized improved methods for endothelial cell isolation and proliferation for and the positive effects on graft patency were significant. The first attempt at human utilization of a fully biological vascular graft was attempted by L'Heureux and colleagues through the company Cytograft Tissue Engineering[68]. These grafts were cultured from allogenic donor fibroblasts as previously described, and the culture process took approximately 7 months. Three of these grafts have been implanted in patients as arteriovenous hemodialysis access shunts with positive results, however the length of time required for manufacturing ultimately lead to the company abandoning this method[116]. Another graft was developed by Shinoka, Bruer and coworkers using a 50:50 blend of PLCL and either PLA or PGA statically seeded with autologous bone marrow-derived mononuclear cells[117]. Scaffolds were implanted as large diameter pediatric vascular grafts. The study found that 11 years after implantation patients exhibited no graft related complications and the original graft material completely degraded in that time frame[118]. This study holds particular significance due to the simplicity of the procedure. Mononuclear cells isolated from the patient's bone marrow are isolated and manually drip seeded onto porous PGA scaffolds merely 2 hours before implantation. This may be attributed to the youth of his subjects if we remember the increased elastin content seen in the rapidly degrading ETVGs implanted in neonatal lambs, however more data is needed before a theory can be determined.

23

Currently, Niklason and colleagues at Humacyte are conducting clinical trials with their human acellular vessel (HAV)[119]. The HAV is constructed by seeding donor smooth muscle cells onto a PGA mesh scaffold. The seeded scaffold is conditioned in a bioreactor 8 weeks to develop de novo tissue structure, and subsequently decellularized before implantation. The HAV is currently in Phase III trials for use in vascular trauma and arteriovenous hemodialysis access and is in phase II trials for use as treatment of peripheral artery disease.

1.5   Objectives

Progress in the ETVG paradigm requires a systematic approach to reach better mechanistic understanding of the cause-effect interplay between implant properties, host reactions, and their modulation with controllable parameters. There are a vast array of variables that are associated with ETVG development such as implant material, manufacturing techniques, scaffold functionalization, cellularization, types of cells utilized, seeding method, preconditioning with a bioreactor and method of bioreactor stimulation. However, it is finally becoming clear which variables hold the most influence in terms of graft patency. The development of a dynamic bioreactor environment and automated cell seeding apparatus will enhance the creation of cellularized biodegradable vascular grafts with increased patency rates.

This dissertation documents the development of methods for the systematic high throughput investigation of the effects mechanical conditioning exert on engineered tissue vascular grafts designed for use in a rat aortic interposition model. The main objective can be split into 3 aims:

(1) To design and manufacture a seed and culture bioreactor system for the cultivation of ETVGs with the capacity to apply biaxial mechanical stimulation.

(2) To fully evaluate the seeding capabilities of the bioreactor system for consistency between samples.

 (3) To develop a pipeline to study the effects of mechanical conditioning on ETVG composition, microstructure, mechanical properties and patency.

In Chapter 2, we develop the animal model used to evaluate the in vivo response to implanted ETVGs. This is a significant step, as the in vivo model directly dictates the target graft size and surgical techniques used. In Chapter 3, we refine our initial bioreactor design and conduct extensive testing on the seeding capabilities of the system, ensuring consistency between samples at culture time t = 0. This is important because it is a confirmation of limited variability between ETVGs, increasing the statistical relevance of results. In Chapter 4, we fully define the mechanical culture capabilities of the bioreactor design and methods used to determine the mechanical properties of the developing ETVGs. Chapter 5 provides a brief summary of our accomplishments and outlines future experiments using the system for its intended purpose.

Chapter 2

Static Culture *in vitro* and *in vivo* deployment in rats

There are a wide variety of variables associated with the manufacturing of ETVGs. Keeping the desired end goal in mind when considering ETVG production is essential to make informed choices. The goal of this work was ultimately to examine the effects of mechanical stimulation on ETVG development as well as the host response following implantation. Of the methods mentioned above, cellularized scaffolds is the most conducive towards the study of developing tissue in vitro. Acellular methods utilize scaffold functionalization to encourage the migration of host cells onto the graft in situ, which is fundamentally different in technique and not relevant to this project. While natural matrices and gels commonly employ mechanical conditioning to achieve the required physiological strength, the timeline of such development is also out of the scope of this project's goals. We determined that seeding porous scaffolds would be the quickest way to assemble a rough ETVG template that could withstand mechanical strain for conditioning and implantation in an animal model.

For our in vivo study, we wanted to evaluate our grafts as small diameter vascular grafts ($<$ 5 mm) and cost effectiveness was critical. Commonly used models for cardiovascular research include mice, rats, rabbits, pigs, sheep, dogs and baboons[120–124]. Large animal studies with pigs, sheep, and baboons are excellent for clinical translation research, however the cost associated with keeping them is high. The presented study is a proof-of-concept approach, so small animal models were chosen as the most appropriate. The aortic interposition model in rats is commonly used to study ETVGs in vivo. The vessel

is approximately 2 – 3 mm in diameter and grafts sections used in this model are typically 1.5 cm in length[125–128].

To facilitate the development of de novo tissue with remodeling capability, we used a biodegradable polymer to construct the scaffold. Options included linear α-hydroxy esters such as poly(lactic acid) (PLA), poly(glycolic acid) (PGA), and poly(ε-caprolactone), (PCL)), elastomeric segmented polyurethanes (PU), and highly crosslinked polyesters (e.g., poly(glycerol sebacate) (PGS)). PLA, PGA and PGS all degrade over the course of a couple weeks in physiological conditions making them ideal for applications were rapid degradation is encouraged[124,129,130]. PU is a highly compliant material which is advantageous for avoiding problem related to compliance mismatch in vivo[131]. The properties of PU are also highly tunable making it a popular choice for those studying the effects of graft properties on cell behavior. PCL is FDA approved for use in medical devices and has a much longer degradation period compared to other biodegradable polymers; 2 years rather than 2 weeks[132]. By blending de novo tissue with a structurally supportive polymer, the overlap of tissue development and scaffold degradation is extended and opportunities for process optimization multiplied. Methods for manufacturing polymer based scaffolds are to numerous to be listed, but one of the most well studied and consistently used in cardiovascular applications is electrospinning[133–135]. The mechanical and biological properties of electrospun vascular grafts can readily be tailored by altering the composition and combination of the blended polymers or copolymers. The structural properties, such as polymer fiber size and scaffold thickness, can be controlled by adjusting electrospinning settings (voltage, speed, time, and concentration of the polymer solutions)[85].

Cell types used in vascular tissue engineering are typically vascular endothelial cells, vascular smooth muscle cells, or stem cells. To avoid an immunological response after implantation, ETVG development methods typically aim to use autologous cell sources. While the benefits of having a fully confluent layer of autologous endothelium are well known, harvesting enough cells for use is a major problem in the field. This problem can be alleviated by using stems cells, which can either be harvested[136] or induced from a different population of host cells such as dermal fibroblasts[126]. However, directing the differentiation of

stem cells in vivo can be challenging, and maintaining the differentiated state is inconsistent. While studying the use of both types of cells in ETVG applications is essential towards advancing the field, neither are truly relevant in the context of this study. The primary provider of mechanical support in vasculature is the VSMC, due to its contractile ability and SEM secretion. By using an immortalized VSMC line we avoid the complication of having to isolate cells from target tissue or having monitor the differentiation of stem cells while still being able to study relevant cell behavior in response to stimuli.

In this section, we review the development of our tissue engineered vascular graft model and initial bioreactor design concept. Methods regarding scaffold materials and manufacturing techniques, postprocessing, seeding methods and bioreactor design will be explained, preliminary analysis techniques for ETVGs optimized, and initial results discussed.

2.1   Methods

2.1.1   Scaffold fabrication

Polycaprolactone (PCL; Mn = 80,000), N,N-Dimethylformamide (DMF) and Tetrahydrofuran (THF) at high performance liquid chromatography grade were obtained from Sigma-Aldrich (St. Louis, MO) and used without further purification. The 14 wt% polymer solution was prepared by dissolving PCL in a solution of THF and DMF with a weight/weight ratio of 1:1 and stirred for 24 hours at 40°C. The solution was observed to be clear and without trapped air before every use.

The mandrel used to collect the PCL fibers and form the scaffold is a stainless-steel rod 2mm in diameter. An aluminum foil strip, 1cm thick and 13 cm long, is wrapped around the mandrel tightly. The wrapped mandrel is then mounted between of lathe chucks designed to suspend the mandrel in the electrospinning system. The aluminum wrap is essential for scaffold removal from the mandrel once the spin is complete. The PCL solution is extruded from a 1 ml syringe with a 26-gauge stainless steel blunt tip needle and a mass flow rate of 1.2 ml/h. The mandrel is mounted 20 cm away from the needle on a stage

set to translate 5 cm continuously at 1 cm/s as the mandrel rotates at 720 rpm. A high voltage (15 kV) was

applied to the base of the needle for 40 min to facilitate fiber collection.
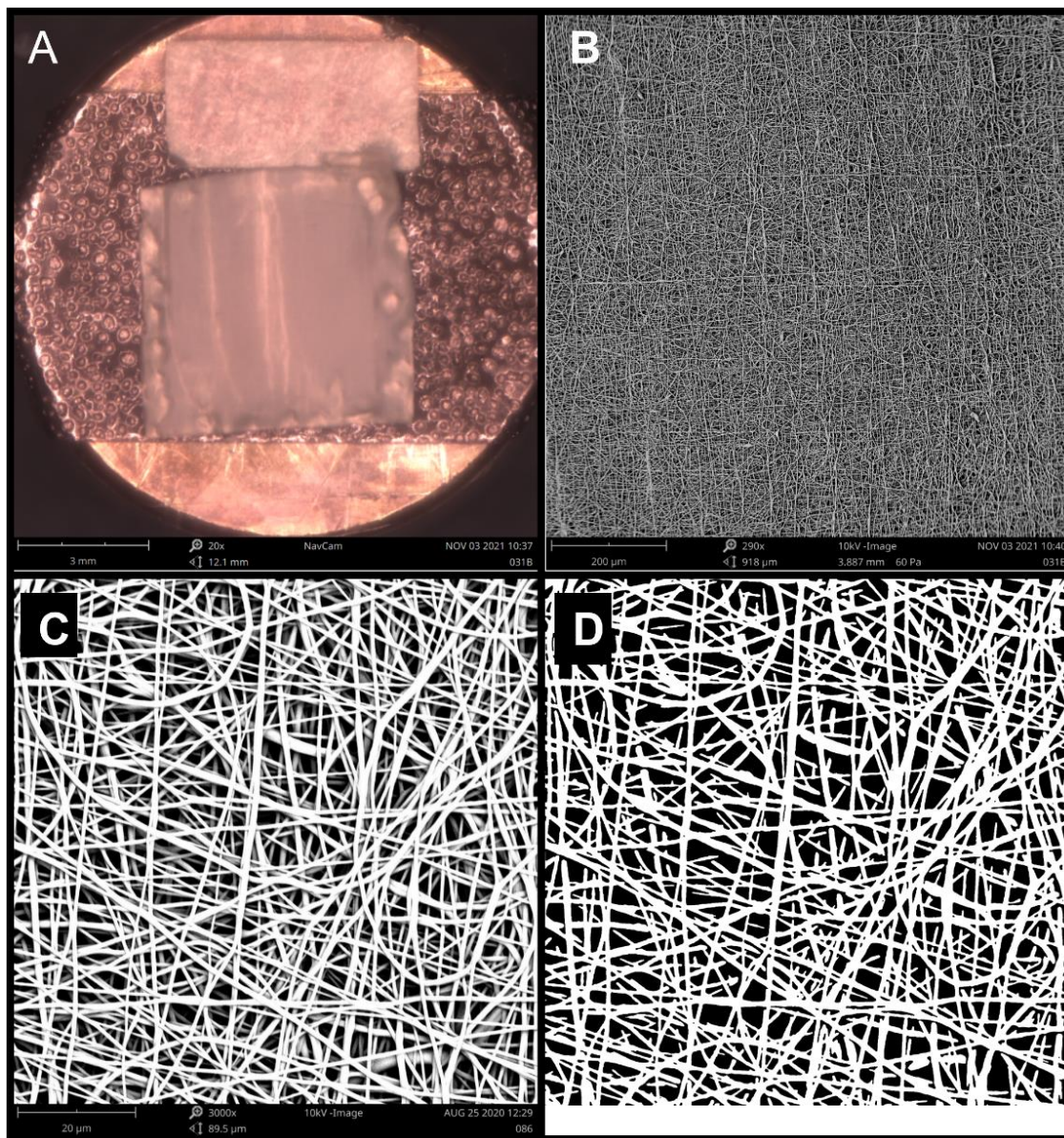
Figure 9. Representative images obtained from SEM imaging at A) 20x, B) 300x and C) 3000x magnification. High magnification images were binarized for further analysis using ImageJ software (D).

When the spin is completed, the aluminum sheet is removed from the mandrel and cut to size

depending on its intended function. Samples are dried overnight in the presence of the blue rocks to

evaporate any remaining solvent and a small section of the scaffold is excised for SEM imaging. Sections

were imaged at 5x, 500x and 3000x at random spatial intervals (Fig 9). 3000x was the optimal magnification for high resolution imaging and analysis of scaffold microstructural properties based on pixel size in relation to fiber diameter.

2.1.2   Scaffold Characterization

2.1.2.1   Mass Distribution

Each spin produced a 12cm long tube of electrospun PCL material. the last centimeter of material on either end was removed and the remaining 10 centimeters used for analysis. The scaffold was cut into 1 cm sections and each section labeled 1-10 in longitudinal order. Section mass was reported as the average of 3 mass measurements taken with a scale. The exact length of each section was measured x3 with calipers and average for the final reported value. Thickness was determined by spreading the scaffold section between two glass coverslips and measuring the thickness with a micrometer. This value was subtracted from the thickness of the coverslips alone and reported.

2.1.2.2   ImageJ Analysis

SEM images of scaffold microstructure were taken at random spatial intervals across the 10 cm length. Scaffold sections were mounted to carbon taped covered pegs with their luminal surface facing out. The scaffold sections were imaged using SEM at 20x and 300x for qualitative analysis, but 3 addition images were acquired at 3000x for quantitative analysis using an ImageJ software called DiameterJ[137]. DiameterJ utilizes a variety of algorithms to binarize the images such that the first 3-4 layers of fibers are white and everything else is black. The selected binary images are then used to quantify average fiber diameter, fiber orientation and pore size for that sample in relevant units given a pixelated length of the scale bar.

2.1.2.3 Uniaxial Mechanical Testing
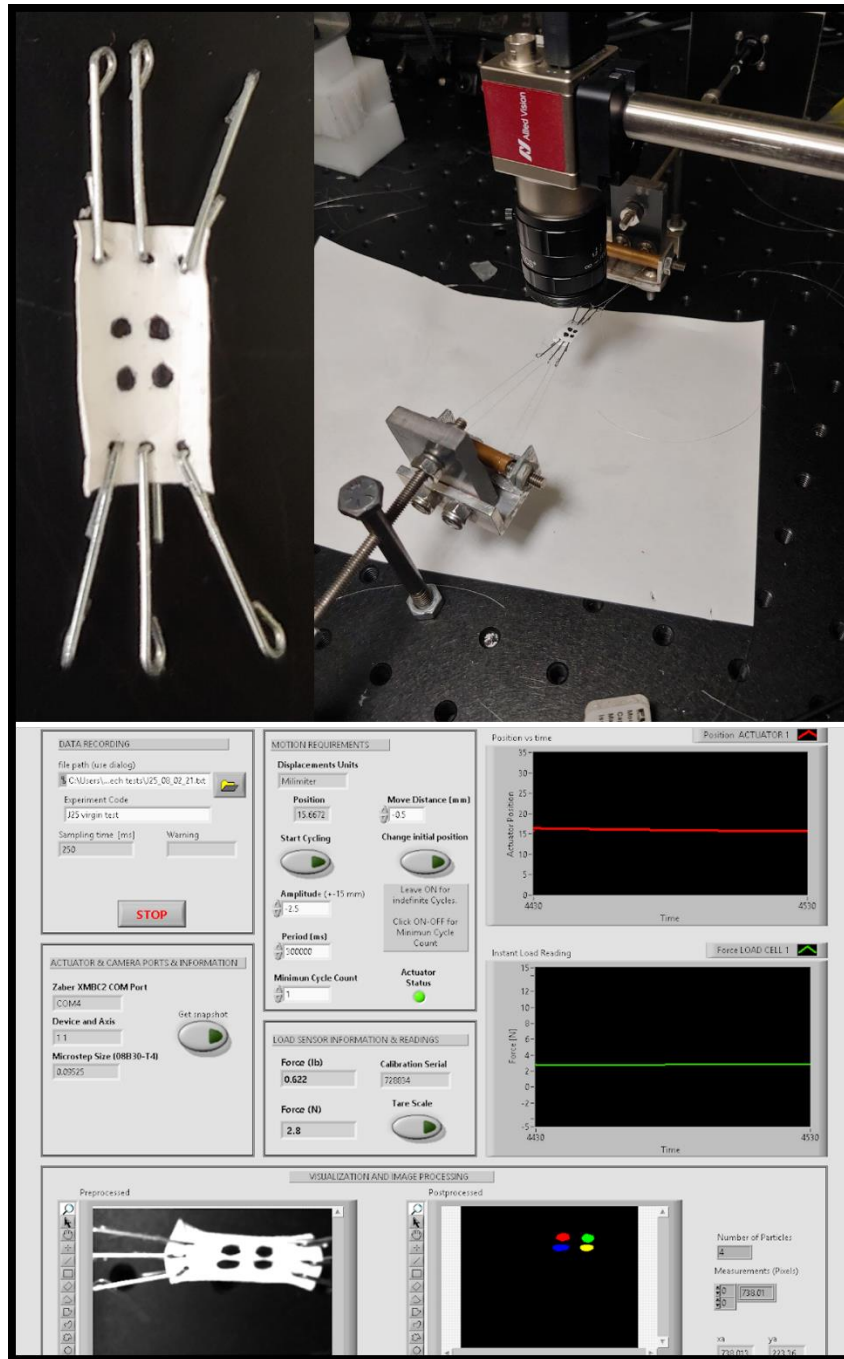
Figure 10. The uniaxial mechanical tester for scaffold material characterization. The scaffold section is fastened to 6 metal hooks (top left) and mounted between two custom fabricated brackets designed to evenly distribute force between the hooks (top right). One bracket is attached to a load cell, while the other is connected to a linear actuator. The camera tracks the movement of 4 dots on the scaffold surface to calculate relative strain. Strain and force measurements from the load cell are saved to a previously indicated file path. The lab view control window is used to dictate testing protocol and manipulate tracking parameters for more precise measurements (bottom).

Scaffold sections 2.5 cm long where mounted via six metal fasteners into the uniaxial testing system (Fig 10). The hooks were connected via fishing line to brackets outfitted to homogenously distribute force along the three points of contact with the material edge. The scaffold surface was marked with 4 dots arrange in a square. A camera was programmed through LabVIEW to track the movement of the four dots, facilitating the calculation of the scaffold material strain (Fig 10). The force applied to the scaffold material was measured via a load cell situated on the distal bracket post. Axial tension was applied with an actuator.

Once the scaffold material is mounted appropriately into the system, a pretension of 2 N is applied and the load cell tared. The material is then prestretched 10 times in quick succession by 1 mm. Once the scaffold is preconditioned this way, the scaffold is subjected to mechanical tests as dictated by the LabVIEW program. Controllable parameters in the LabVIEW program include stretch amplitude of the actuator, stretch period and number of stretch cycles from 1 to infinite. Our sample test protocol utilized a 5%, 8% and 10% stretch level over a period of 30 seconds to determine the elastic modulus. Mechanical properties after degradation have also been evaluated by subjecting scaffold material to NaOH solutions of varying PH before mechanical testing.

2.1.3   Vascular Smooth Muscle Cell Culture

Murine vascular smooth muscle SV40LT-SMC cells (VSMCs) (ATCC; Manassas, VA, USA) were cultured full growth medium containing Dulbecco Modified Eagle's Medium (DMEM), 10% fetal bovine serum (FBS) and 200 mcg/mL geneticin (G418), all produced by Gibco. Cells were lifted for passage using 0.025% trypsin solution, At passage 6, cells were harvested for seeding.

2.1.4   Bioreactor Design

The first iteration of our bioreactor cultured 4 scaffolds vertically in a polypropylene jar, and all four scaffolds were fed from the same media reservoir. Scaffolds were mounted by suture over tubing connectors, fit snugly into a bracket made of 2 stainless steel washers connected via 2 threaded stainless-steel rods. The bracket structure was attached to the jar lid via the stainless-steel rods as well. The lid

contained 9 holes: 2 for the stainless-steel rods, 4 for the individual tubes that feed the proximal scaffold ends, 2 for the drainage tubes that cycle the media from the bioreactor jar to the reservoir, and 1for the filter that allowed for sterile air exchange (Fig 11). Circulation of culture media was facilitated via peristatic pumps. To control the fluid level in the bioreactor jar, the pump hosting the tubes that drained the bioreactor into the reservoirs was set to a speed of 10 RPM while the ETVG feeder tube pump was set to 5 RPM. Drainage tubing only went 1 inch into the bioreactor jar, well above the proximal end of the scaffold, ensuring the level of media never dipped enough to expose the scaffold to air.
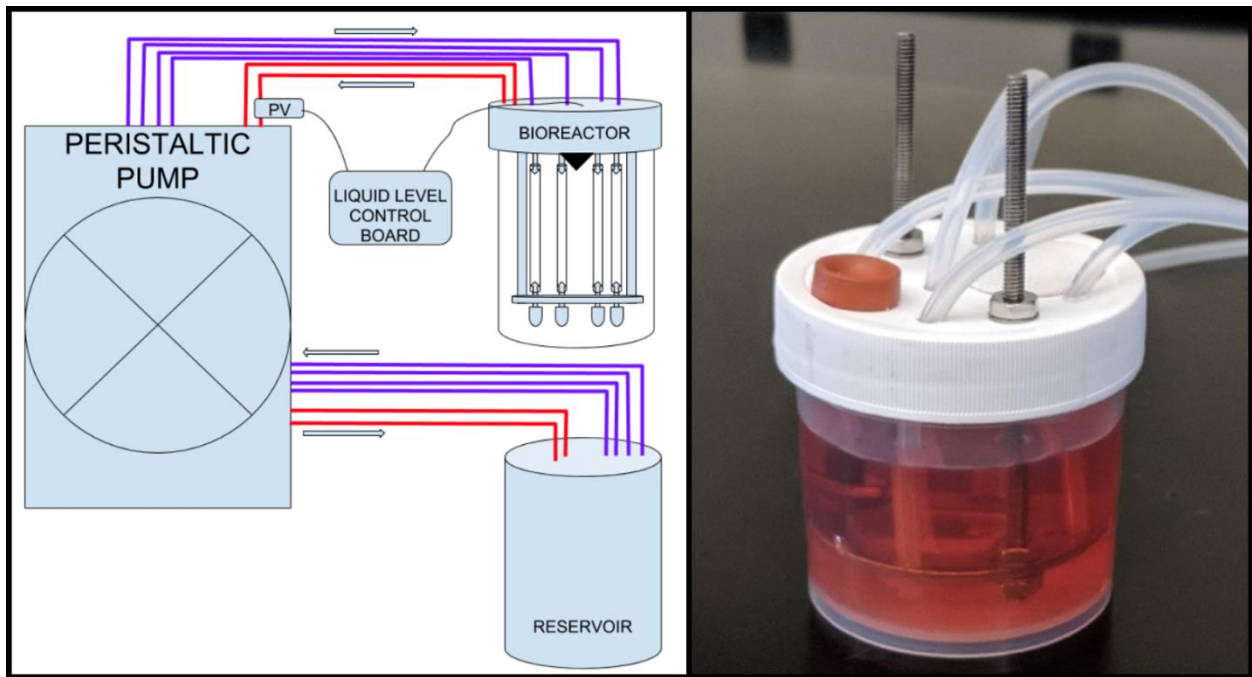
Figure 11. ETM3 Bioreactor Version 1, for static culture. A) Schematic diagram of bioreactor flow loop, featuring 2 bioreactor draining tubes and a liquid level control sensor. Should media touch the sensor, the pinch valve is programed to open, facilitating an increased drainage rate from the bioreactor chamber. B) the bioreactor chamber components are localized to the lid to enhance ease of handling. When changing media or manipulating the ETVGS the bioreactor lid could be held suspended in the air, allowing for the use of both hands for the procedure and limiting contact with possible contaminating surfaces.

Scaffold seeding was conducted via forced transmural flow due to a plug located at the distal end of the scaffold material. Briefly, approximately 8 million cells were suspended in 50 ml of solution. The cell suspension was deposited into the media reservoir and the peristatic pump set to 30 RPM to drive the cell suspension through the connective tubing and transmurally through the scaffold walls. After completion

of seeding, the plug was removed from the distal end of each scaffold, allowing media to move through the lumen of the scaffold unimpeded. Media was switched on a weekly basis by removing the media from the bioreactor chamber, filling the cell media reservoir with 250 ml of fresh culture medium, and resuming flow to allow the refill of media in the bioreactor system. ETVGs for initial analysis were cultured for 1-2 weeks in this system.

2.1.5 *In vivo* Studies
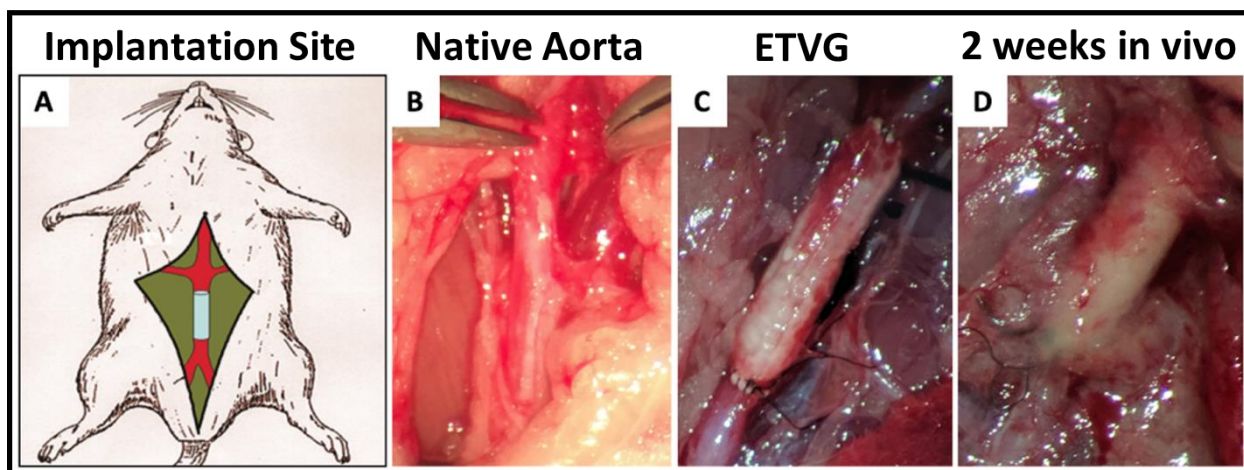
Figure 12. In vivo rat model. A) schematic of the surgical deployment of an ETVG as an infra-renal aortic interposition graft. B) native rat aorta before excision. C) an ETVG immediately following suture to the native aorta. D) the same ETVG at explant after 2 weeks of in vivo deployment.

Following culture periods of 1-2 weeks, ETVGs were harvested from the bioreactor and place into ice cold phosphate buffered saline (PBS) for transport to the surgical site. All experimental animals were treated in accordance with institutional guidelines and the Guide for the Care and Use of Laboratory Animals, published by the National Institutes of Health (NIH Publication No. 86-23, revised 2011). Select samples were implanted as aortic grafts in Sprague-Dawley rats through bisection of the abdominal aorta above the renal bifurcation, a well described aortic interposition by-pass graft in rats[78,138] (Fig 12). Isoflurane (3%) was used as general anesthesia. Anesthesia depth was monitored by checking for the absence of pedal reflexes. The recipient rat was then placed supine on a warming pad on the operative field with sodium heparin given intravenously. A long midline abdominal incision was made and the intestine

retracted outside the abdomen using a gauze to expose the infra- renal abdominal aorta and the inferior vena cava. The aorta was carefully cleaned and isolated and a proximal and a distal control of the vessel obtained with vascular clamps. A 1.5 cm portion of the abdominal aorta was then excised with micro-scissors to match the length of the vascular grafts. The anastomosis of the recipient's abdominal aorta to vascular graft was completed with continuing 8-0 monofilament suture. After completion of the anastomosis, the distal clamp was removed to assess for bleeding and then the proximal clamp was removed. The intestines were returned to the abdomen, which was then closed with 4-0 continuous sutures. The recipient rat was placed on a warm area, treated with painkillers and allowed to recover. The rats were observed in the surgical suite until fully recovered from anesthesia and then returned to the housing area. Buprenorphine and cefuroxime were administered subcutaneously for the first 3 days after surgery, and anti-aggregation therapy started after surgery with aspirin and dypiridamole.

At the scheduled explant time point, animals were be anesthetized with 3.0% isoflurane inhalation with oxygen followed by 1 mL of hyper-potassium chloride (2 mEq/mL) cardiac arrest solution intravenous injection to obtain rapid cardiac arrest at the diastolic phase without additional pain. This method is within the recommendations of the Panel on Euthanasia of the American Veterinary Medical Association.

2.1.6   Histology Analysis

ETVGs cultured in vivo were stain with H&E and picrosirius *en bloc* and embedded in OCT Compound (Electron Microscopy Sciences; Hatfield, PA, USA) to cut 8 μm-thick cross-sections with a cryotome. Samples harvest from in vivo were immediately embedded in OCT freezing medium and cryosectioned. Samples were subsequently stained with H&E and Picrosirius red for analyzing the developing tissue structure. Stained cross sections were imaged with an Eclipse LV100D microscope (Nikon Instruments; Melville, NY, USA)

2.2   Results

2.2.1   Scaffold Morphology
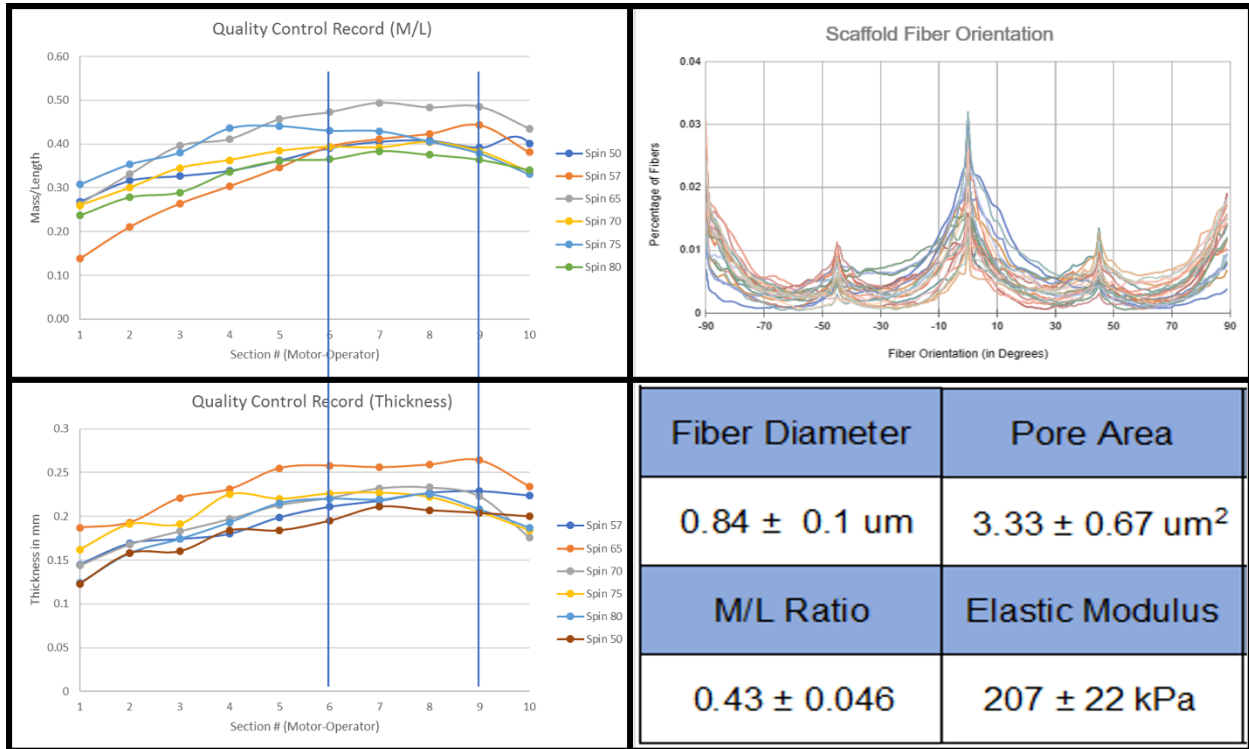
Figure 13. Virgin Scaffold Analysis. Graphs depicting gradient of mass/length measurements and thickness of unprocessed 10 cm scaffolds. Reveal a restricted area of homogenous properties common to most manufactured scaffolds (left, outlined in blue). SEM images were analyzed to determine the orientation of individual fibers in the graft material. The resulting graph reveals that fibers are randomly oriented with no more than 3% of fibers aligned in one direction. 0° associates with fibers aligning in the circumferential direction while 90° associates fibers aligned in the axial direction. SEM analysis also revealed the average fiber diameter and pore size of electrospun fibers. Material stiffness was determined with the uniaxial mechanical tester. These results are reported at the bottom right.

An appropriate section of homogeneous and reproducible scaffold properties was identified from the gross 10 cm produced with each spin (Fig 13). This section produces scaffolds 4cm long, 2mm inner diameter, ~150-200 µm thick with a mass ratio of ~.36-.41 mg/mm. We repeat this process every 10 scaffolds we make to monitor for any changes and preserve our current scaffold quality. SEM analysis of our scaffold material shows an average fiber diameter of 0.84 µm and an average pore area of 3.33 µm^2 (Fig 13). Scaffolds present linear elastic behavior under 10% axial strain with a Young's modulus of 207±22kPa. Static and dynamic degradation experiments have revealed that no significant changes in mass

or microstructure occur over a 4-week period under physiologic pH and temperature, clearing them for use

in our experiments (Fig 14).
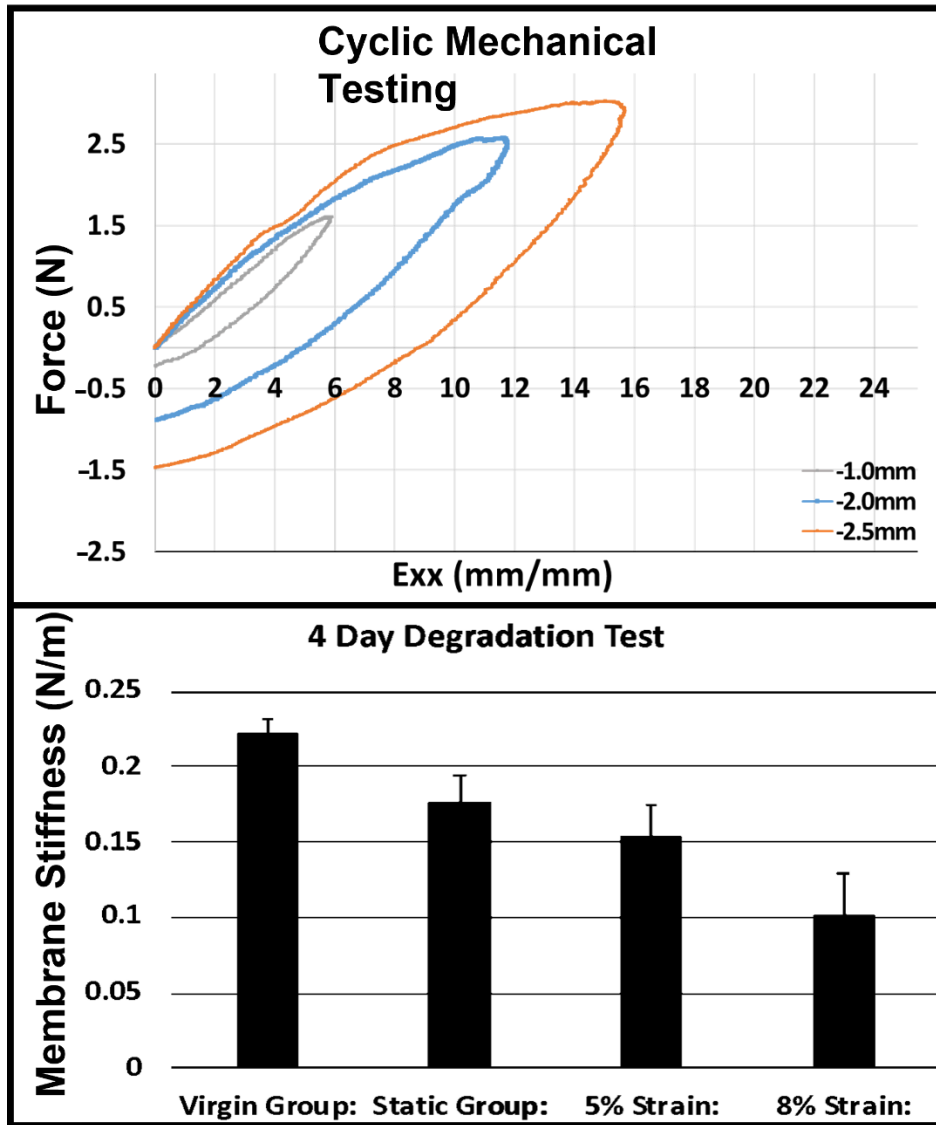
Figure 14. Mechanical testing analysis. A plot of force vs strain in the x direction is obtained to determine the young's modulus from the linear portion of the plot (top). The young's modulus of 3 sequential tests are averaged to obtain the experimental modulus. Further evaluation of scaffold properties in terms of degradation rate is being conducted by evaluating the stiffness of the material after being subjected to cyclic stretch in a NaOH of pH 12.5, however statistically viable data has yet to be produced. Initial results are shown (bottom).

2.2.2 *In vitro* Development
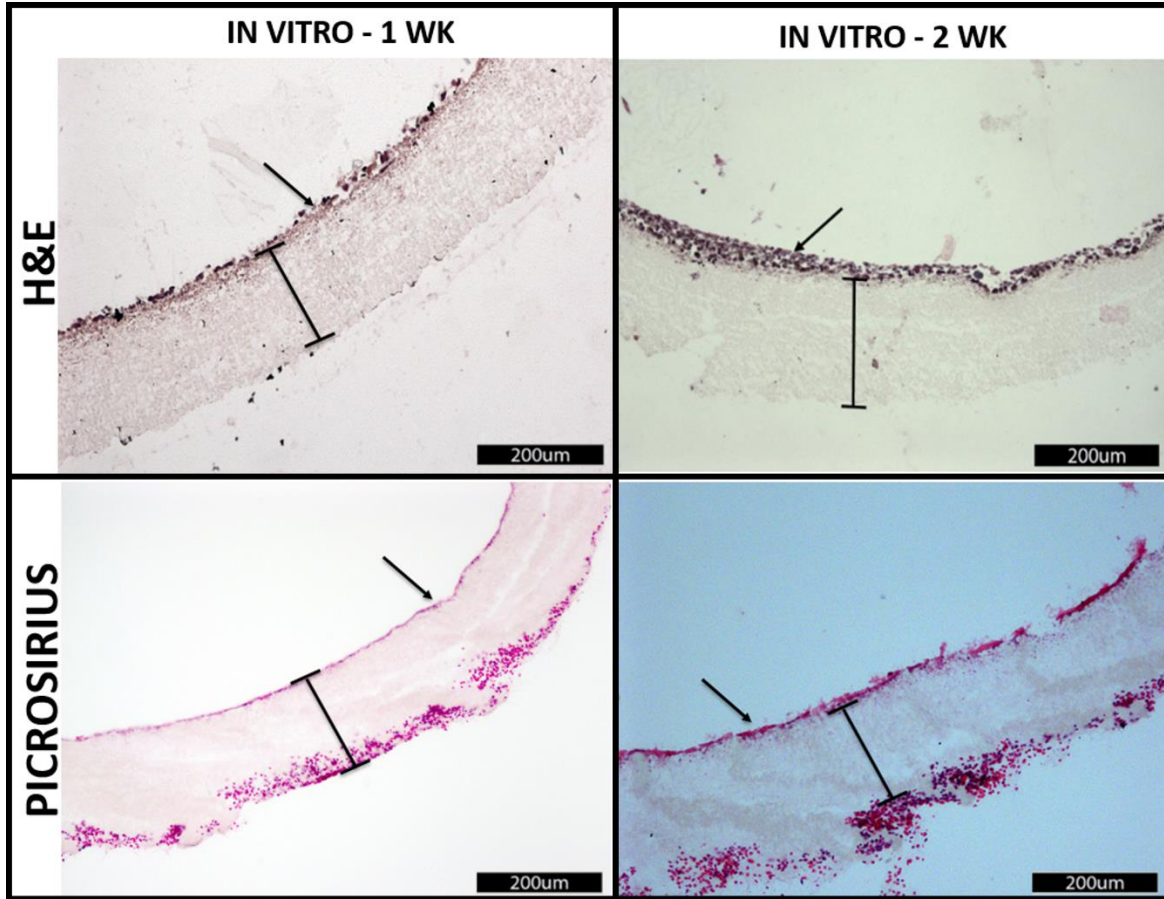
Figure 15. Histology of ETVGs after in vitro culture. In our static bioreactor we successfully seeded and cultured cells for up to 2 weeks. The cells grew in random layers (H&E) and deposited collagen in an unorganized manner (Picrosirius). Two weeks of culture appeared to result in thicker cell layers and increased collagen deposition. Scaffold lumen is show with arrows, scaffold thickness highlighted by bars. Cells located on the external side of picrosirius stained sections are blood cells from contact with the blood of the intended graft recipient during implantation, graft sections were cut to size at the implant site and excess used for histology.

Culture methods were confirmed to be successful qualitatively, resulting in full even circumferential coverage after one week of incubation in the system (Fig 15). Cells appeared to remain viable and continued to proliferate and deposit ECM over 2 weeks of in vitro incubation according to histological analysis. Comparison between the two time points suggest that collagen content was increased significantly, but organization appeared to be random, consistent with results of other studies.

2.2.3 *In vivo* Response
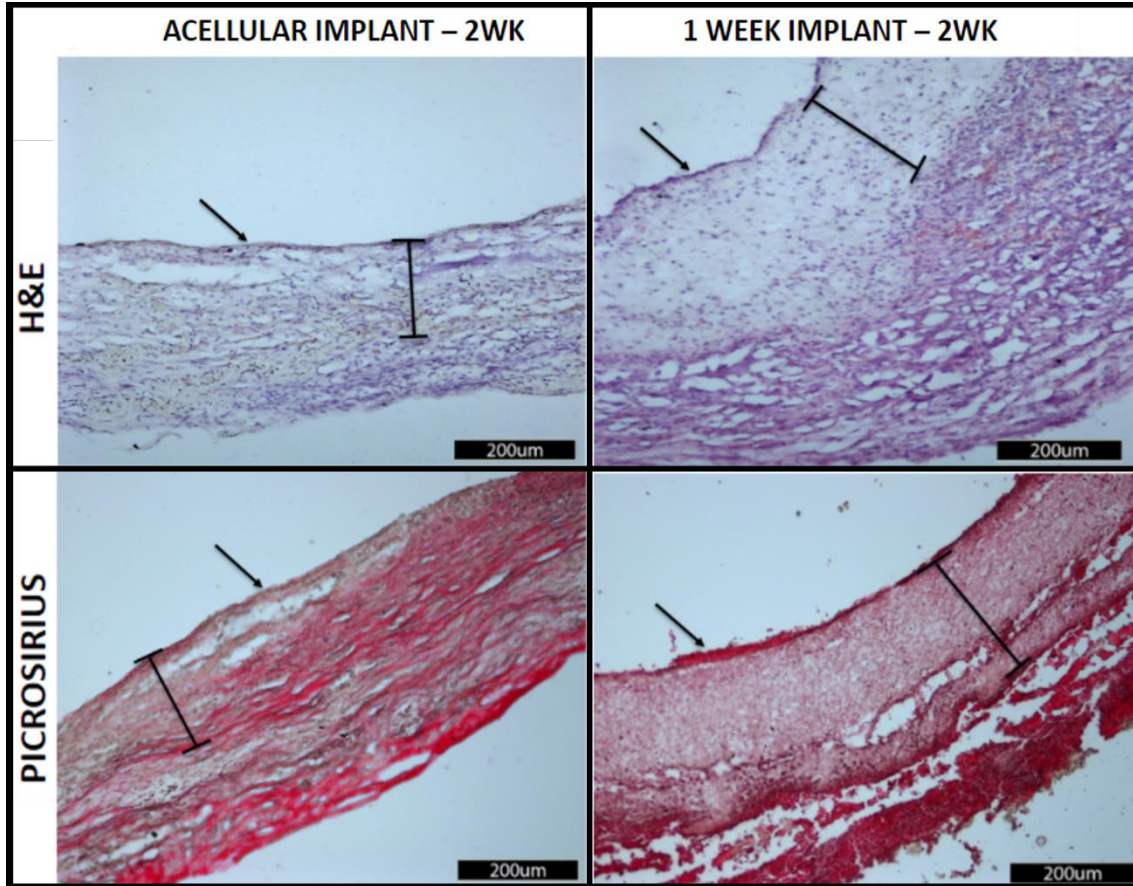
Figure 16. Histology of ETVGs after in vivo deployment. Acellular grafts without modification and ETVGs after one week of culture were compared 2 weeks after implantation. Scaffold lumen is show with arrows, scaffold thickness highlighted by bars. Both grafts exhibited heavy infiltration of cells into the graft material. Scaffolds with a cellular component demonstrated massive fibrotic tissue deposition around the scaffold edge, clearly visible to the naked eye at explant.

Scaffolds cultured for 1 and 2 weeks under static conditions were implanted in successfully Sprague-Dawley rats. Our survival rate was approximately 60% among subjects that did not die due to surgical complications. Qualitative observation showed the expected signs of inflammatory response consisting of fibrous tissue accumulation around the scaffold and thrombus formation within, usually at the proximal anastomosis. Histology further shows that the thickness of the fibrotic tissue varies between the in vitro time points (Fig 16).

PCL scaffolds exhibit degradation of microstructure over time both in vitro and in vivo with the most extensive being after 2 weeks in vitro and 2 weeks in vivo consistently throughout samples. The 2:2 samples also exhibited increased infiltration of cells into the scaffold material from the outer edge

2.3   Discussion

The methods available for the construction of tissue engineered vascular grafts are numerous and have been met with varying levels of success. It is well established that scaffold functionalization is a critical factor in promoting cell adhesion and tissue development in polymer scaffolds. However, the relative success of different functional molecules and functionalization methods used in the field have not revealed a superior method. While enhanced results may have been achieved if a functional element was included during scaffold processing, by simplifying the model we reduce the level of variability affecting results. The ultimate intention is to characterize the effect mechanical strain has on 3D de novo tissue development, which can be affected a great deal by the protein composition of the cell's environment[139,140]. The wide variety of functionalization techniques can be translated into an opportunity for functionalization tailored to produce a specific development outcome when used in tandem with mechanical stimulation techniques. However, to study the effects of functionalization, a non-functionalized base line must be established.

The first version of the bioreactor was a positive first attempt that revealed many opportunities for improvement. A major area that required optimization was the seeding method, which, though very simple, fostered a high degree of variability between samples. The channels of the peristaltic pump do not facilitate a fine degree of control over flowrate in the circuit. By depositing the total cell load required for seeding all four scaffolds collectively in the media reservoir, there was no way to confirm homogenous delivery between samples. Additionally, variable levels of pressure developed within the ETVG lumen led to the occasional blowout of the distal end of the ETVG from its tubing connector mount. The consistency of this occurrence also highlighted the need for a better ETVG mounting system that gripped the scaffold better if mechanical stimulation was ever applied. Axial mechanical stimulation would also be difficult to apply

vertically because a vertical stage would need to be designed to house the required components. Finally, the positioning of the micro-porous filters affixed to the bioreactor lids lead to a buildup of condensation in the filter material and ultimately contamination of the bioreactor environment when subjected to long term culture.

Methods of ETVG analysis had to be optimized according to the limitations incurred by our choice of scaffold material. The melting point of PCL is 60, which is the temperature paraffin wax is heated to when embedding tissue sections for histological analysis. This prompted the choice of cryosectioning for structural tissue analysis for the experiments. PCL is also a hydrophobic material, making adherence to microscope slides after sectioning tenuous when there is minimal tissue present in the sample. As such, samples developed in vitro were stained *en bloc* prior to cryosectioning to minimize the number of washes that needed to be applied to scaffold cross sections after they had been adhered to the microscope slide. We attempted to use the Fastin elastin assay and Syrcol collagen assay by Biocolor to determine the level of elastin and collagen deposition at each of the time points, however levels were too low to be detected. This is unsurprising, as other studies site periods of up to 8 weeks to achieve significant tissue development. The study would have been strengthened with the addition of a viability test to confirm cells are healthy and continuously proliferating between time points.

Initially, the scaffolds were intended to be used as interposition grafts in the rate abdominal aorta, however the diameter of the ETVG and the diameter of the target vessel were significantly different, leading to improper suturing and surgical failure. By suturing the grafts into the side of the vessel wall, the diameter of the incision can be manipulated, and the graft can be sutured appropriately. This study lacks true clinical relevance since the length of the graft is not sufficient to emulate human CABG condition. However, endothelialization of the graft lumen is not the focus of this research, the host reaction to graft mechanical properties is. As such, the consideration is irrelevant for this level of study. When comparing samples developed in vitro to their counterparts employed in vivo, it is apparent that no further development of the

VSMC layer occurs after implantation. However, there is heavy recruitment of cells on the adventitial surface that can most likely be attributed to macrophage recruitment in response to vascular injury.

Chapter 3

Characterization of seeding efficiency of bioreactor V2

This section is an abridged version of the publication Saunders et al. *Evaluation of perfusion-driven cell seeding of small diameter engineered tissue vascular grafts with a custom-designed seed-and-culture bioreactor*. PLoS ONE 2022

The method of cell seeding onto any scaffold determines the number of cells initially present for in vitro culture and their spatial distribution, which in turn dictates the proliferation, migration, and phenotype of cells as neo-tissue develops[141]. Achieving an even distribution of viable cells can prove challenging as the methods currently utilized are inherently inconsistent. Various techniques have been investigated to seed small diameter tubular scaffolds due to the unique problems associated with this class of geometries [142]. The most widely employed is dripping cell suspension onto the scaffold surface. However, this method is unreliable due to the manual nature of the procedure, and user independent consistency is challenging to achieve [143]. Various uncommon and less well-established cell seeding techniques that aim to use specific directing forces to control the seeding outcomes of the constructs are too hampered by the complexity of devices and procedures to be considered for regular use. Perfusion-based cell seeding, also called vacuum cell seeding or filtration cell seeding, has been employed in many applications such as seeding bone grafts, vascular grafts, heart valves, and other scaffolds of unique geometries. Perfusion based seeding has consistently been shown to improve cell adhesion to surfaces, increase proliferation, and encourage uniform cell distribution compared to traditional static methods[110,144].

Herein, we investigate perfusion seeding as a preferred method for luminal seeding of scaffolds with tubular geometries and quantify the performance of a custom-built perfusion seed-and-culture bioreactor against static seeding methods of cell delivery regarding spatial distribution of seeded cells and their viability. The seed-and-culture bioreactor design was developed as a controlled environment capable of seeding and culturing 4 ETVGs simultaneously under identical conditions. Using the bioreactor system, a variety of environmental stimuli including dual axial mechanical stimulation and the addition of environmental growth factors may be administered to the developing ETVGs semi automatically with minimal handling. Having multiple directly comparable data points is essential to increasing the speed at which research may be conducted but scaling up these experimental processes can be difficult. We suggest bioreactor-mediated perfusion seeding as a simple method that can be easily and reproducibly applied to 4 scaffolds concurrently in a bioreactor environment. Furthermore, the automatic process reduces variability in the seeding method, further reducing variability in ETVG quality between samples.

3.1   Methods

3.1.1   Seeding experiment.

Murine vascular smooth muscle SV40LT-SMC cells (VSMCs) (ATCC; Manassas, VA, USA) were cultured as previously described. Prior to seeding, all scaffolds were prewetted with full growth medium overnight. During and after seeding, scaffolds were maintained in a 5% CO_2 incubator at 37 ºC. Twenty-four hours after seeding, scaffolds were collected for analysis. Harvested scaffolds were split into 5 equal sections approximately 6 mm long for analysis of seeding efficiency across the full length (Fig 17D). Section 1 represents the upstream entry, whereas section 5 is the distal end of the scaffold.

Seeding took place in three distinct methods: 1) bioreactor-mediated perfusion seeding, 2) static injection counterpart seeding, and 3) drip seeding (Fig 17 A-C).
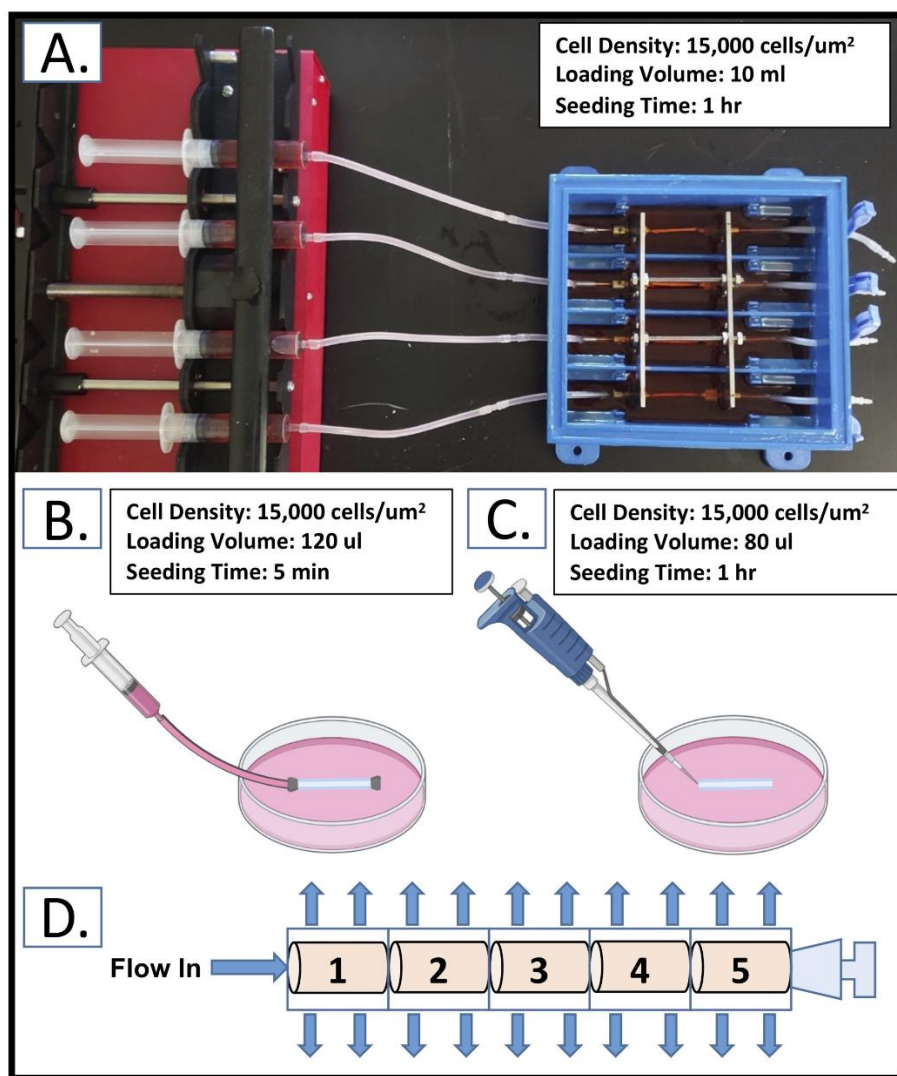
Figure 17. Seeding methodology. Seeding method diagrams for (A) the bioreactor mediated perfusion seeding method, (B) static injection counterpart seeding method and (C) drip seeding. (D) Operating principle of bioreactor mediated perfusion seeding method. Numbers indicate sample organization for analysis.

3.1.1.1 Bioreactor-mediated perfusion (BMP) seeding

Four scaffolds at the time were mounted into the custom-designed seed-and-culture bioreactor (Fig 17 A). The design of the bioreactor chamber is fully described in Chapter 4. 10 mL of cell suspension, containing 2 x 106 VSMCs, was drawn into sterile syringes and connected to the flow loop upstream of each scaffold. The tubing at the downstream end of each scaffold was clamped shut and the cell suspension

was driven through the porous scaffold (Fig 17 D) at a rate of 10 ml/hr with a syringe pump (New Era Pump Systems; Farmingdale, NY, USA).

3.1.1.2   Static injection counterpart (SIC) seeding

Scaffolds were mounted onto modified stainless steel cannulas and filled with 100 ul of concentrated cell suspension containing approximately 2 x 106 VSMCs (Fig 17 B). Each end of the construct was closed, and the scaffold submerged in full growth medium. This method replicated all the conditions of the perfusion-driven seeding method except the transmural pressure gradient supplied by the syringe pump.

3.1.1.3   Drip seeding

Using standard aseptic procedures, 80 µl of a concentrated cell suspension containing approximately 2 x 106 VSMCs was carefully pipetted directly onto the luminal surface of the tubular scaffolds (Fig 17 C). Seeded scaffolds were placed in individual 100 mm culture dishes and incubated for 1 hour at 37°C. During this period the scaffold was rotated every 15 min to encourage even cell distribution. After one hour, scaffolds were submerged in full growth medium. This method replicated the target cell density of the previous methods, while depositing cells inside the scaffold manually.

3.1.2   Viability assessment and cell number.

Scaffold sections produced for viability testing and seeding efficiency analysis were placed in 1000 µl of full growth medium supplemented with 100 µl of alamarBlue (BioRad; Hercules, CA, USA). The samples were incubated for 4 hours at 37 C with intermittent shaking. After incubation, 200 µl of the solution from each sample was placed into separate wells of a 96 well plate. Viable cells reduce resazurin, the active ingredient in alamarBlue, to resorfin which is highly fluorescent. This reaction was quantified with the hybrid microplate reader BioTek Synergy H1 (BioTek; Winooski, VT, USA). The cell number was obtained with a standard curve calculated using known concentration suspensions of cells from 25,000 – 275,000 cells in increments of 25,000.

Additionally, the spatial organization of viable cells was determined via a live/dead viability assay kit (BioVision, Waltham, MA, USA), which marks live and dead cells based on membrane integrity and esterase activity. Ethidium homodimer-1, enters cells with a compromised plasma membrane to bind DNA and emit a red fluorescence. Living cells are identified by Calcein AM, a fluorogenic dye that can permeate through the cell membrane to be converted to a green fluorescence after interaction with intracellular esterase. The middle section of 4 bioreactor-mediated perfusion-seeded scaffolds where harvested and incubated in a 1000:1:2 mixture of PBS, ethidium homodimer-1, Calcein AM for 15 minutes. ETVG circular cross-sections sections were cut into 3 sub-sections and grid-imaged from the luminal surface on a Nikon C2 confocal microscope system in z stacks of eight to twelve 16 μm slices. Images where stitched together using a 3D image stitcher plugin available through FIJI image manipulation software[145].

3.1.3 Immunohistochemical assessment.

Scaffold sub-sections produced for spatial distribution analysis with haematoxylin and eosin stain (H&E) were fixed in 10% neutral buffered formalin overnight. Sections were stained en bloc with H&E and embedded in OCT Compound (Electron Microscopy Sciences; Hatfield, PA, USA) to cut 8 μm-thick cross-sections. Stained cross sections were imaged with an Eclipse LV100D microscope (Nikon Instruments; Melville, NY, USA)

Additional spatial distribution analysis was conducted by staining cell nuclei with DAPI. Scaffold sub-sections were harvested from the bioreactor and briefly rinsed in PBS before fixation in ice cold methanol for 5 minutes. Similar to the H&E samples, sections were stained *en bloc* before embedding in OCT medium and cutting. After fixation, scaffolds were rinsed in three 5-minute PBS baths. Membrane permeabilization was achieved by submersion in room temperature 0.1% Triton solution for 15 minutes. This was followed by another set of three PBS rinses and incubation with 300 nM DAPI solution for 5 minutes. Sections where imaged at 10x on the confocal microscope.

Raw H&E images were converted to binary with ImageJ software[137]. Binary images were post-processed to remove artifacts not relevant to analysis. Total cell load was determined by the total area of

cells present (i.e. area of black pixels in the image). Circumferential cell coverage was calculated by measuring the length of the perimeter covered by cells and dividing by the total luminal perimeter of the scaffold. Average cell-layer thickness was determined by dividing the total cell load by the length of the perimeter covered by cells.

3.1.4   Scanning electron microscopy (SEM) assessment.

Scaffold sections produced for surface coverage analysis were cut along the top most edge and placed in 10% neutral buffered formalin solution overnight. Sections were then rinsed 3x in PBS before dehydration in a series of graded ethanol (ETOH) washes from 50% to 100%. Chemical drying was achieved with graded washes of ETOH and hexamethyldisilane (HMDS) (MilliporeSigma; Burlington, MA, USA), followed by submersion in HMDS until fully evaporated.

After dehydration was completed, samples were mounted for imaging with the luminal side of the scaffold facing up and the circumferential direction corresponding to the horizontal direction of the sample. Samples were handled such that the middle section represents the bottom most section of the scaffold during seeding. Samples were gold sputter coated (Cressington 108, Ted Pella; Redding, CA, USA) and imaged with scanning electron microscopy (Phenom ProX Desktop SEM, NanoScience Instruments; Pheonix, AZ, USA) operated at 15kV. Imaging was conducted at 300x in a 3x3 grid across the full surface of the scaffold section to best approximate total surface coverage.

Raw SEM images were converted to binary with the ImageJ plugin DiameterJ Segment[137]. Of the multiple binary images created from each raw SEM image, the one that was the most accurate in determining where cells were located (i.e. the black spaces in the image covered wherever cells were present in the original) was chosen for further evaluation. Another ImageJ function, Analyze Particles, was then employed for the quantification of percent area coverage. Binarized images were checked to determine the general accuracy of the segmentation method before reporting. Accuracy was determined by randomly selecting 5 images from each seeding method and comparing results with cell coverage determined by manual segmentation.

48

3.1.5   Statistics.

For all the analysis, three to four samples were used (n = 3+1). Values were reported as the average of all the samples, and the error was reported as either the standard deviation or 95% confidence interval (CI) in cases where the standard deviation was larger than the mean. The effect of seeding method and scaffold section within the seeding method on cell viability, surface coverage, and cell layer thickness were assessed with a standard ANOVA, and multiple pair-wise comparisons were carried out using the Tukey-HSD method. Differences were considered significant if $p \leq 0.05$.

3.2   Results

3.2.1   Viability assessment and cell number.

The seeding method had a significant effect on the number of viable cells present per section on electrospun PCL tubular scaffolds (p=0.005). The average number of viable cells present per sample by method is 282,598 ± 53,957 cells, 237,220 ± 43,243 cells, and 163,929± 110,537 cells for BMP seeding, SIC seeding, and drip seeding, respectively. While these averages are not significantly different, the number of viable cells by section showed that perfusion-driven seeding results in significantly more cells by section, 56,519± 15,463 cells, than drip seeding, 42,182± 29,725 cells (p=0.04). The average number of viable cells by section of SIC seeding, 47,444± 15,437 cells, was not significantly different than BMP seeding or drip seeding and the level of variability in longitudinal cell distribution between samples was high.

Perfusion-driven seeding also resulted in the most consistent pattern of cell distribution of the three methods. While section 1 consistently resulted in lower numbers of viable cells than sections 2-5, sections 2-5 were indistinguishable (with p > 0.95, Fig 18 A). SIC seeding also showed no significant difference between sections and when averaged showed a normal distribution pattern with higher concentration of cells in section 3, the middle of the scaffold (Fig 18 B). The standard deviation between SIC samples was larger than in BMP seeded samples, showing that while there is no observable significant difference between averages, the results were not as consistent. Drip seeded scaffolds did have a distinct pattern of cell distribution identifiable in all samples analyzed (Fig 18 C). Drip seeding did not achieve uniformity

across the entire length of the scaffolds, most cells were found at either end of the scaffolds, sections 1 and 5, with very few to be found in the middle section. Sections 1 and 5 were found to be significantly different from sections 2, 3 and 4 (p=0.01, 0.0009, 0.009 and p=0.03, 0.0003, 0.003 respectively, the latter set not included in Fig 18 C).
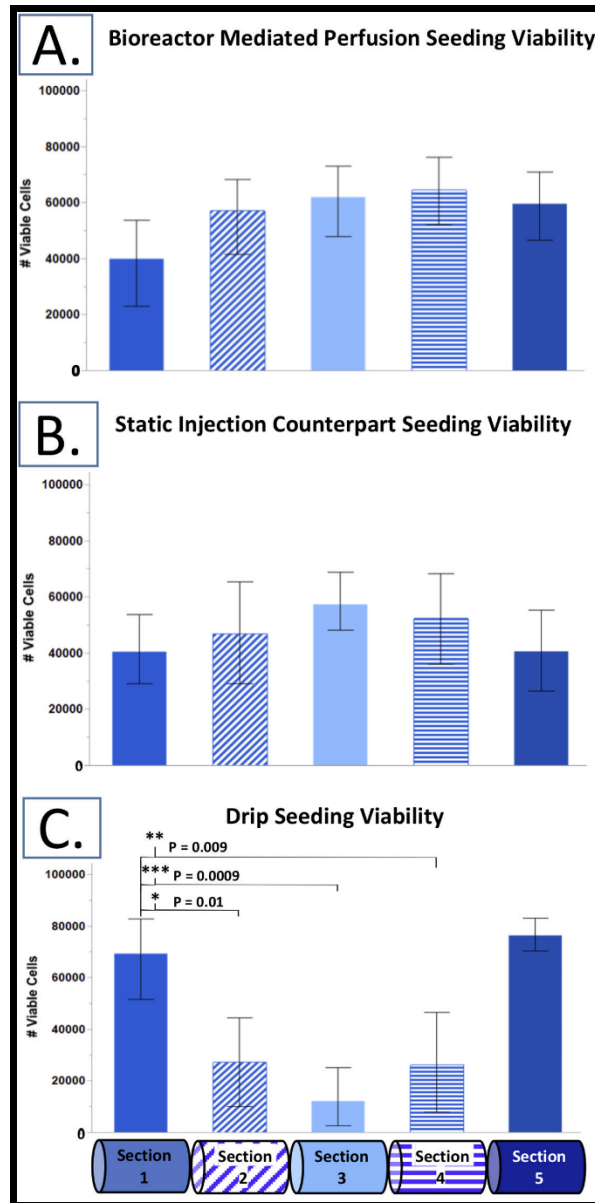
Figure 18. AlamarBlue viability assay results. Section average viable cell numbers for (A) perfusion bioreactor seeding, (B) static counterpart seeding, and (C) drip seeding. (n = 4; mean with 95% confidence intervals.)

The live dead cell imaging of bioreactor mediated perfusion seeded scaffolds revealed a thick, confluent layer of living cells covering approximately two thirds of the scaffold luminal surface (Fig 19). The 4 other scaffolds evaluated this way also follow this pattern. Non-viable cells can be found amongst the live cells, but they are mostly concentrated near the edges where the scaffolds sub-sections were cut, and along major defects in the scaffold structure. The third section of the scaffold that does not contain a confluent layer of cells shows small live cell clumps interspersed throughout the area.
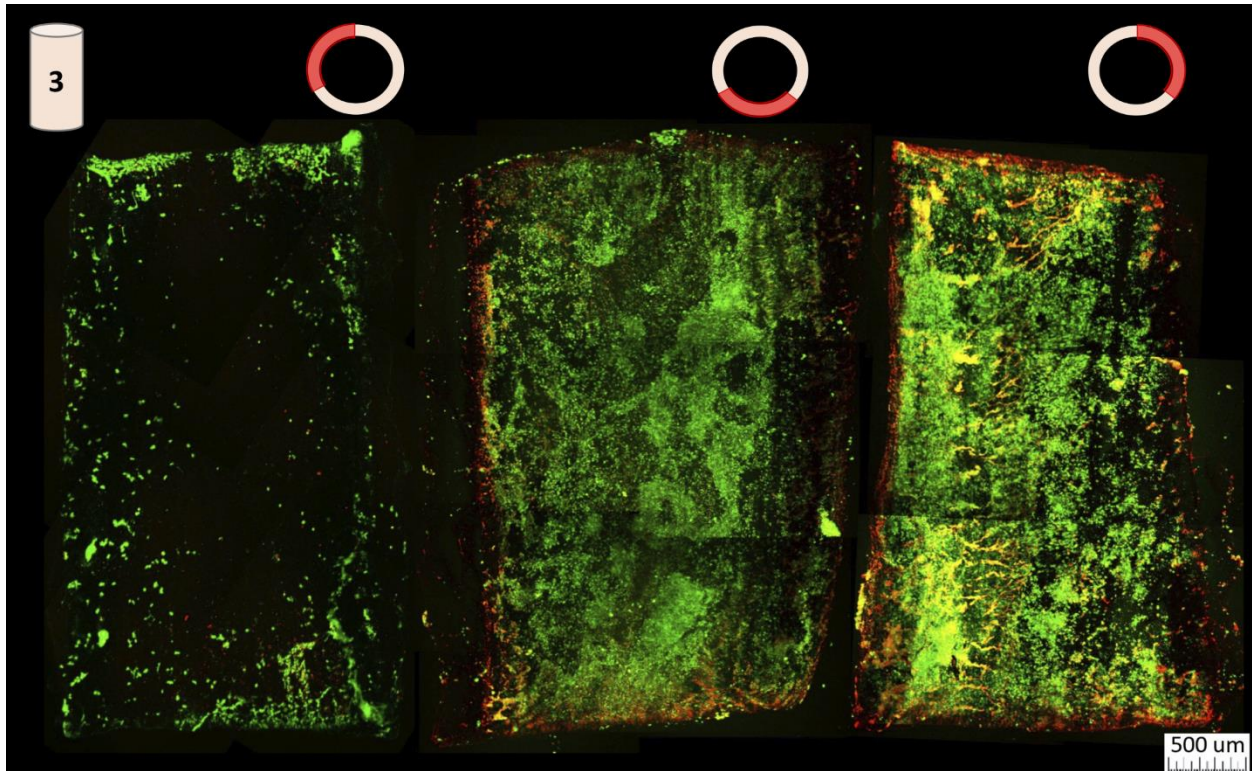
Figure 19. Spatial live/dead cell imaging. The middle section of a perfusion seeded scaffold is represented in 3rds.The left most portion is the top right edge of the scaffold, the middle portion is the bottom of the scaffold, and the right most portion is the top left side of the scaffold. Each section length was approximately 5mm, and its circumference was 6.28mm.

In summary, BMP seeding resulted in the most viable cells with the most consistent distribution across the samples. SIC seeding resulted in a comparable number of cells but with a more inconsistent distribution, and drip seeding resulted in the least number of cells but a high degree of consistency in distribution pattern that featured most of the cells focalized at either end, and middle sections remaining bare.

3.2.2 Immunohistochemical spatial distribution analysis.

BMP seeding resulted in the most consistent cell coverage across the five sections in terms of cell presence around the circumference, though cell-layer thickness varied spatially (Fig 20). Both the SIC and drip seeded samples resulted in cells restricted to a few smaller locations, with inconsistent coverage between sections, and variable thickness of cell layers within each section, often settling in clumps and large regions remaining bare. Drip seeding in particular resulted in multiple sections entirely without cells, usually sections 2-4. Due to such, quantitative analysis was conducted on the BMP and SIC seeded scaffolds only. Perfusion-driven seeding consistently showed cells dispersed across about 60% of the scaffold area, with the highest concentration being located along the bottom edge of the scaffold. BMP seeding also resulted in sporadic cell patches occasionally adhered to the top edge of the scaffold, something rarely seen in SIC or drip seeding methods.
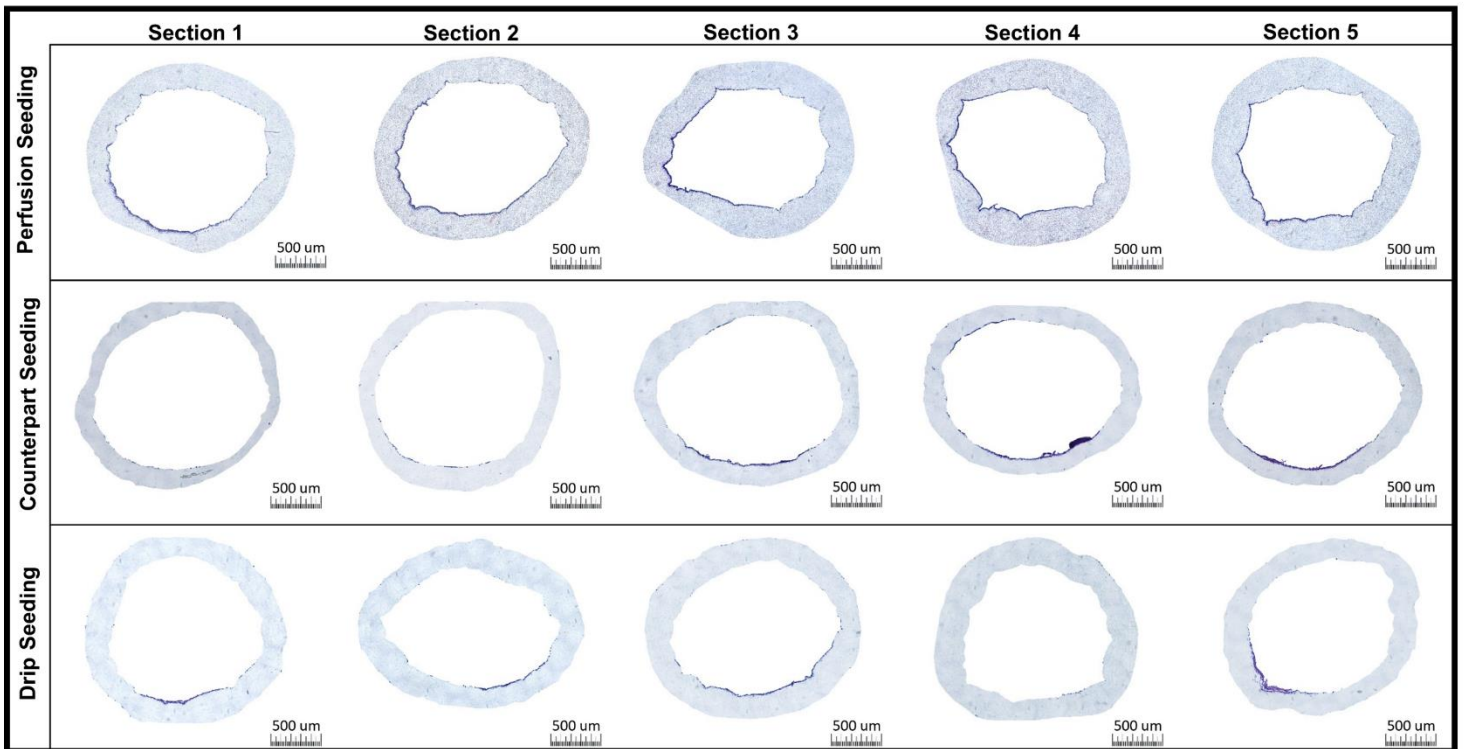
Figure 20. H&E cross-sections. Representative haematoxylin and eosin (H&E) stained cross sections of each seeding method 24 hrs after seeding in longitudinal order.

DAPI stained cross sections show a similar distribution of cells when compared to H&E stained sections, with emphasis on individual nuclei (Fig 21). This confirms that the cell layer deposited by bioreactor-mediated perfusion-seeding is indeed composed by cells with DAPI stainable nuclei and typically one layer thick covering > 60% of the luminal surface. DAPI results obtained with both static methods corroborate H&E histology showing inconsistency in the cell layer thickness and circumferential distribution between sections.
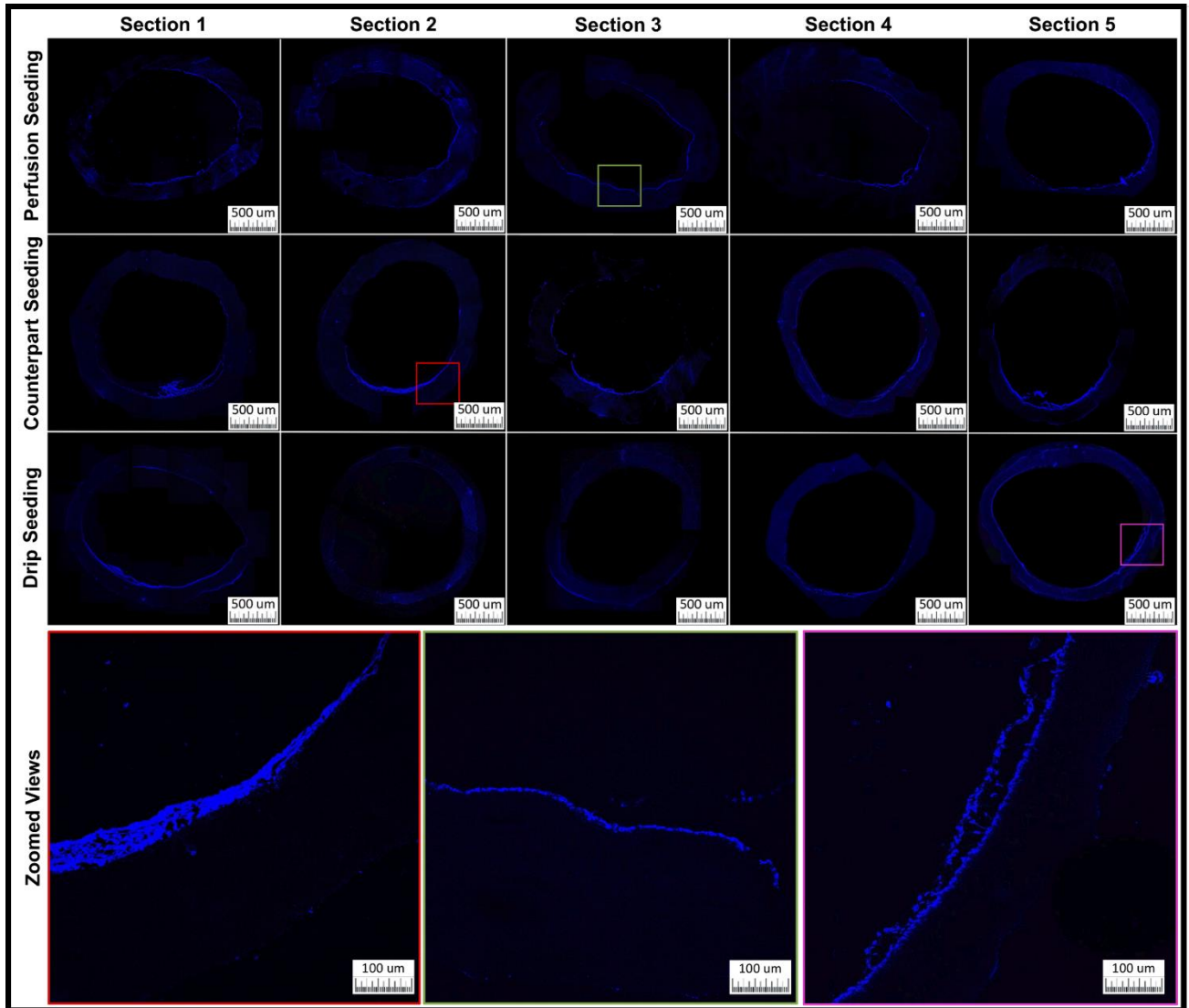
Figure 21. DAPI cross-sections. DAPI stained nuclei of cells in cross sections of each seeding method 24 hrs after seeding in longitudinal order.

Quantitative analysis of histology sections largely agrees with viability results. BMP seeding resulted in a significantly higher total cell load being deposited to the scaffold lumen than SIC seeding (p=0.007, Fig 22 A and 22 C). The variability of total cell load and average cell-layer thickness between sections in the SIC seeded samples corroborates with variations observed in the cell viability analysis (Fig 22 B). Though there was no significant difference in the average cell layer thickness between the two methods (27.8 vs 29.1 µm), the standard deviation was observed to be larger for individual sections in the SIC method. The proportion (or percentage) of circumferential coverage between BMP seeding and SIC seeding was significantly different (p<0.0001), on average achieving 62.8± 20.7 % and 23.6± 15.2 % respectively.
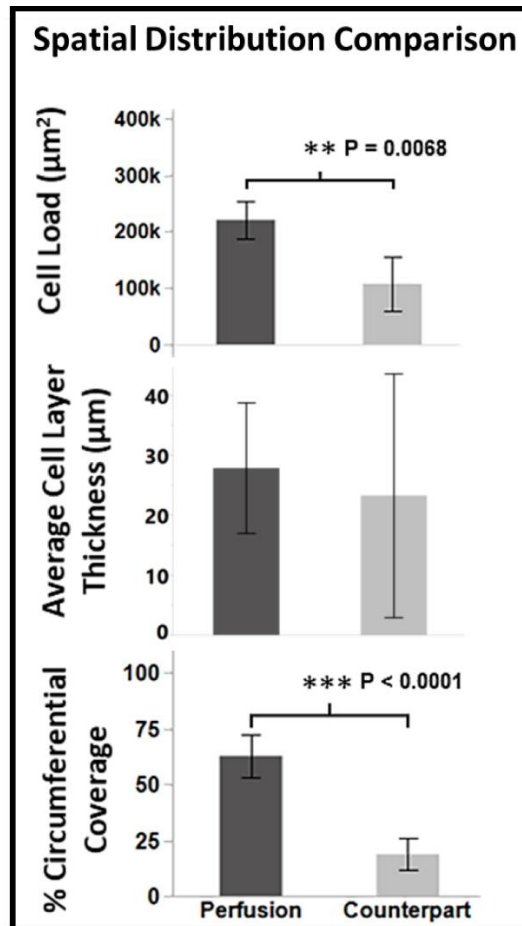
Figure 22. Quantitative assessment of uniformity. Quantitative analysis of H&E images for bioreactor mediated perfusion and static injection counterpart seeding methods preformed with rVSMCs onto electrospun PCL scaffolds. Uniformity judged in terms of total cell load, average cell layer thickness, and % circumferential coverage per section. (n = 20, n=15; mean ± standard deviation).

In summary, BMP seeding achieves significantly more cell load and percent circumferential coverage than static methods while also maintaining a consistent cell layer thickness and distribution between all five sections.

3.2.3   SEM surface coverage analysis.
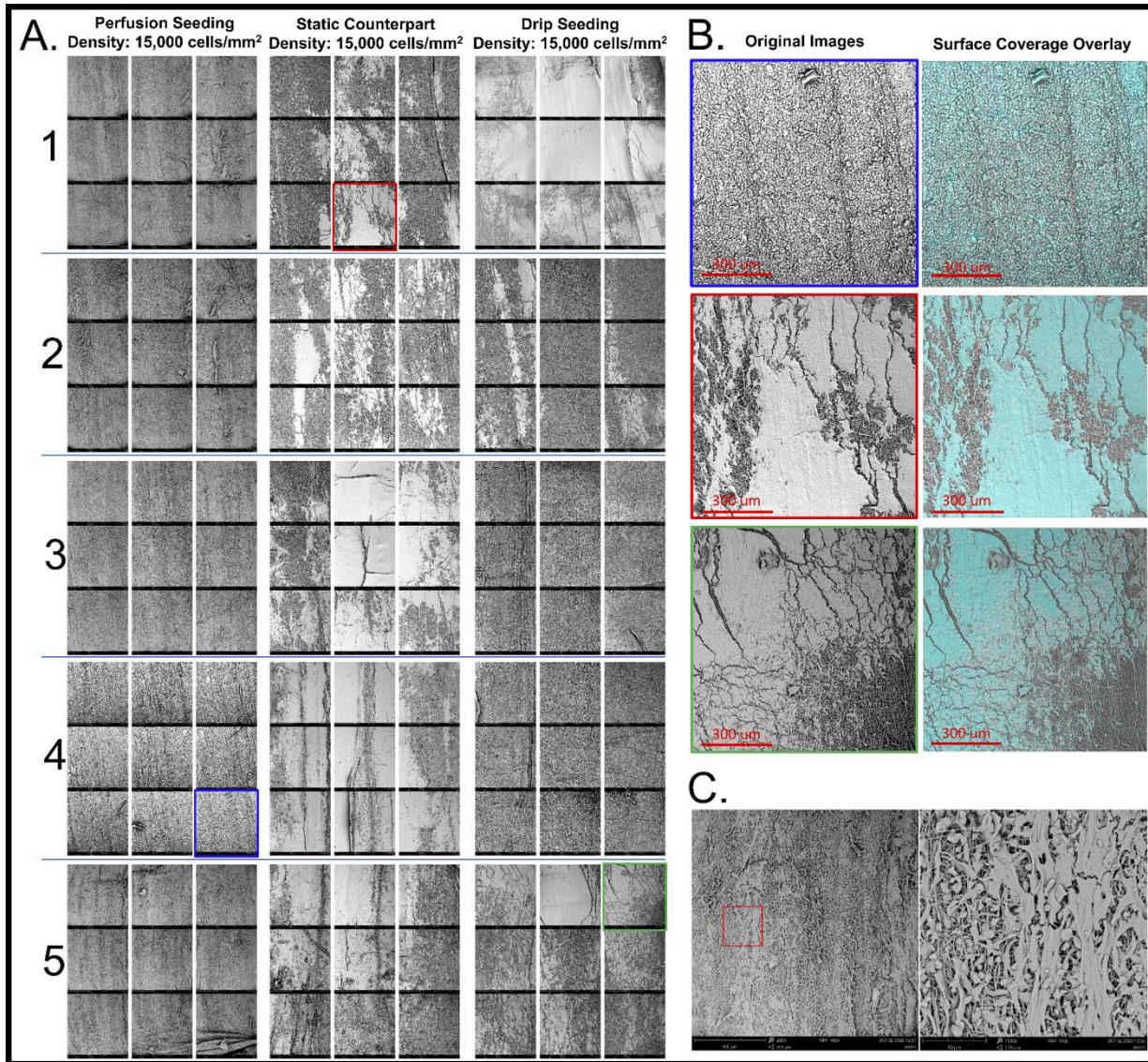
Figure 23. Interpretation of SEM images. (A) Representative SEM images of luminal surface of seeded electrospun PCL scaffolds for each seeding method, (B) Sample images representing quantitative analysis of luminal surface coverage per method. (C) Zoomed in view of perfusion seeded scaffold.

Analysis of the topography of scaffold sections agrees with viability and histology results. BMP seeding showed consistent coverage across the full scaffold surface (Fig 23 A) Additionally, perfusion-

driven seeding resulted in individual cells spaced apart from each other while both static methods led to clumps of cell aggregates from which individual cells could not be identified in the SEM images (Fig 23 B). Cells tend to concentrate along the bottom of the scaffold (middle column of the SEM 3x3 sample views) in the SIC method, and drip seeded scaffolds showed large concentrations of cells at the ends while typically achieving fuller surface coverage in these sections. BMP seeded cells did not appear to be damaged from the perfusion treatment, the morphology of the individual cells qualitatively showed evidence of adherence to the scaffold surface (Fig 23 C).
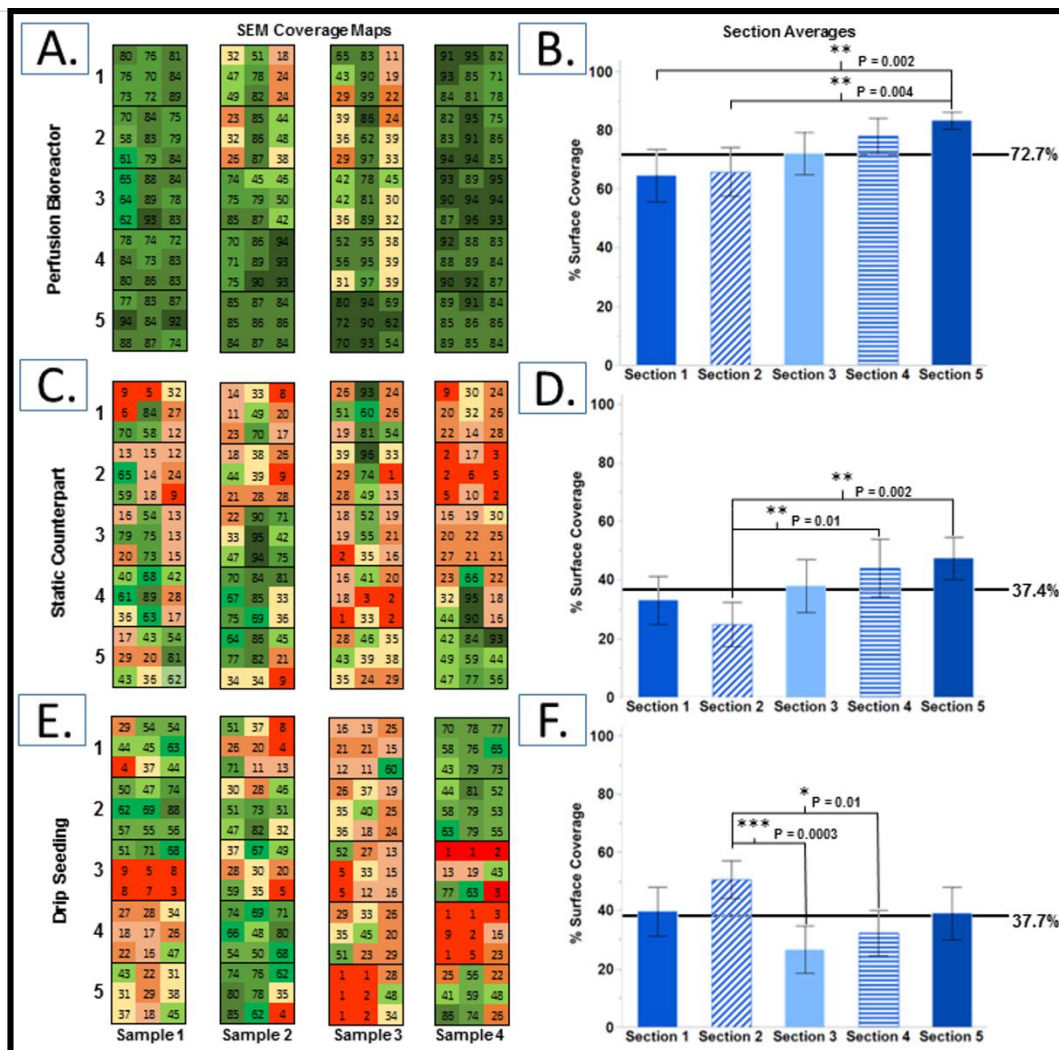
Figure 24. Quantitative analysis of surface coverage. Color map of surface coverage and section averages respectively for (A,B) perfusion bioreactor seeding, (C,D) static counterpart seeding, and (E,F) drip seeding (n = 36; mean with 95% confidence intervals).

Quantitative analysis shows that BMP seeding resulted in significantly higher surface coverage across the scaffold surface, $72.7 \pm 21.7\%$, when compared to static methods, which averaged $37.4 \pm 25.8\%$ and $37.7 \pm 24.7\%$ ($p<0.0001$, Fig 24 A vs. 24 C and 24 E respectively). BMP seeded sections did reveal a gradient of increasing surface coverage from sections 1 to 5, i.e. upstream to downstream. Sections 1 and 2 on average achieved significantly less surface coverage than section 5 ($p=0.002$ and $p=0.004$ respectively, Fig 9B). Though more inconsistent than previous results suggest, the average surface coverage of sections 1 and 2 are $64.6 \pm 26.32\%$ and $65.8 \pm 24.5\%$ respectively, which is still higher than the approximately 37% surface coverage achieved by either static method per section on average. The percent area coverage in SIC and drip seeded scaffolds were variable between sample sections. The distribution pattern for SIC scaffolds tends to be along the bottom edge of the scaffold with patches of high cell density, while drip seeded scaffolds tended to have more surface coverage at either end. Both static methods show a high level of intra-sample variability in cell distribution, either along the length or the circumference of the scaffolds. (Fig 24 B, D, F) Analysis of accuracy showed that manual segmentation vs. automatic segmentation did not deviate more than 2% in the 15 random SEM images analyzed.

3.2.4 Combined results.

Establishing correlations between the data reveals that BMP seeding resulted in the most consistent seeding pattern across all five sections (grouped in blue in Fig 25). When comparing the number of viable cells to percent surface coverage, perfusion-driven seeded scaffolds outperformed static methods in both aspects, achieving comparable viable cell load with higher cell coverage ($> 60\%$ vs. $< 50\%$ of either static method, Fig 25). Comparing the number of viable cells obtained from the alamarBlue viability assay to the total cell load determined by histology resulted in a linear correlation (Fig 25). Correlation of histology determined cell load or SEM-determined surface coverage vs. cell-layer thickness demonstrated again the improved performance and consistency achieved with perfusion-driven seeding method compared to static methods (Fig 25).
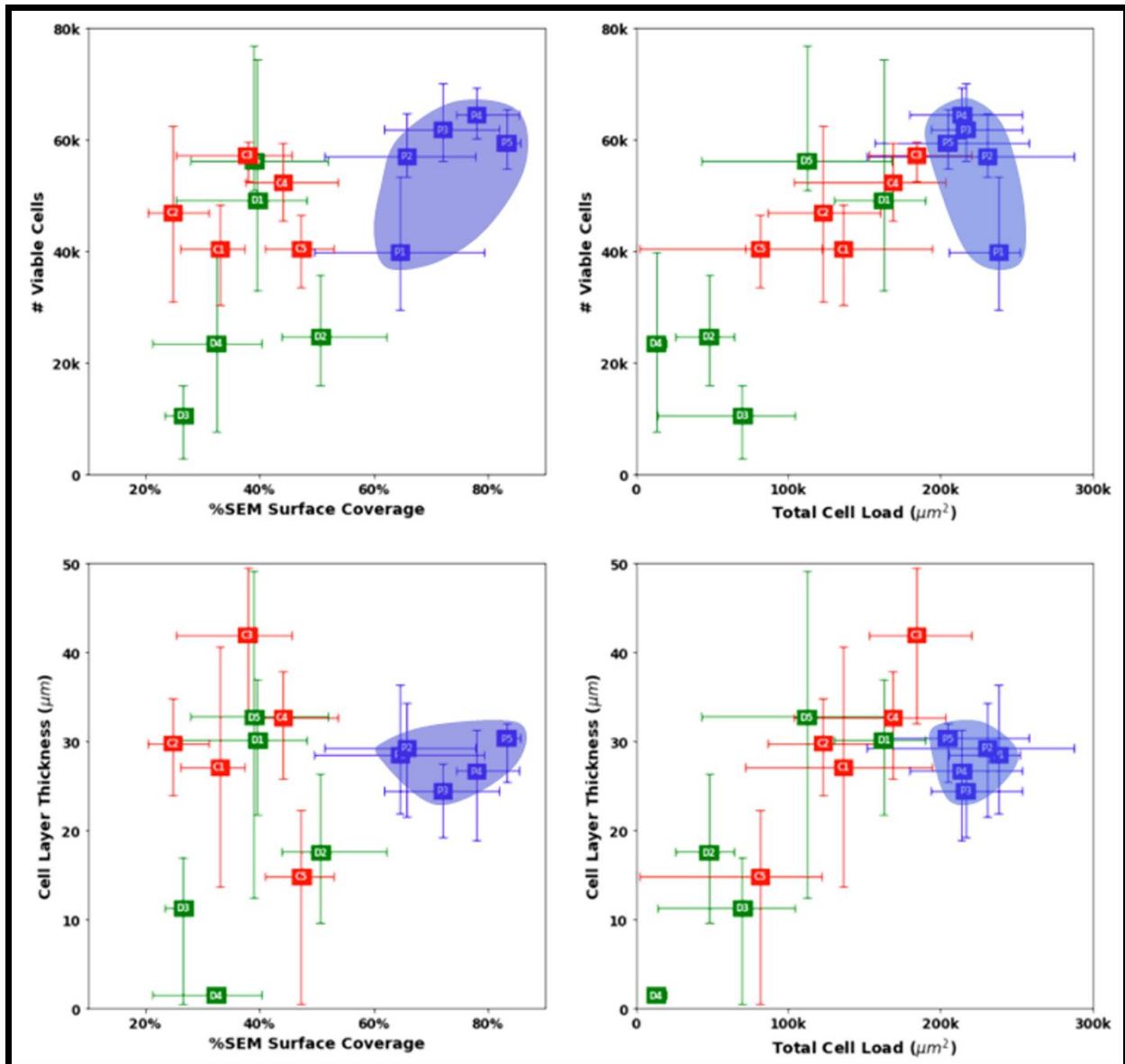
Figure 25. Scatter plots of combined data. The top left graph compares the average number of viable cells present on each scaffold section to the surface coverage determined with SEM analysis. The top right graph compares the number of viable cells and the cell load area as determined by H&E analysis. The bottom left graph compares the average cell layer thickness to SEM surface coverage and the bottom right graph compares cell layer thickness to cell load. Bioreactor mediated perfusion data is highlighted in blue..

3.3 Discussion

Automatic seeding within bioreactors has the benefit of limiting the manual handling of scaffolds, which in turn limits possible contamination scenarios. Due to this major benefit, it has been investigated repeatedly since its initial development in 1990 by Wildevuur and coworkers[146]. Originally, this method

was developed as a quick way to seed vascular grafts during the operating procedure at the patient's bedside. In one exploratory study by Noishiki et al., an 8 cm section of vasculature was finely minced and suspended in 20 ml of physiological saline solution. The resulting suspension was pushed transmurally through the lumen of a highly porous fabric scaffold via repeated pressurized injection[147]. After implantation in a canine model, it was reported that the grafts experienced increased thrombus formation; however, localization of cell types to their natural physiological locations was also observed and after 14 days the grafts were reported to be fully endothelialized. This result was initially promising, but the study failed to address the rapid transanastomotic endothelial outgrowth observed in animals, and the requirement of a sacrificial vessel fragment for the seeding does not reduce patient risk associated with multiple surgeries.

Since then, several groups have developed and employed other perfusion-based methods to create small diameter ETVGs. Feijen and co-workers have cannulated porous tubular polytrimethylene carbonate scaffolds with 3mm inner diameter in custom-made glass flow chambers and injected 20 ml of SMC cell suspension through their lumen[76,148]. The cell suspension was injected with two syringes, one positioned at either end of the scaffold. Scaffolds were manually rotated every 30-60 min during the first 2.5 hours after seeding to promote homogeneous cell adhesion, and cultured with either static or dynamic flow conditions up to 14 days. Cell presence after 7 days was observed transmurally throughout the bulk of the scaffold. However, a full analysis along the scaffold length or circumference was not demonstrated, so more detailed spatial distributions of cell seeding could not be determined. Furthermore, rotating after injection when dealing with thick, porous scaffolds, is counter intuitive, as a dense pore network may impede cell migration due to gravity. This is supported by the study observation that thicker scaffolds took a longer time to seed, suggesting the structure impeded cell movement within the scaffold thickness. If in fact the study achieved a homogenous circumferential distribution, it would be interesting to see if a similar result could be achieved without the rotation period.

Vorp and colleagues have developed and refined methods for seeding of vascular grafts that combine double injection filtration perfusion, vacuum perfusion and a rotational element concurrently[103,105].

59

Studies were conducted to examined the effectiveness of the seeding method on two distinct scaffold types [149]. One had small pore sizes and infiltration into the scaffold thickness was limited, while the other contained larger pores and allowed cellular infiltration. Cell distribution across the full length of the scaffold was investigated and found to be homogenous and viable in both cases. Furthermore in 2020, Cunnane et al. revised the system to accommodate grafts with lengths comparable to those used for human arterial replacement[106]. Instead of two syringes seeding the graft at both ends, a diffuser was inserted into the scaffold lumen. Over the course of the seeding period, the diffuser would translate across the graft length while dispensing cell suspension from the distal end. Results indicated that this method also achieved a uniform distribution both longitudinally and circumferentially with a scaffold six times the length of those in the previous study (12 cm vs 2 cm). While the results are overwhelmingly positive, the complexity of the seeding systems and experimental protocol limits further manipulation of the scaffold environment after seeding as well as limiting similar application to systems that attempt to culture more than one graft at a time.

Seeded scaffolds were evaluated longitudinally and circumferentially in terms of cell load, viability, cell layer thickness, and surface coverage distribution. BMP seeding resulted in comparable numbers of viable cells as static drip seeding and the SIC methods. However, the distribution of the cells present varied greatly between methods. Drip seeding onto the luminal surface resulted in high concentrations of cells at either end of the scaffold and very few in the middle, as expected. The SIC and BMP seeding had similar longitudinal cell distributions, but static injection resulted in 35% less circumferential coverage on average. Interestingly, our histology analysis revealed a more significant difference between BMP and static seeding methods in terms of cell load than suggested by the results obtained in our alamarBlue viability assay. We surmise that the histology washes may have washed away some of the cells present after static seeding. BMP seeding was seemingly unaffected by this possible phenomenon, leading us to believe that perfusion not only leads to better cellular coverage but also enhances cell attachment to our scaffolds.

Differences in apparent SMC morphology perceived from close inspection of the SEM images could be related with the phenotypic modulation of SMCs, which could change from synthetic to contractile if part of a large aggregate as seen in the denser regions of drip seeded and statically infused scaffolds. Contractile SMCs are elongated, spindle-shaped cells, whereas synthetic/proliferative SMCs are less elongated and have a cobblestone morphology[31]. However, SEM imaging is purely topographical and the boundary between cells can be difficult to define if cells form aggregates with multiple layers and have deposited ECM into the interstitial space between cells. In the bioreactor mediated perfusion seeding method, cells are distributed more homogenously and typically in a monolayer, with different degrees of sparsity, so it is easier to distinguish individual cells from one another. In the other static methods, cells would typically aggregate in a small region of the scaffold area which presents itself as a smooth surface with individual cells difficult to identify.

There are many limitations associated with the work presented here as there often are with ETVG-related experiments. To determine feasibility in the clinical setting, the system would need to be scaled up to the appropriate size. Vascular grafts for human CABG are typically 5 mm in diameter and 18 cm long resulting in an aspect ratio of 45, compared to the aspect ratio employed here, which is about $20^{150,151}$. Additional determinations of cell morphology, such as staining with vascular SMC contractile markers like alpha smooth muscle actin (α-SMA), smoothelin, or smooth muscle myosin heavy chain (SM-MHC) would provide more information towards determining how the seeding process may affect SMC phenotype and behavior relevant for the subsequent steps of in vitro culture. Furthermore, we have looked into additive agents that are used to prevent cell sedimentation in syringes and tubing, but none were used in this study, which may be considered an oversite when determining the effectiveness of our method. Additive agents in 3D culture media can be expensive, and there are a great number to choose from. We believe that the positive results obtained in this study are encouraging and promote the possibility of future studies to tailor those aspects to address a variety of problems.

Chapter 4

Development of dynamic culture capabilities and analysis methods.

Though the correlation between biophysical stimulation and increased ECM synthesis can readily be observed, the mechanism behind the interaction remains undefined. The response is undoubtably multichannel, a highly integrative collection of cellular pathways responding and influencing cell behavior at the microscopic scale. Studying the response of individual cells to the addition of molecules or mechanical strain to a system can reveal highly significant information, however, cellular behavior varies drastically between 2-D and 3-D constructs in vitro[152]. Progress in the field demands a highly controllable and consistent microenvironment to study how the effect of physiologically relevant mechanical stimulation translates to 3D ECM development and organization.

Huang, Niklason and coworkers investigated biaxial mechanical strain as previously mentioned [114]. In the bioreactor system, 3 ETVGs sheathing silicone tubing were seeded with bovine SMCs and cultured in parallel. One scaffold was used as a static control, experiencing no form of stimulation. The second was connected to a flow circuit that cyclically pumped PBS through the silicone tube in the ETVG lumen, facilitating the application of circumferential stretch. The third and final scaffold was also subjugated to circumferential stretch, but experienced additional application of axial stretch from an axially movable connector controlled by a linear motor. Prior to the application of stretch, all three scaffolds were cultured under static conditions for 1 week, then dynamic conditions were applied to the designated scaffold for a period up to 12 weeks. The axial strain applied to the biaxially developed ETVG was 8% and was maintained at a rate of 0.033 Hz for the duration of the culture period. Circumferential stretch application was added a week after axial. Both the uniaxial and biaxial ETVGs experienced a simulated pulse rate of

62

245 bpm and achieved circumferential strains up to 2% facilitated by the silicone tubing. After a period of 13 weeks, there was an obvious difference between the ETVGs.

Mechanical stretch resulted in thicker, stronger tissues, and the benefit of biaxial over uniaxial techniques was pronounced, especially when considering the significant increase in elastin content which contributed to increase compliance[153]. Further exploration revealed that not only the composition and mechanical properties were improved, but also the microstructural organization of the tissue. The ECM of biaxially developed ETVGs was extensive and highly organized, featuring mature elastin fibers. Collagen fibers experienced an orientation gradient transmurally through the scaffold thickness from circumferential orientation along the lumen to axial orientation along the adventitia. Collagen fibers also experienced a higher level of undulation, a feature relevant to native vasculature. When the elastin was removed in the constructs, the undulation of the collagen fibers decreased and the ETVG stiffened, suggesting that elastin functionally was also increased when ETVGs are subjected to biaxial stimulation. Mechanical mismatch between host arteries and ETVGs is thought to cause blood flow disturbances resulting in pathological tissue response and neointimal hyperplasia at the distal anastomosis. Higher graft compliance has a positive effect on graft patency, suggesting that grafts developed this way may reduce graft failure in vivo.

In this study, we sought to address the limitations of the first bioreactor design and further progress the system towards the reliable application of dual axial mechanical strain on mounted tubular constructs. The final iteration of the main bioreactor chamber was a 3-D printed construct that features 4 separate troughs for individual scaffold cultivation. Each scaffold is also on its own flow loop, eliminating possible crosstalk between samples and further limiting possible contamination scenarios. Tubes facilitating the transfer of cell media from bioreactor chamber to the reservoirs were placed on the secondary fast-moving pump while tubes feeding the ETVGs from the reservoirs were on the primary slower moving pump. This feature aided in reliable fluid level management in the bioreactor system, preventing possible overflow into neighboring troughs as well as reservoir emptying which introduces air into the scaffold lumen. The orientation of scaffold culture was shifted horizontally, to ease the application of axial stretch to the system.

Additionally, the process for cell loading was revised extensively (See Chapter 3). The fully defined design and experimental procedure is outlined in the following sections.

4.1 Bioreactor V2.1
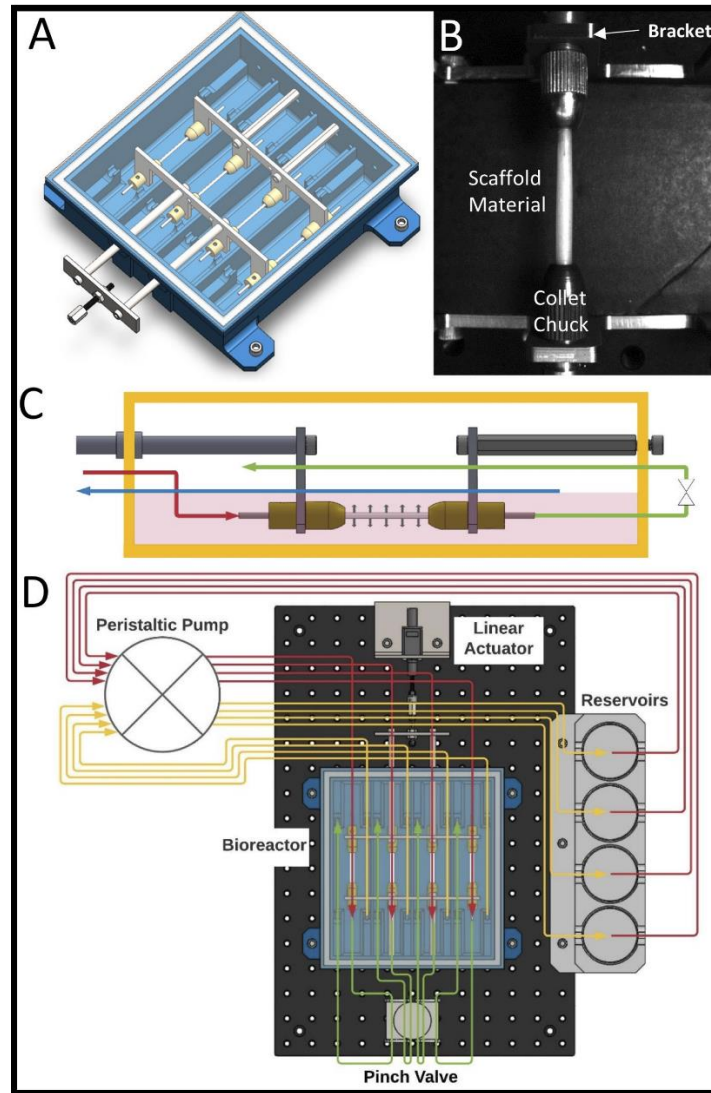
Figure 26. Bioreactor design. (A) The fully assembled bioreactor chamber. Intake and outtake tube holders are found on each side of the individual ETVG chambers. (B) An electrospun PCL tubular scaffold mounted with collet chucks in a four-pronged stainless-steel bracket. The 2mm cannulas affixed to either end of the scaffold form a tight seal with the tightened collet chucks. This connection makes tensile stretch and luminal pressurization possible while also leaving the lumen of the ETVG in direct contact with media flow. (C) Flow diagram within the bioreactor chamber. The red arrow shows media traveling from a reservoir to the ETVG lumen, the green arrow shows media movement out of the ETVG, out of the bioreactor, through the pinch valve, and back into the bioreactor. The blue arrow represents media being drawn from the bioreactor chamber to return to the reservoir. (D) Full schematic of bioreactor flow loop and intended features. Color coded as in panel C.

The bioreactor chamber (Fig 26A) was 3-D printed (Stratasys F170, Eden Prairie, MN) with a 13% infill using acrylonitrile butadiene styrene (ABS) with water-soluble QSR support material. The 3-D printed bioreactor chamber was coated with resin to prevent fluid leakage. The bioreactor was designed to seed-and-culture four tubular scaffolds in parallel channels (175 mm x 38 mm x 25 mm). The tubular scaffolds are fitted onto 2mm outer diameter stainless steel cannulas on each end such that 30mm of the graft length was available for seeding. Scaffolds were secured to the cannulas with parafilm and mounted into two 4 pronged brackets with collet chucks (Fig 26B). The brackets are fastened at a fixed distance apart keeping the 20 mm length of the scaffolds straight and unstressed. Once assembled, the mounting bracket was placed in the bioreactor chamber and the scaffolds connected to their individual flow paths through the cannulas.

4.2   Experimental Procedure

Robust experimental processes are important for systematic study. Here we outline the procedure for using the seed and culture bioreactor system. The activities are split up into days, however there can be periods of inactivity between the active days that span more than 24 hours depending on the experimental protocol and length of culture period. The described procedures can easily accommodate a variety of ETVG scaffolds and allow for easy manipulation of relevant culture parameters within a controlled environment to study the effects of mechanical conditioning on ETVG development.

4.2.1   Day 1

4.2.1.1   Bioreactor Sterilization

The bioreactor chamber is scrubbed thoroughly in warm soapy water and special attention is payed to crevices which like to harbor bacteria. Following a rinse in clean water, the bioreactor chamber is sterilized via immersion in 70% ethanol and placed in the BSC. The UV function of the BSC is used to further sterilize the bioreactor interior as it air dries. The bioreactor chamber can be stored in the BSC to maintain sterility until it is used.

The ETVG mounting bracket assembly is disassembled, and each piece thoroughly scrubbed with ultrafine steel wool and soap. Assembly pieces are rinsed once in clean water and once in 70% ethanol before being left to air dry. Components are packaged by order of assembly in sealable autoclave bags and subjected to 121 F for 30 minutes. Sterilized components can be stored in their bags indefinitely prior to use.

Bioreactor tubing remains connected in the culture flow loop following the end of an experiment. ETVG feeder tubes are connected to bioreactor drainage tubes after removal from the bioreactor chamber. The system is flushed by filling the culture reservoirs with warm soapy water and the tubes gently massaged to dislodge possible build up. The system is drained, rinsed with clean water, and drained again before 70% ethanol is allowed to run through the system uninterrupted for 1 hour. The tubing is then fully disassembled and allowed to dry. Cell reservoirs and extraneous pieces of tubing are washed separately following the same procedure but using a syringe to facilitate the rinsing. Flow loop components are packaged by order of assembly and autoclaved at 121 F for 30 minutes. Sterilized components can be stored in their bags indefinitely prior to use.

4.2.1.2 Scaffold Preparation

The following method is specific for use with electrospun PCL scaffolds. To reduce the hydrophobicity of the PCL material, processed scaffolds are submerged in 1M NaOH solution (pH = 12) for 4 hours. Scaffolds are then rinsed x3 via submersion in 10 ml of DI water and 5 minutes on the shaker. Following the DI rinses, scaffolds are placed into sterile test tubes and totally submerged in 70% ETOH over night to sterilize.

4.2.2 Day 2

4.2.2.1 Scaffold Mounting

In the biosafety cabinet, the bioreactor box tubing is assembled. This includes the ETVG feeder tubes, ETVG exit tubes, and bioreactor drainage tubes. The bioreactor drainage tubes are sealed off to prevent contamination access when not hooked into the full flow loop.
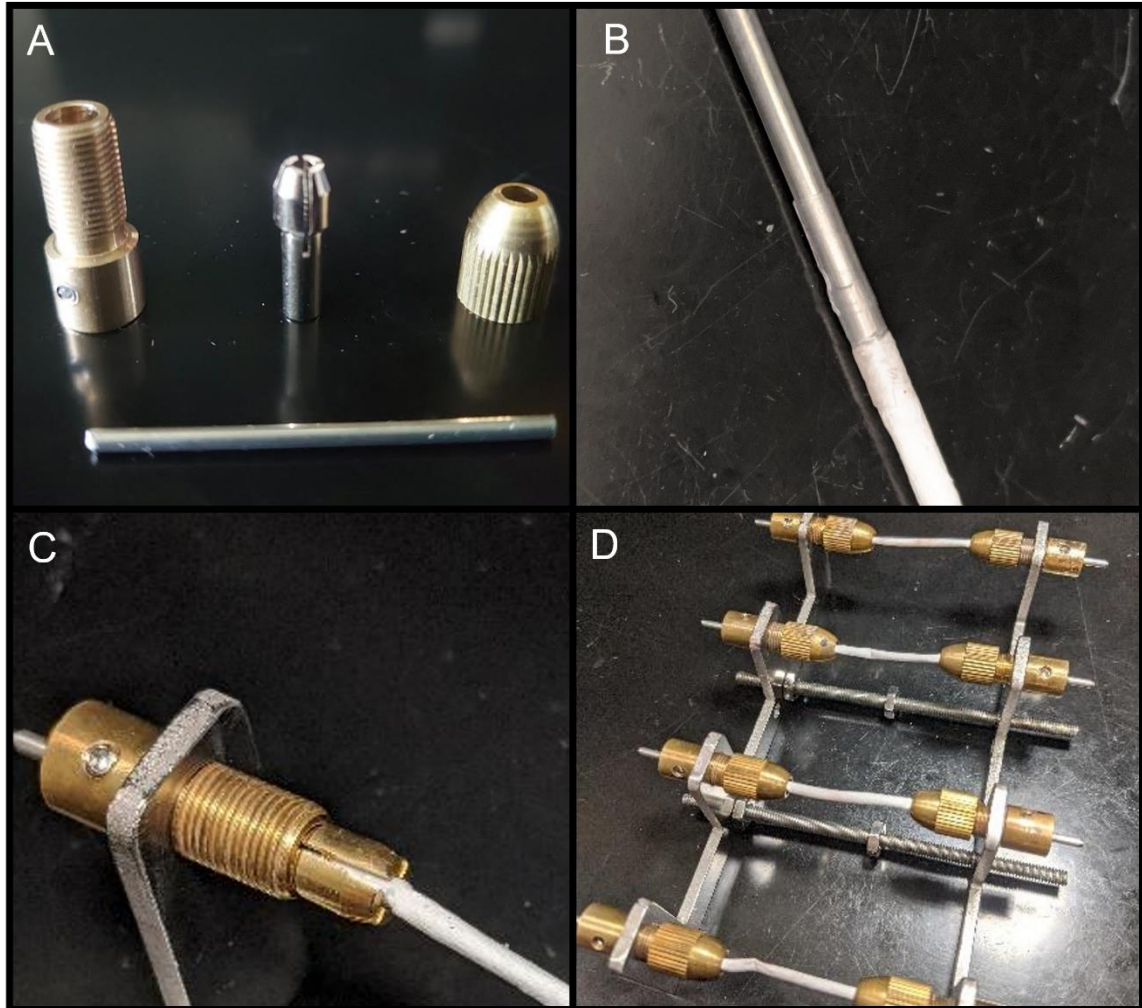
Figure 27. Mounting scaffolds into the bracket assembly. A) Scaffolds are fastened into the bracket assembly via a collet chuck assembly featuring a base, stainless steel collet, and a taper. B) The scaffolds are secured to the 2mm stainless steel cannulas, by tightly wrapping with parafilm. C) The collect is then slide into place on the cannula, with the front face planar to the end of the cannula and fastened into the base with set screws. The collet is then tightened via the taper screw, holding the scaffold securely in place. D) This process is repeated on the other side. Due to one end already being secured, the opposite taper screw needs to be gently slid over the scaffold material before collet placement.

Sterilized scaffolds are secured between 4 cm long metal cannulas via parafilm wrap (Fig 27 B). One of the four pronged brackets is secured into a specially designed mounting table, and a collet chuck base is screwed through each prong. One collet is slid into place, entrance parallel to the end of the cannula concealed within the scaffold material and parafilm wrap, for each scaffold (Fig 27 C). The collet is slid into its appropriate base and its position secured with set screws in the base. Then each collet is tightened by screwing on the taper. For each scaffold, the other taper is slid over the opposite cannula until it sits face to face with the first taper, then the second collet is slid into place on the opposite end, with its entrance parallel to the end of the second cannula hidden by the scaffold material. The whole construct is then very carefully manipulated to coax the remaining cannulas into the bases on the second 4 pronged bracket (Fig 27 D). The cannulas are fixed into the appropriate position via set screws and the collets are tightened by screwing on the tapers. The two brackets are fastened a fixed distance apart via threaded rods, and tubing connecters fixed to each cannula end to facilitate insertion into the bioreactor flow circuit. The proximal entrance of the ETVG is connected to the ETVG feeder tube, and the distal end is connected to the ETVG exit tube.

Figure 28. Comparison between the static and dynamic bioreactor chamber assemblies. The main difference between the static and dynamic bioreactor chambers correlates to the bracket assembly. In static culture, scaffolds are held at a fixed distance apart, so the only bracket attachment required is between the two brackets themselves (left). The dynamic assembly requires one bracket to be fixed in relation to the bioreactor wall, while the other can move in relation to the linear actuator positioned outside of the box. To achieve this affect, 2 linear motion bearings were set into the bioreactor wall to allow the passage of linear motion shafts (right).

For static culture, the rods fastening the 4 pronged brackets together are kept and the whole assembly simply placed into the static bioreactor box (Fig 28). However, scaffolds undergoing dynamic culture will be culture in the dynamic box. The dynamic box assembly features and additional step securing the distal 4 pronged bracket to the bioreactor box edge and the proximal 4 pronged bracket to linear shafts connected outside the bioreactor chamber by a bracket that facilitates connection to a linear actuator. Once the brackets are secured properly, the original rods connecting the 4 pronged brackets are removed and the system fit for dynamic culture.

4.2.2.2   Prewetting

A sterile 10 ml syringe is filled with 70% ethanol and connected to the ETVG feeder tube. The solution is pushed through the scaffold slowly to flush any final possible impurities from the assembly. An additional syringe filled with sterile PBS is flushed through the scaffold the same way. Following this step, the ETVG exit tube at the distal end of the bioreactor is clamped shut, and an additional syringe of sterile PBS flushed through the scaffold at a rate of 20ml an hour with a syringe pump. This step is repeated with an additional syringe of sterile PBS. Following this rinse, the excess fluid in the bioreactor is aspirated and a fresh syringe filled with full culture medium is connected to the ETVG feeder tube. The clamp on the ETVG exit tube is undone and the bioreactor exit tube is fully flushed with medium. Immediately following this the exit tubes are clamped again and the whole assembly placed into an incubator over night for scaffold prewetting.

4.2.3   Day 3

4.2.3.1   ETVG Seeding

Day 3 is seeding day. Cell seeding onto the scaffold is fully characterized in CH3 and Publication reference.

4.2.4   Day 4

4.2.4.1   Static Culture

After the seeding period, the 4 ETVGs within the bioreactor are switched into culture mode each with their own independent flow loops. For static culture, the switch is relatively simple because the only requirement is insertion into the bioreactor flow loop. The bioreactor flow loop is primed by connecting the tube destined for the ETVG feeder connection and the tube destine for bioreactor draining, filling the media reservoir with full culture medium and using the peristalitic pump to drive flow though the tubes, priming the system. Clamps are used to seal the feeder tube and the drainage tube prior to their disconnection. Once disconnected, the tubes are fastened to the appropriate ports on the bioreactor box and the system is ready for slow flow static culture.

Culture medium is drawn from the media reservoir with a peristaltic pump, and pushed through the ETVG lumen, and returned to the ETVG chamber. For fluid level balancing in each ETVG system, an additional flow line draws media from the bioreactor chamber back to the media reservoir. The intake and outtake tubes are located at opposite ends of the ETVG chamber, facilitating gentle media flow around the outer surface of the scaffold during culture.

4.2.4.2   Dynamic Culture

For dynamic culture, the bioreactor box with specialized bracket connections is fastened into the specially design dynamic breadboard featuring a linear actuator (Fig 29 B), 4 pressure sensor connections (Fig 29 C), and 4 parallel pinch valves (Fig 29 D). The bioreactor chamber is hooked into the flow system as previously described. The box is placed onto the dynamic breadboard, and the linear shaft connecting bracket slid into place on the linear actuator shaft and secured with a stainless-steel nut. The base of the bioreactor chamber is then secured to the dynamic breadboard in each corner by 4 screws. The ETVG exit tubes are securing into the pinch valve chamber, and pressure sensors plugged into their appropriate ports. Additionally, a single Texas Instruments data acquisition board controls all the electronic components of the bioreactor.
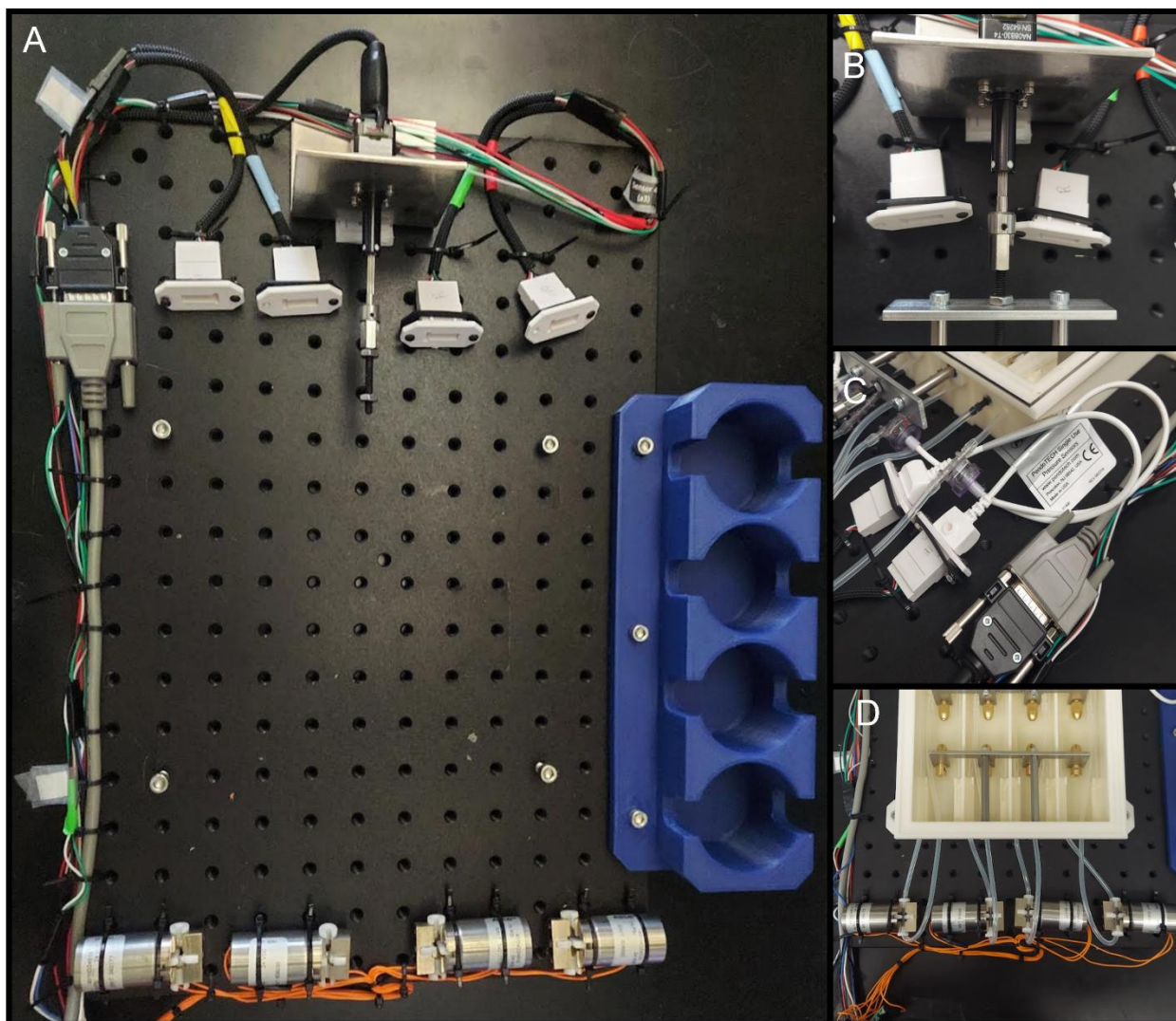
Figure 29. Dynamic culture components. A) The fully assembled dynamic breadboard. Four screws denote intended bioreactor placement. Demonstrations of connections to the actuator (B), pressure sensors (C), and pinch valves (D) are also shown.

4.2.5 Day 5

4.2.5.2 Media Switch

Once a week following the start of slow flow static culture, the media will need to be replace in the bioreactor system. This process is begun by turning the peristatic pump facilitating bioreactor draining of and allowing the reservoirs to drain nearly completely into the bioreactor chamber. Media is then aspirated from the bioreactor chamber, and the reservoirs filled with 100 ml of fresh culture medium, warmed to 37

in the hot water bath. The entire system is returned to the incubator and connected back to the peristatic pumps to resume normal culture conditions.

4.2.5.3   Dynamic Programming

A custom user interface was developed to control the bioreactor system in LabView (Fig 30). The user can adjust all inputs to control the pump velocity, axial stretch, max pressure, time to hold pressure, number of cycles, etc. The fine control over these parameters allows for future experimentation with different mechanical stimulation procedures on the scaffolds. Base controls of the program included the ability to remotely turn the pump on at a desired speed. This is useful to prime the bioreactor system with media prior to culture start and remove bubbles that may interfere with pressure measurements. You also have the ability to control the pinch valve to open and close remotely and tare the pressure sensors. Initial actuator position can also be set before starting an experiment. It is important to note that the number designated to move the bioreactor is in relation to its absolute position, not its current position. The program facilitates the recording of data to any text file designated by the file path, and the sampling rate can also be defined.

Experimentally the program allows you to exert influence over the mechanical conditioning regimen in the follow order. At $t = 0$, the parameter you dictate is pump velocity, which is the default value the pump will take if it is turned on. The length of time the pump is held at this speed without the addition of stimulation can also be dictated. The next phase incorporates graft pressurization with controls over pump velocity 2, the speed for pressure buildup, and the period of pressurization by closure of the pinch valve. Pressure can be held for a specified time, which the program facilitates by turning the pump off while keeping the pinch valve closed. This step is critical for evaluating possible ETVG leakage, signaled by decreasing pressure during this period. At the end of the specified time the pinch valve is released and flow allowed to resume. The next phase incorporates axial stretch with dictated strain and hold period. Axial strain and circumferential pressurization cannot be exerted concurrently by the program unless a significant is place on the ETVGs through setting of the initial actuator position. The cycle switches back and forth

72

between circumferential and axial stimulation, but either phase may be programmed to repeat a set number of times in their block. Also, a wait period can be established between each action. The bioreactor program can be run indefinitely in theory, but we suggest that stimulation be applied periodically, over periods of 6 hours or less, in order to reduce stress on electrical components.
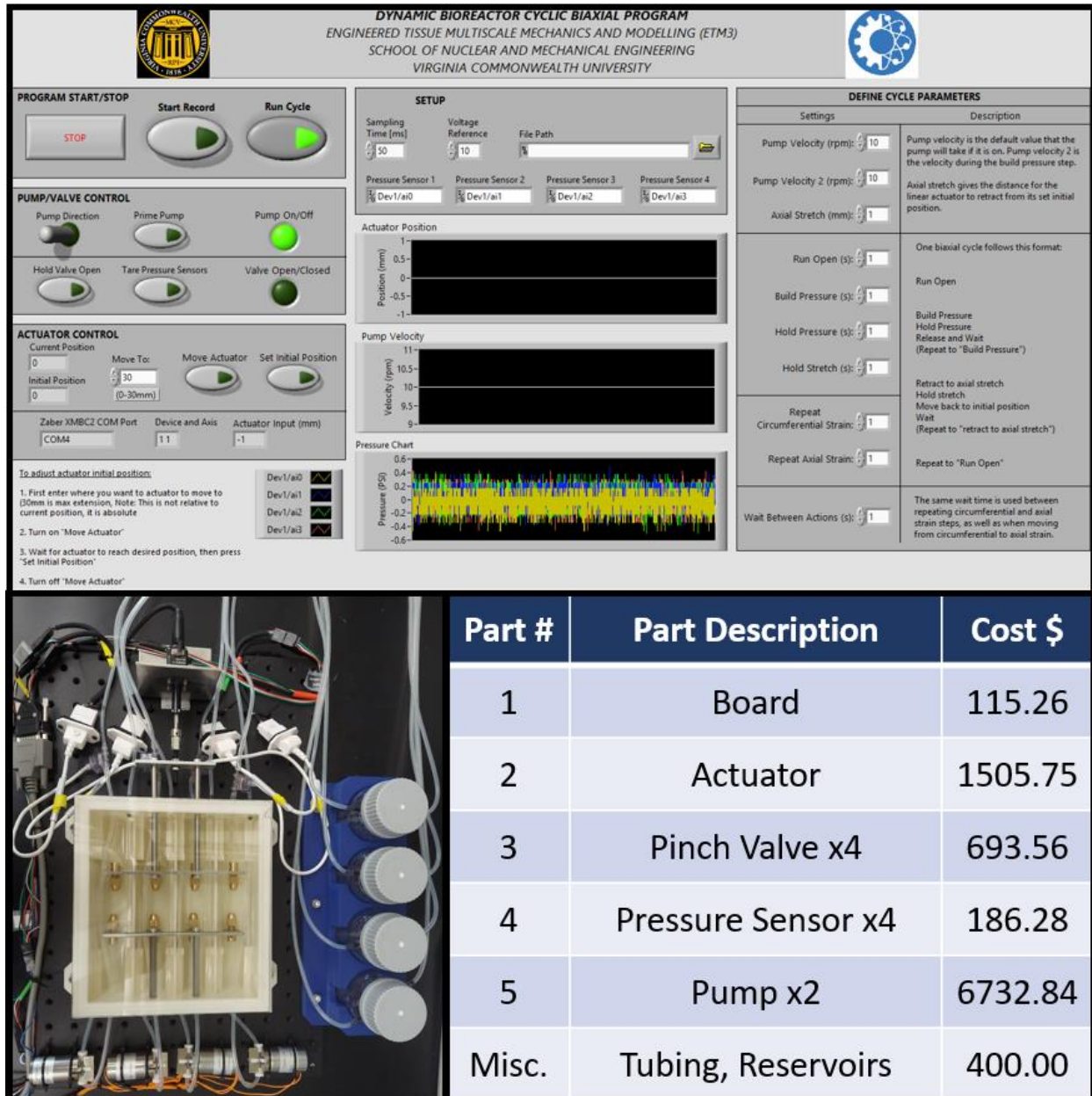
Figure 30. Programming dynamic culture. The LabVIEW interface (top) can be used to dictate the period, magnitude and pattern of circumferential and axial stimulation. Each of the dynamic culture components (bottom) can also be controlled individually via DAQ board connection.

4.3   Biaxial Mechanical Tester

Determination of the mechanical properties of cultured ETVGs is an essential part of future studies evaluating the effect of mechanical strain on tissue development. A custom designed biaxial mechanical tester was created for this purpose and has been a useful tool for testing the conditioning programming capabilities of the bioreactor.

4.3.1   Biaxial Mechanical Tester Assembly

The biaxial tester assembly can facilitate mechanical property measurements both in open air and submerged in liquid through a custom-designed 3D printed mounting stage (Fig 31). When recording measurements of submerged scaffolds, it is essential that the camera is recording through a window in direct contact with the medium to prevent possible image distortion. The design features a clear, bottom panel and lifted stage such that the camera may be mounted to record from the bottom of the assembly.
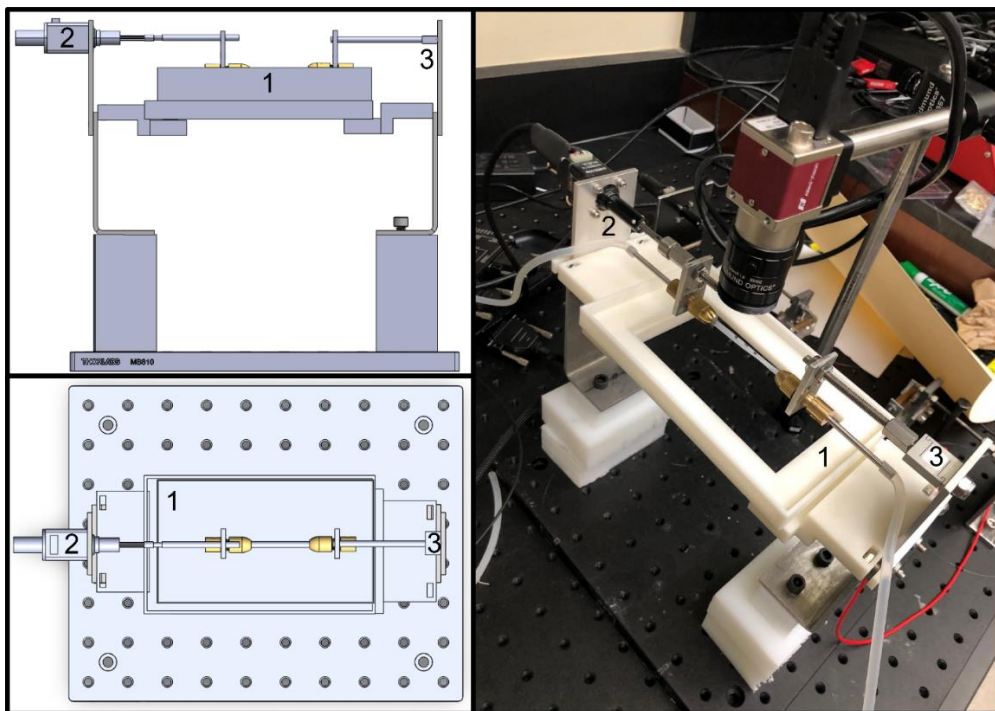
Figure 31. Biaxial mechanical tester. The center box (1) houses mounted scaffolds. The center box may be modified to hold the scaffold submerged underwater. The bottom of the box is clear plastic to facilitate

camera viewing from the bottom. A linear actuator (2) mounted via support brackets provide axial stretch. The system is composed of a peristaltic pump, load sensor (3), and pressure sensor downstream.

Measurements of circumferential hydrostatic pressure is facilitated by an in-line pressure sensor located at the distal end of the scaffold in relation to flow. Pressure is applied via the closing of a pinch valve at the distal end of the pressure sensor. Measurements of tensile force exerted by the actuator at the proximal bracket are facilitated by a load cell fastened to the distal bracket.

4.3.2   Geometry and Stress Calculations
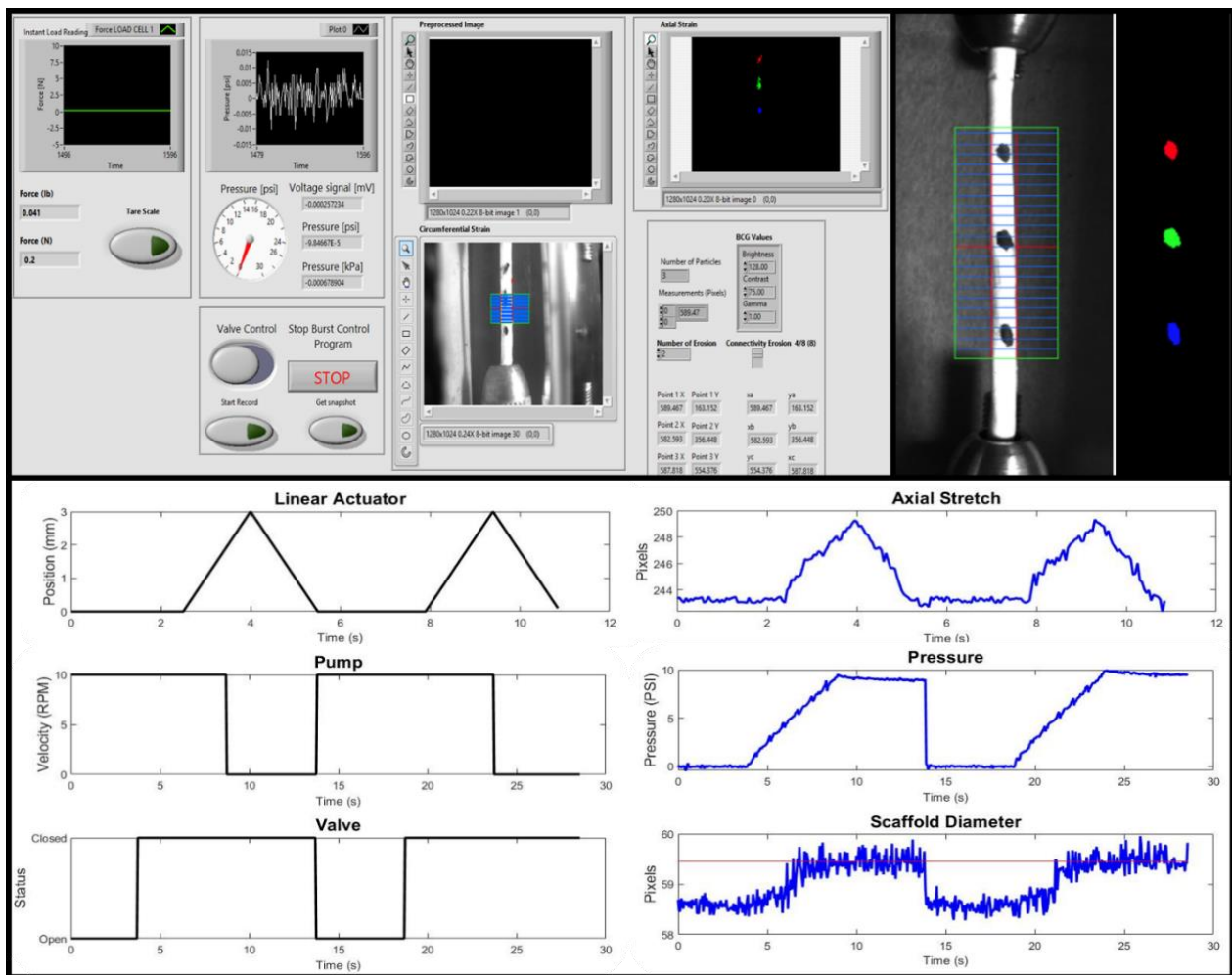
Figure 32. Geometry monitoring. Scaffolds mounted in the biaxial mechanical tester system are evaluated by tracking the change in diameter and distance between three markings place on the scaffold surface via LabVIEW monitoring software (top). The biaxial mechanical tester is a useful to for evaluating possible dynamic culture conditions. Silicone tubes were mounted in the tester and subjected to conditioning cycles similar to those programmed by the dynamic bioreactor. Measurements corresponded to the activation of dynamic components.

A computer vision program was implemented for tracking the circumferential and axial strain response of the scaffolds (Fig 32). Grayscale-based edge tracking of the scaffold reports changes in the diameter. For the axial component, three dots are drawn on the scaffolds and the distances between them are used to detect stretch on the scaffold. The computer vision measurement system was capable of recording deformations less than 0.1mm in the scaffolds. Camera measurements are compared to measurements of tensile force and hydrostatic pressure to determine the stress experienced by the material and the material stiffness.

4.4   Discussion

Before the success of Huang and coworkers, a bioreactor for the biaxial mechanical stimulation of vascular constructs was developed by Mironov and colleagues[154]. The design supported the recording of diameter and pressure during culture with the incorporation of a camera and pressure transducers and is one of the earliest documented attempts at applying axial strain to arterial constructs. Zaucha and colleagues later developed a more sophisticated version featuring a computer-controlled bioreactor and biomechanical testing system capable of (i) enabling simultaneous and independent control of circumferential pressure and axial load on TEVs; and (ii) performing biaxial mechanical testing on the same vessel at multiple time-points in culture. Additionally, a multi-photon microscope was incorporated to facilitate real time imaging of active ECM synthesis and organization within the bioreactor under a variety of loading conditions[155]. The bioreactor proved to be a thorough tool for the study of ETVG development, however due to the system's complexity only one vessel could be cultured and examined at a time. Additionally, the cost associated with such high-definition monitoring equipment is significant. Commercially made bioreactors such as the Bose ElectroForce BioDynamic Test Instrument and the Tissue Growth Tech LumeGen Bioreactor are designed to conduct mechanical testing on vascular constructs have been developed, however such systems were not developed with ETVG manufacturing in mind and the cost is often prohibitive.

To our knowledge, the bioreactor system presented here is the first to be developed that incorporates semi-automated cell seeding and subsequent culture in a system conducive to the application of biaxial mechanical stimulation on four small diameter tubular scaffolds simultaneously and independently. To culture multiple ETVGs in parallel greatly increases experimental through put, facilitating rapid progress in the field. The variety of conditioning regimens that can be facilitated by the system combined with its ability to adapt to scaffolds of different lengths, diameters, and structures make it a versatile and cost-effective tool for the rapid study of ETVG development under the influence of mechanical forces. The plug and play nature of the bioreactor chamber simplifies the design and reduces cost. The ability to conduct tissue engineering experiments in a cost- and resource-effective experimental program is crucial to refine methods and obtain reproducible and statistically reliable data to provide a better mechanistic understanding of engineered tissue growth and remodeling during its in vitro incubation stage.
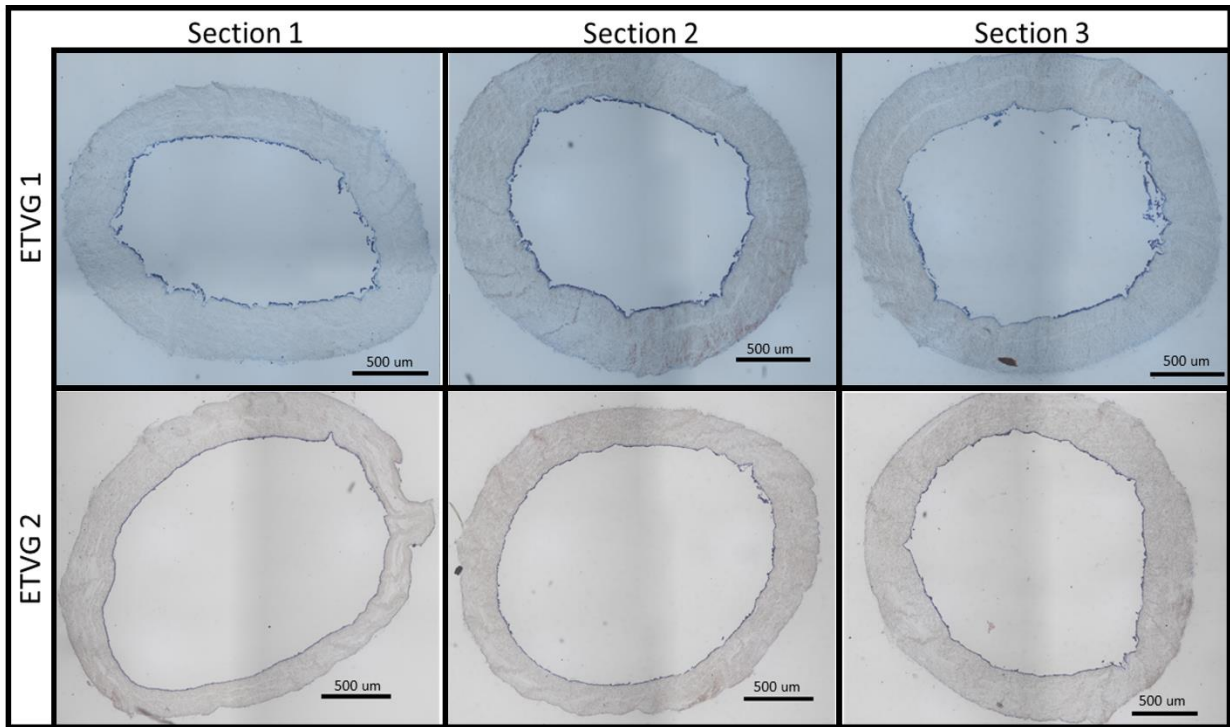

Figure 33. Initial results of in vitro culture using the bioreactor system. Scaffolds were seeded as previously described and allowed to rest for two days before hooked into the culture flow loop. ETVGs pictured experienced 3 days of slow flow through the lumen. Circumferential distribution of cells was improved over the 24 hr time points previously evaluated.

Electrospun PCL scaffolds seeded with rat vascular smooth muscle cells have been successfully cultured in the bioreactor for a period of 5 days without becoming contaminated (Fig 33). On the second day, the system was exposed to slow flow of approximately 2 ml/min. Initial histology revealed ETVGs developed improved surface coverage when compared to samples 24 hours after seeding, as described in Chapter 3. This suggests that cell adhesion to the scaffold is strong enough to with stand mild shear stress exposure, which is a promising initial result. The protocol needs to be optimized in terms of how long tissue is allowed to develop before external forces are applied. Starting dynamic conditioning too early can result in scaffold leaking due to insufficient tissue development and dislodging of developing tissue from the scaffold. Following continued experiments characterizing the basic effects of mechanical stimulation on ETVG development, running experiments with different scaffold types to see if experimental application and results are conserved would strengthen the study considerably. One area of concern is pump placement in relation to the bioreactor. Tubes linking the bioreactor chamber to the reservoirs run out of the incubator and through a peristatic pump before returning. Cooling of media due to this exposure has resulted in increased condensation on the lid of the bioreactor box, which eventually redistributes the fluid between ETVG flow loops. During periods of extended ETVG culture, this is combated by insulating the tubes outside of the incubator. Moving the pumps into the incubator would eliminate this effect, but the size of the pumps in relation to the incubator limit the feasibility of this option. Possible solutions include buying a different pump or a larger incubator.

The biaxial tester uses methods similar to other biaxial mechanical testing systems to determine axial and circumferential strain, further validating our adoption of the method[129,155]. Ultimately, combining the two systems would allow for real time monitoring of mechanical properties providing valuable insight into the stages of ETVG development. Until then, the current tester needs to be modified to accommodate specimens of native vasculature. Physiological specimens can be notoriously difficult to hold for mechanical testing applications, often requiring some sort of suture or treatment that hardens a section of

tissue, making it easier to grip. Testing the mechanical properties of native vessels provides target values

for ETVG development.

Chapter 5

Conclusion and Future Work

Overall, there is a trend in the field of tissue engineering to bridge the past 50 years of empirically-based trial-and error experimentation towards a rational approach based on engineering principles and critical reasoning[90]. Developing a thorough understanding of the underlying structural and mechanical factors responsible for the formation and maturation of functional ECM structures remains elusive, but significant progress is being made in characterizing the macroscopic effects of multiaxial mechanical loading in 3D tissue development.

The methods outline in each chapter of this dissertation describe a pipeline for the evaluation of the effects of mechanical conditioning on ETVG microstructure, stiffness, mechanical properties and patency. Bioreactors are a premier tool for studying the effects of environmental stimuli on ECM remodeling and ETVG development. The concurrent development of 4 ETVGs under identical conditions is a novel concept which will facilitate a quicker rate of discovery in the field. Additionally, carefully developed user interfaces mediate the easy programming of mechanical conditioning regimens with a high degree of specificity. Finally, due to the design simplicity and the primary use of generic parts, the described bioreactor can be modified to accommodate grafts of different sizes and structures relatively hassle free. The development of this vital tool not only marks the transition of vascular tissue engineering from a field of empirical discovery to one of systematic characterization but contributes significantly towards progress in the field.

5.1 Dynamic Conditioning Characterization

While studies similar to ours have revealed the paramount importance of vascular mechanotransduction, they do not achieve actual quantification due to the fact that they focus on single level conditions – i.e., no stretch vs. a single level of stretch. With the bioreactor we can begin to evaluate the extent mechanical stimulation can be utilized to affect ETVG properties. Our hypothesis is that different levels of strain magnitude and frequency will result in ETVGs of varying microstructural and mechanical properties. By fine tuning the relevant range of mechanical stimulation for ETVGs we can save time and resources in future experiments.

The bioreactor will also be modified to conduct hands free, non-destructive testing of mechanical properties during culture so we can measure the response to mechanical conditioning in real time. Intermittent biomechanical testing in combination with detailed structural analysis will allow us to gain further insights into both microstructure influence on tissue level biomechanics as well as constituent production, removal and reorganization in response to mechanical stimuli.

5.2 Characterization of Foreign Body Response in vivo

The ultimate goal is to be able to predict the in vivo response to ETVGs with different properties. The implantation of a biomaterial into the body initiates a foreign body reaction. This begins with protein absorption and acute inflammation, then typically chronic inflammation, and in some cases leads to granulation tissue formation[156,157]. Several different factors including extent of the injury created with the implantation, biomaterial chemical composition, surface free energy, surface charge, porosity, roughness, and implant size and shape have been indicated to have a role in the duration and extent of each step and still a lot of research is being performed to better understand this response[158].

The duality between fully functional tissue regeneration vs. pathobiological fibrotic repair is dependent on a multi-phased cascade involving the cause-effect interplay between implant properties, host reactions, and their modulation with controllable parameters[158,159]. ETVGs should be designed not to

diminish host responses, but instead, to trigger desired immunological responses and therefore enable their integration and subsequent growth and remodeling. Using the body's own mechanisms to continue ETVG development in vivo lessens the need for outside involvement such as immunosuppressant drugs and additional surgeries[160]. Developing a detailed understanding of this response through systematic experiments will provide guidelines to achieve cell and tissue homeostasis quickly, while preventing maladaptive tissue formation.

5.3   Simulating culture environments for improved outcomes

This experimental device promises to provide new insights towards mechanically induced growth and remodeling of TEBVs. Using experimental results, theoretical models can be developed to mathematically describe these complex processes. Studies with validated mathematical models have the advantage over experimental research in that individual parameters can be altered to understand how these individual components affect the overall function. In addition, the time and cost savings using mathematical models makes them significantly more valuable.

References

1.   Mensah GA, Brown DW. An overview of cardiovascular disease burden in the United States. *Health Affairs*. 2007;26(1):38–48.

2.   Haimov H, Giron F, Jacobson JH. The Expanded Polytetrafluoroethylene Graft: Three Years' Experience with 362 Grafts. *Archives of Surgery*. 1979;114(6):673–677.

3.   De Bakey ME, Jordan GL, Abbott JP, Halpert B, O'neal RM. The Fate of Dacron Vascular Grafts. *Archives of Surgery*. 1964;89(5):755–782.

4.   Chester JF. The causes of synthetic vascular graft failure. *Annals of the College of Surgeons of Hong Kong*. 2002;6(4):97–101.

5.   Goldman S, Zadina K, Moritz T, Ovitt T, Sethi G, Copeland JG, Thottapurathu L, Krasnicka B, Ellis N, Anderson RJ, Henderson W. Long-term patency of saphenous vein and left internal mammary artery grafts after coronary artery bypass surgery: Results from a Department of Veterans Affairs Cooperative Study. *Journal of the American College of Cardiology*. 2004;44(11):2149–2156.

6.   Marasco S. Total Arterial Revascularization. *Operative Techniques in Thoracic and Cardiovascular Surgery*. 2016;21(1):20–30.

7.   Hayatsu Y, Ruel M, Sun LY. Renal insufficiency and severe coronary artery disease: Should coronary artery bypass grafting, off-pump coronary artery bypass grafting or percutaneous coronary intervention be performed? *Current Opinion in Cardiology*. 2019;34(6):645–649.

8.   Rehman ZU, Riaz A, Nazir Z. Peripheral Arterial Injuries in Children: An Audit at a University Hospital in Developing Country. *Annals of Vascular Diseases*. 2020;13(2):158–162.

9. Morão S, Ferreira RS, Camacho N, Vital VP, Pascoal J, Ferreira ME, Capitão LM, Gonçalves FB. Vascular Trauma in Children—Review from a Major Paediatric Center. *Annals of Vascular Surgery*. 2018;49(February):229–233.

10. Baram A, Ahmad BJ, Izac AY, Falah F, Sherzad H. Pediatric vascular reconstruction after trauma and malignancy; a single centere case series. *International Journal of Surgery Open*. 2021;36:2–7.

11. Lord JW, Sadranagani B, Bajwa G, Rossi G. New technique for construction of composite dacron vein grafts for femoro distal popliteal bypass in the severely ischemic leg. *Annals of Surgery*. 1975;181(5):670–675.

12. Pashneh-Tala S, MacNeil S, Claeyssens F. The tissue-engineered vascular graft - Past, present, and future. *Tissue Engineering - Part B: Reviews*. 2016;22(1):68–100.

13. Li S, Henry JJD. Nonthrombogenic approaches to cardiovascular bioengineering. *Annual Review of Biomedical Engineering*. 2011;13(1):451–475.

14. Peck M, Gebhart D, Dusserre N, McAllister TN, L'Heureux N. The evolution of vascular tissue engineering and current state of the art. *Cells Tissues Organs*. 2011;195(1–2):144–158.

15. Standring S, Gray H. *Gray's anatomy : the anatomical basis of clinical practice*. Elsevier; 2021.

16. Chamley JH, Gröschel-Stewart U, Campbell GR, Burnstock G. Distinction between smooth muscle, fibroblasts and endothelial cells in culture by the use of fluoresceinated antibodies against smooth muscle actin. *Cell and Tissue Research*. 1977;177(4):445–457.

17. Radke D, Jia W, Sharma D, Fena K, Wang G, Goldman J, Zhao F. Tissue Engineering at the Blood-Contacting Surface: A Review of Challenges and Strategies in Vascular Graft Development. *Advanced Healthcare Materials*. 2018;7(15):1–24.

18. Larsen M, Artym V V., Green JA, Yamada KM. The matrix reorganized: extracellular matrix remodeling and integrin signaling. *Current Opinion in Cell Biology*. 2006;18(5):463–471.

19.   Mozafari H, Zhou C, Gu L. Mechanical contribution of vascular smooth muscle cells in the tunica media of artery. *Nanotechnology Reviews*. 2019;8(1):50–60.

20.   O'Connell MK, Murthy S, Phan S, Xu C, Buchanan JA, Spilker R, Dalman RL, Zarins CK, Denk W, Taylor CA. The three-dimensional micro- and nanostructure of the aortic medial lamellar unit measured using 3D confocal and electron microscopy imaging. *Matrix Biology*. 2008;27(3):171–181.

21.   Bou-Gharios G, Ponticos M, Rajkumar V, Abraham D. Extra-cellular matrix in vascular networks. *Cell Proliferation*. 2004;37(3):207–220.

22.   Leloup AJA, Van Hove CE, Heykers A, Schrijvers DM, De Meyer GRY, Fransen P. Elastic and muscular arteries differ in structure, basal NO production and voltage-gated Ca2+-channels. *Frontiers in Physiology*. 2015;6(DEC):1–9.

23.   Bellmunt-Montoya S, Escribano JM. Vein diameter and vein surgery. *European Journal of Vascular and Endovascular Surgery*. 2019;57(6):858.

24.   Shadwick RE. Mechanical design in arteries. *Journal of Experimental Biology*. 1999;202(23):3305–3313.

25.   CB W, DW G, JFR P, DJ C. A New Radically Improved Model of the Circulation With Important Clinical Implications. *American Journal of Surgery and Clinical Case Reports*. 2020;2(06).

26.   Rocha R V., Tam DY, Karkhanis R, Nedadur R, Fang J, Tu J V., Gaudino M, Royse A, Fremes SE. Multiple arterial grafting is associated with better outcomes for coronary artery bypass grafting patients. *Circulation*. 2018;138(19):2081–2090.

27.   Humphrey JD. Vascular adaptation and mechanical homeostasis at tissue, cellular, and sub-cellular levels. *Cell Biochemistry and Biophysics*. 2008;50(2):53–78.

28.   Valdez-Jasso D, Bia D, Zocalo Y, Armentano RL, Haider MA, Olufsen MS. Linear and Nonlinear

Viscoelastic Modeling of Aorta and Carotid Pressure-Area Dynamics under in vivo and ex vivo Conditions. *Annals of Biomedical Engineering*. 2011;39(5):1438–1456.

29.   Silver FH, Horvath I, Foran DJ. Viscoelasticity of the vessel wall: The role of collagen and elastic fibers. *Critical Reviews in Biomedical Engineering*. 2001;29(3):279–301.

30.   Qiu J, Zheng Y, Hu J, Liao D, Gregersen H, Deng X, Fan Y, Wang G. Biomechanical regulation of vascular smooth muscle cell functions: From in vitro to in vivo understanding. *Journal of the Royal Society Interface*. 2014;11(90).

31.   Rensen SSM, Doevendans PAFM, Van Eys GJJM. Regulation and characteristics of vascular smooth muscle cell phenotypic diversity. *Netherlands Heart Journal*. 2007;15(3):100–108.

32.   Feil S, Fehrenbacher B, Lukowski R, Essmann F, Schulze-Osthoff K, Schaller M, Feil R. Transdifferentiation of vascular smooth muscle cells to macrophage-like cells during atherogenesis. *Circulation Research*. 2014;115(7):662–667.

33.   Birukov KG, Shirinsky VP, Stepanova O V., Tkachuk VA, Hahn AWA, Resink TJ, Smirnov VN. Stretch affects phenotype and proliferation of vascular smooth muscle cells. *Molecular and Cellular Biochemistry*. 1995;144(2):131–139.

34.   Thyberg J, Blomgren K, Roy J, Tran PK, Hedin U. Phenotypic modulation of smooth muscle cells after arterial injury is associated with changes in the distribution of laminin and fibronectin. *Journal of Histochemistry and Cytochemistry*. 1997;45(6):837–846.

35.   Wong JY, Velasco A, Rajagopalan P, Pham Q. Directed movement of vascular smooth muscle cells on gradient-compliant hydrogels. *Langmuir*. 2003;19(5):1908–1913.

36.   Sazonova O V., Isenberg BC, Herrmann J, Lee KL, Purwada A, Valentine AD, Buczek-Thomas JA, Wong JY, Nugent MA. Extracellular matrix presentation modulates vascular smooth muscle cell mechanotransduction. *Matrix Biology*. 2015;41:36–43.

37. Shyy JYJ, Chien S. Role of integrins in cellular responses to mechanical stress and adhesion. *Current Opinion in Cell Biology*. 1997;9(5):707–713.

38. Kim BS, Nikolovski J, Bonadio J, Mooney DJ. Cyclic mechanical strain regulates the development of engineered smooth muscle tissue. *Nature Biotechnology*. 1999;17(10):979–983.

39. Leight JL, Wozniak MA, Chen S, Lynch ML, Chen CS. Matrix rigidity regulates a switch between TGF-β1-induced apoptosis and epithelial-mesenchymal transition. *Molecular Biology of the Cell*. 2012;23(5):781–791.

40. Gimbrone MA, García-Cardeña G. Endothelial Cell Dysfunction and the Pathobiology of Atherosclerosis. *Circulation Research*. 2016;118(4):620–636.

41. Bulick AS, Muñoz-Pinto DJ, Qu X, Mani M, Cristancho D, Urban M, Hahn MS. Impact of endothelial cells and mechanical conditioning on smooth muscle cell extracellular matrix production and differentiation. *Tissue Engineering - Part A*. 2009;15(4):815–825.

42. Bhatt DL. Percutaneous coronary intervention in 2018. *JAMA - Journal of the American Medical Association*. 2018;319(20):2127–2128.

43. Doenst T, Haverich A, Serruys P, Bonow RO, Kappetein P, Falk V, Velazquez E, Diegeler A, Sigusch H. PCI and CABG for Treating Stable Coronary Artery Disease: JACC Review Topic of the Week. *Journal of the American College of Cardiology*. 2019;73(8):964–976.

44. Kraeger RR, Lagos JA, Barner HB. Long term evaluation of allogenic veins as arterial grafts. *Vascular and Endovascular Surgery*. 1976;10(2):121–127.

45. Carpenter EW, Lindenauer SM. Immunosuppression in Arterial and Venous Allografts. *Archives of Surgery*. 1973;106(1):75–78.

46. Bortolotti U, Casarotto D, Frugoni C. Coronary artery bypass with glycerol-preserved saphenous vein allografts. *Cardiovascular Diseases*. 1981;8(2):250–258.

47. Drezner AD, Turner RJ. Technical Requirements for a Successful Human Umbilical Vein Implant. *Vascular and Endovascular Surgery*. 1980;14(3):158–167.

48. Dardik H, Dardik II. Successful arterial substitution with modified human umbilical vein. *Annals of Surgery*. 1976;183(3):252–258.

49. Rubio PA, Farrell EM. Maintenance Hemodialysis With Modified Human Umbilical Vein Graft Angioaccess. *Vascular and Endovascular Surgery*. 1980;14(3):186–191.

50. Aalders GJ, van Vroonhoven TJMV. Polytetrafluoroethylene versus human umbilical vein in above-knee femoropopliteal bypass: Six-year results of a randomized clinical trial. *Journal of Vascular Surgery*. 1992;16(6):816–824.

51. Silver GM, Katske GE. Clinical Experiences with the Stabilized Human Umbilical Vein in Coronary Bypass Surgery. *Vascular and Endovascular Surgery*. 1980;14(3):192–196.

52. Silver GM, Katske GE, Stutzman FL, Wood NE. Umbilical Vein for Aortocoronary Bypass. *Angiology*. 1982;33(7):450–453.

53. Gupta P, Mandal BB. Tissue-Engineered Vascular Grafts: Emerging Trends and Technologies. *Advanced Functional Materials*. 2021;31(33):1–28.

54. Nasiri B, Row S, Smith RJ, Swartz DD, Andreadis ST. Cell-Free Vascular Grafts That Grow with the Host. *Advanced Functional Materials*. 2020;30(48):2005769.

55. Wu J, Hu C, Tang Z, Yu Q, Liu X, Chen H. Tissue-engineered Vascular Grafts: Balance of the Four Major Requirements. *Colloids and Interface Science Communications*. 2018;23(December 2017):34–44.

56. Matsuzaki Y, John K, Shoji T, Shinoka T. The evolution of tissue engineered vascular graft technologies: From preclinical trials to advancing patient care. *Applied Sciences (Switzerland)*. 2019;9(7).

57. Yuan H, Chen C, Liu Y, Lu T, Wu Z. Strategies in cell-free tissue-engineered vascular grafts. *Journal of Biomedical Materials Research - Part A*. 2020;108(3):426–445.

58. Berger K, Sauvage LR, Rao AM, Wood SJ. Healing of arterial prostheses in man: its incompleteness. *Annals of surgery*. 1972;175(1):118–127.

59. Zilla P, Bezuidenhout D, Human P. Prosthetic vascular grafts: Wrong models, wrong questions and no healing. *Biomaterials*. 2007;28(34):5009–5027.

60. Pennel T, Bezuidenhout D, Koehne J, Davies NH, Zilla P. Transmural capillary ingrowth is essential for confluent vascular graft healing. *Acta Biomaterialia*. 2018;65:237–247.

61. Pennel T, Zilla P, Bezuidenhout D. Differentiating transmural from transanastomotic prosthetic graft endothelialization through an isolation loop-graft model. *Journal of Vascular Surgery*. 2013;58(4):1053–1061.

62. Mallis P, Kostakis A, Stavropoulos-Giokas C, Michalopoulos E. Future perspectives in small-diameter vascular graft engineering. *Bioengineering*. 2020;7(4):1–40.

63. Zhang L, Zhou J, Lu Q, Wei Y, Hu S. A novel small-diameter vascular graft: In vivo behavior of biodegradable three-layered tubular scaffolds. *Biotechnology and Bioengineering*. 2008;99(4):1007–1015.

64. Wagner M, Benjamin HB, Zeit W, Kuzma J. Experiences with the autoplastic cutis vascular graft. *Angiology*. 1958;9(5):253–255.

65. Wagner M, Benjamin HB, Zeit W. Clinical experience with the cutis vascular graft: Progress reports. *Angiology*. 1961;12(2):57–60.

66. Carrabba M, Madeddu P. Current strategies for the manufacture of small size tissue engineering vascular grafts. *Frontiers in Bioengineering and Biotechnology*. 2018;6(APR):1–12.

67.   Konig G, Mcallister TN, Dusserre N, Garrido S a, Iyican C, Marini A, Fiorillo A, Avila H, Wystrychowski W, Zagalski K, Maruszewski M, Jones AL, Cierpka L, de la Fuente LM, L'Heureux N. Mechanical properties of completely autologous human tissue engineered blood vessels compared to human saphenous vein and mammary artery. *Biomaterials*. 2009;30(8):1542–1550.

68.   Wystrychowski W, McAllister TN, Zagalski K, Dusserre N, Cierpka L, L'Heureux N. First human use of an allogeneic tissue-engineered vascular graft for hemodialysis access. *Journal of Vascular Surgery*. 2014;60(5):1353–1357.

69.   L'heureux N, Pâquet S, Labbé R, Germain L, Auger FA. A completely biological tissue-engineered human blood vessel. *The FASEB Journal*. 1998;12(1):47–56.

70.   Asakawa N, Shimizu T, Tsuda Y, Sekiya S, Sasagawa T, Yamato M, Fukai F, Okano T. Pre-vascularization of in vitro three-dimensional tissues created by cell sheet engineering. *Biomaterials*. 2010;31(14):3903–3909.

71.   Mosadegh B, Xiong G, Dunham S, Min JK. Current progress in 3D printing for cardiovascular tissue engineering. *Biomedical Materials (Bristol)*. 2015;10(3).

72.   Freeman S, Ramos R, Alexis Chando P, Zhou L, Reeser K, Jin S, Soman P, Ye K. A bioink blend for rotary 3D bioprinting tissue engineered small-diameter vascular constructs. *Acta Biomaterialia*. 2019;95:152–164.

73.   Ligon SC, Liska R, Stampfl J, Gurr M, Mülhaupt R. Polymers for 3D Printing and Customized Additive Manufacturing. *Chemical Reviews*. 2017;117(15):10212–10290.

74.   Abaci A, Guvendiren M. Designing Decellularized Extracellular Matrix-Based Bioinks for 3D Bioprinting. *Advanced Healthcare Materials*. 2020;9(24):1–18.

75.   Tamay DG, Usal TD, Alagoz AS, Yucel D, Hasirci N, Hasirci V. 3D and 4D printing of polymers

for tissue engineering applications. *Frontiers in Bioengineering and Biotechnology*. 2019;7(JUL).

76.   Song Y, Wennink JWH, Kamphuis MMJ, Vermes I, Poot AA, Feijen J, Grijpma DW. Effective

        seeding of smooth muscle cells into tubular poly(trimethylene carbonate) scaffolds for vascular

        tissue engineering. *Journal of Biomedical Materials Research Part A*. 2010;95A(2):440–446.

77.   Niklason LE, Abbott W, Gao J, Klagges B, Hirschi KK, Ulubayram K, Conroy N, Jones R,

        Vasanawala A, Sanzgiri S, Langer R. Morphologic and mechanical characteristics of engineered

        bovine arteries. *Journal of Vascular Surgery*. 2001;33(3):628–638.

78.   Soletti L, Nieponice A, Hong Y, Ye SH, Stankus JJ, Wagner WR, Vorp DA. In vivo performance

        of a phospholipid-coated bioerodable elastomeric graft for small-diameter vascular applications.

        Journal of Biomedical Materials Research - Part A. 2011;96 A(2):436–448.

79.   Nezarati RM, Eifert MB, Dempsey DK, Cosgriff-Hernandez E. Electrospun vascular grafts with

        improved compliance matching to native vessels. *Journal of Biomedical Materials Research - Part

        B Applied Biomaterials*. 2015;103(2):313–323.

80.   De Mel A, Cousins BG, Seifalian AM. Surface modification of biomaterials: A quest for blood

        compatibility. *International Journal of Biomaterials*. 2012;2012.

81.   Deutsch M, Meinhart J, Zilla P, Howanietz N, Gorlitzer M, Froeschl A, Stuempflen A,

        Bezuidenhout D, Grabenwoeger M. Long-term experience in autologous in vitro

        endothelialization of infrainguinal ePTFE grafts. *Journal of Vascular Surgery*. 2009;49(2):352–

        362.

82.   Pan J feng, Liu N hua, Shu L yuan, Sun H. Application of avidin-biotin technology to improve cell

        adhesion on nanofibrous matrices. *Journal of Nanobiotechnology*. 2015;13(1):1–14.

83.   Kim BS, Putnam AJ, Kulik TJ, Mooney DJ. Optimizing seeding and culture methods to engineer

        smooth muscle tissue on biodegradable polymer matrices. *Biotechnology and Bioengineering*.

1998;57(1):46–54.

84.   Best C, Strouse R, Hor K, Pepper V, Tipton A, Kelly J, Shinoka T, Breuer C. Toward a patient-specific tissue engineered vascular graft. *Journal of Tissue Engineering*. 2018;9:204173141876470.

85.   Nottelet B, Pektok E, Mandracchia D, Tille JC, Walpoth B, Gurny R, Möller M. Factorial design optimization and in vivo feasibility of poly(ε-caprolactone)-micro- and nanofiber-based small diameter vascular grafts. *Journal of Biomedical Materials Research - Part A*. 2009;89(4):865–875.

86.   Drilling S, Gaumer J, Lannutti J. Fabrication of burst pressure competent vascular grafts via electrospinning: Effects of microstructure. *Journal of Biomedical Materials Research - Part A*. 2009;88(4):923–934.

87.   Greenwald SE, Berry CL. Improving vascular grafts: The importance of mechanical and haemodynamic properties. *Journal of Pathology*. 2000;190(3):292–299.

88.   Dean EW, Udelsman B, Breuer CK. Current Advances in the Translation of Vascular Tissue Engineering to the Treatment of Pediatric Congenital Heart Disease. *Yale Journal of Biology and Medicine*. 2012;85(2):229–238.

89.   Post A, Diaz-Rodriguez P, Balouch B, Paulsen S, Wu S, Miller J, Hahn M, Cosgriff-Hernandez E. Elucidating the role of graft compliance mismatch on intimal hyperplasia using an ex vivo organ culture model. *Acta Biomaterialia*. 2019;89:84–94.

90.   Zilla P, Deutsch M, Bezuidenhout D, Davies NH, Pennel T. Progressive Reinvention or Destination Lost? Half a Century of Cardiovascular Tissue Engineering. *Frontiers in Cardiovascular Medicine*. 2020;7(September):1–32.

91.   Skovrind I, Harvald EB, Juul Belling H, Jørgensen CD, Lindholt JS, Andersen DC. Concise Review: Patency of Small-Diameter Tissue-Engineered Vascular Grafts: A Meta-Analysis of

Preclinical Trials. *Stem Cells Translational Medicine*. 2019;8(7):671–680.

92.   Matsumura G, Ishihara Y, Miyagawa-Tomita S, Ikada Y, Matsuda S, Kurosawa H, Shin'oka T. Evaluation of tissue-engineered vascular autografts. *Tissue Engineering*. 2006;12(11):3075–3083.

93.   Niklason LE, Gao J, Abbott WM, Hirschi KK, Houser S, Marini R, Langer R. Functional arteries grown in vitro. *Science*. 1999;284(5413):489–493.

94.   Kim YB, Kim G. Rapid-prototyped collagen scaffolds reinforced with PCL/β-TCP nanofibres to obtain high cell seeding efficiency and enhanced mechanical properties for bone tissue regeneration. *Journal of Materials Chemistry*. 2012;22(33):16880–16889.

95.   Udelsman B V., Khosravi R, Miller KS, Dean EW, Bersi MR, Rocco K, Yi T, Humphrey JD, Breuer CK. Characterization of evolving biomechanical properties of tissue engineered vascular grafts in the arterial circulation. *Journal of Biomechanics*. 2014;47(9):2070–2079.

96.   Matsumura G, Ishihara Y, Miyagawa-Tomita S, Ikada Y, Matsuda S, Kurosawa H, Shin'oka T. Evaluation of Tissue-Engineered Vascular Autografts. *Tissue Engineering*. 2006;12(11):3075–3083.

97.   Perea H, Aigner J, Hopfner U, Wintermantel E. Direct magnetic tubular cell seeding: A novel approach for vascular tissue engineering. *Cells Tissues Organs*. 2006;183(3):156–165.

98.   Yaman S, Anil-Inevi M, Ozcivici E, Tekin HC. Magnetic force-based microfluidic techniques for cellular and tissue bioengineering. *Frontiers in Bioengineering and Biotechnology*. 2018;6(DEC).

99.   Shimizu K, Ito A, Arinobe M, Murase Y, Iwata Y, Narita Y, Kagami H, Ueda M, Honda H. Effective cell-seeding technique using magnetite nanoparticles and magnetic force onto decellularized blood vessels for vascular tissue engineering. *Journal of Bioscience and Bioengineering*. 2007;103(5):472–478.

100.   Arrigoni C, Chittò A, Mantero S, Remuzzi A. Rotating versus perfusion bioreactor for the culture

of engineered vascular constructs based on hyaluronic acid. *Biotechnology and Bioengineering*. 2008;100(5):988–997.

101. Callanan A, Davis NF, McGloughlin TM, Walsh MT. Development of a rotational cell-seeding system for tubularized extracellular matrix (ECM) scaffolds in vascular surgery. *Journal of Biomedical Materials Research - Part B Applied Biomaterials*. 2014;102(4):781–788.

102. Nasseri BA, Pomerantseva I, Kaazempur-Mofrad MR, Sutherland FWH, Perry T, Ochoa E, Thompson CA, Mayer JE, Oesterle SN, Vacanti JP. Dynamic rotational seeding and cell culture system for vascular tube formation. *Tissue Engineering*. 2003;9(2):291–299.

103. Soletti L, Nieponice A, Guan J, Stankus JJ, Wagner WR, Vorp DA. A seeding device for tissue engineered tubular structures. *Biomaterials*. 2006;27(28):4863–4870.

104. Udelsman B, Hibino N, Villalona GA, McGillicuddy E, Nieponice A, Sakamoto Y, Matsuda S, Vorp DA, Shinoka T, Breuer CK. Development of an operator-independent method for seeding tissue-engineered vascular grafts. *Tissue Engineering - Part C: Methods*. 2011;17(7):731–736.

105. Nieponice A, Soletti L, Guan J, Deasy BM, Huard J, Wagner WR, Vorp D a. Rotational Vacuum Seeding Technique. *Biomaterials*. 2008;29(7):825–833.

106. Cunnane EM, Lorentz KL, Soletti L, Ramaswamy AK, Chung TK, Haskett DG, Luketich SK, Tzeng E, D'Amore A, Wagner WR, Weinbaum JS, Vorp DA. Development of a Semi-Automated, Bulk Seeding Device for Large Animal Model Implantation of Tissue Engineered Vascular Grafts. *Frontiers in Bioengineering and Biotechnology*. 2020;8(October):1–10.

107. Alvarez-Barreto JF, Linehan SM, Shambaugh RL, Sikavitsas VI. Flow perfusion improves seeding of tissue engineering scaffolds with different architectures. *Annals of Biomedical Engineering*. 2007;35(3):429–442.

108. Wendt D, Marsano A, Jakob M, Heberer M, Martin I. Oscillating perfusion of cell suspensions

through three-dimensional scaffolds enhances cell seeding efficiency and uniformity. *Biotechnology and Bioengineering*. 2003;84(2):205–214.

109. Amadeo F, Boschetti F, Polvani G, Banfi C, Pesce M, Santoro R. Aortic valve cell seeding into decellularized animal pericardium by perfusion-assisted bioreactor. *Journal of Tissue Engineering and Regenerative Medicine*. 2018;12(6):1481–1493.

110. Patel NM, Yazdi IK, Tasciotti E, Birla RK. Optimizing cell seeding and retention in a three-dimensional bioengineered cardiac ventricle: The two-stage cellularization model. *Biotechnology and Bioengineering*. 2016;113(10):2275–2285.

111. L'Heureux N, Pâquet S, Labbé R, Germain L, Auger FA. A completely biological tissue-engineered human blood vessel. *The FASEB Journal*. 1998;12(1):47–56.

112. Quint C. Tissue-engineered vessel derived from human fibroblasts with an electrospun scaffold. *Journal of Tissue Engineering and Regenerative Medicine*. 2020;14(11):1652–1660.

113. Jeong SI, Kwon JH, Lim JI, Cho SW, Jung Y, Sung WJ, Kim SH, Kim YH, Lee YM, Kim BS, Choi CY, Kim SJ. Mechano-active tissue engineering of vascular smooth muscle using pulsatile perfusion bioreactors and elastic PLCL scaffolds. *Biomaterials*. 2005;26(12):1405–1411.

114. Huang AH, Lee YU, Calle EA, Boyle M, Starcher BC, Humphrey JD, Niklason LE. Design and Use of a Novel Bioreactor for Regeneration of Biaxially Stretched Tissue-Engineered Vessels. *Tissue Engineering - Part C: Methods*. 2015;21(8):841–851.

115. Syedain ZH, Meier LA, Bjork JW, Lee A, Tranquillo RT. Implantable arterial grafts from human fibroblasts and fibrin using a multi-graft pulsed flow-stretch bioreactor with noninvasive strength monitoring. *Biomaterials*. 2011;32(3):714–722.

116. McAllister TN, Maruszewski M, Garrido SA, Wystrychowski W, Dusserre N, Marini A, Zagalski K, Fiorillo A, Avila H, Manglano X, Antonelli J, Kocher A, Zembala M, Cierpka L, de la Fuente

LM, et al. Effectiveness of haemodialysis access with an autologous tissue-engineered vascular graft: a multicentre cohort study. *The Lancet*. 2009;373(9673):1440–1446.

117. Matsumura G, Hibino N, Ikada Y, Kurosawa H, Shin'oka T. Successful application of tissue engineered vascular autografts: Clinical experience. *Biomaterials*. 2003;24(13):2303–2308.

118. Hibino N, McGillicuddy E, Matsumura G, Ichihara Y, Naito Y, Breuer C, Shinoka T. Late-term results of tissue-engineered vascular grafts in humans. *The Journal of Thoracic and Cardiovascular Surgery*. 2010;139(2):431-436.e2.

119. Lawson JH, Glickman MH, Ilzecki M, Jakimowicz T, Jaroszynski A, Peden EK, Pilgrim AJ, Prichard HL, Guziewicz M, Przywara S, Szmidt J, Turek J, Witkiewicz W, Zapotoczny N, Zubilewicz T, et al. Bioengineered human acellular vessels for dialysis access in patients with end-stage renal disease: Two phase 2 single-arm trials. *The Lancet*. 2016.

120. Branson DF, Picha GJ, Desprez J. Expanded polytetrafluoroethylene as a microvascular graft: A study of four fibril lengths. *Plastic and Reconstructive Surgery*. 1985;76(5):754–763.

121. Rothuizen TC, Damanik FFR, Lavrijsen T, Visser MJT, Hamming JF, Lalai RA, Duijs JMGJ, van Zonneveld AJ, Hoefer IE, van Blitterswijk CA, Rabelink TJ, Moroni L, Rotmans JI. Development and evaluation of in vivo tissue engineered blood vessels in a porcine model. *Biomaterials*. 2016;75:82–90.

122. Aussel A, Thébaud NB, Bérard X, Brizzi V, Delmond S, Bareille R, Siadous R, James C, Ripoche J, Durand M, Montembault A, Burdin B, Letourneur D, L'Heureux N, David L, et al. Chitosan-based hydrogels for developing a small-diameter vascular graft: In vitro and in vivo evaluation. *Biomedical Materials (Bristol)*. 2017;12(6).

123. Conklin BS, Richter ER, Kreutziger KL, Zhong DS, Chen C. Development and evaluation of a novel decellularized vascular xenograft. *Medical Engineering and Physics*. 2002;24(3):173–183.

124.   Lee KW, Stolz DB, Wang Y. Substantial expression of mature elastin in arterial constructs. *Proceedings of the National Academy of Sciences of the United States of America*. 2011;108(7):2705–2710.

125.   de Valence S, Tille JC, Mugnai D, Mrowczynski W, Gurny R, Möller M, Walpoth BH. Long term performance of polycaprolactone vascular grafts in a rat abdominal aorta replacement model. *Biomaterials*. 2012;33(1):38–47.

126.   Gui L, Dash BC, Luo J, Qin L, Zhao L, Yamamoto K, Hashimoto T, Wu H, Dardik A, Tellides G, Niklason LE, Qyang Y. Implantable tissue-engineered blood vessels from human induced pluripotent stem cells. *Biomaterials*. 2016;102:120–129.

127.   Best C, Fukunishi T, Drews J, Khosravi R, Hor K, Mahler N, Yi T, Humphrey JD, Johnson J, Breuer CK, Hibino N. Oversized Biodegradable Arterial Grafts Promote Enhanced Neointimal Tissue Formation. *Tissue Engineering - Part A*. 2018;24(15–16):1251–1261.

128.   He W, Nieponice A, Soletti L, Hong Y, Gharaibeh B, Crisan M, Usas A, Peault B, Huard J, Wagner WR, Vorp DA. Pericyte-based human tissue engineered vascular grafts. *Biomaterials*. 2010;31(32):8235–8244.

129.   Udelsman B V., Khosravi R, Miller KS, Dean EW, Bersi MR, Rocco K, Yi T, Humphrey JD, Breuer CK. Characterization of evolving biomechanical properties of tissue engineered vascular grafts in the arterial circulation. *Journal of Biomechanics*. 2014;47(9):2070–2079.

130.   Gui L, Zhao L, Spencer RW, Burghouwt A, Taylor MS, Shalaby SW, Niklason LE. Development of novel biodegradable polymer scaffolds for vascular tissue engineering. *Tissue Engineering - Part A*. 2011;17(9–10):1191–1200.

131.   Soletti L, Hong Y, Guan J, Stankus JJ, El-Kurdi MS, Wagner WR, Vorp DA. A bilayered elastomeric scaffold for tissue engineering of small diameter vascular grafts. *Acta Biomaterialia*.

2010;6(1):110–122.

132. Ghasemi-Mobarakeh L, Morshed M, Karbalaie K, Fesharaki MA, Nematallahi M, Nasr-Esfahani MH, Baharvand H. The thickness of electrospun poly (ε-caprolactone nanofibrous scaffolds influences cell proliferation. *International Journal of Artificial Organs*. 2009;32(3):150–158.

133. Marelli B, Achilli M, Alessandrino A, Freddi G, Tanzi MC, Farè S, Mantovani D. Collagen-Reinforced Electrospun Silk Fibroin Tubular Construct as Small Calibre Vascular Graft. *Macromolecular Bioscience*. 2012;12(11):1566–1574.

134. Lannutti J, Reneker D, Ma T, Tomasko D, Farson D. Electrospinning for tissue engineering scaffolds. *Materials Science and Engineering C*. 2007;27(3):504–509.

135. Ekram B, Abdel-Hady BM, El-Kady AM, Amr SM, Waley AI, Guirguis OW. Optimum parameters for the production of nano-scale electrospun polycaprolactone to be used as a biomedical material. *Advances in Natural Sciences: Nanoscience and Nanotechnology*. 2017;8(4).

136. Huang NF, Li S. Mesenchymal stem cells for vascular regeneration. *Regenerative Medicine*. 2008;3(6):877–892.

137. Hotaling NA, Bharti K, Kriel H, Simon CG. DiameterJ: A validated open source nanofiber diameter measurement tool. *Biomaterials*. 2015;61:327–338.

138. Roh JD, Nelson GN, Brennan MP, Mirensky TL, Yi T, Hazlett TF, Tellides G, Sinusas AJ, Pober JS, Saltzman WM, Kyriakides TR, Breuer CK. Small-diameter biodegradable scaffolds for functional vascular tissue engineering in the mouse model. *Biomaterials*. 2008;29(10):1454–1463.

139. Sazonova O V., Isenberg BC, Herrmann J, Lee KL, Purwada A, Valentine AD, Buczek-Thomas JA, Wong JY, Nugent MA. Extracellular matrix presentation modulates vascular smooth muscle cell mechanotransduction. *Matrix Biology*. 2015;41:36–43.

140. Reusch P, Wagdy H, Reusch R, Wilson E, Ives HE. Mechanical strain increases smooth muscle

and decreases nonmuscle myosin expression in rat vascular smooth muscle cells. *Circulation Research*. 1996;79(5):1046–1053.

141. Li Y, Ma T, Kniss DA, Lasky LC, Yang ST. Effects of filtration seeding on cell density, spatial distribution, and proliferation in nonwoven fibrous matrices. *Biotechnology Progress*. 2001;17(5):935–944.

142. Villalona GA, Udelsman B, Duncan DR, McGillicuddy E, Sawh-Martinez RF, Hibino N, Painter C, Mirensky T, Erickson B, Shinoka T, Breuer CK. Cell-seeding techniques in vascular tissue engineering. *Tissue Engineering - Part B: Reviews*. 2010;16(3):341–350.

143. Burg KJL, Holder WD, Culberson CR, Beiler RJ, Greene KG, Loebsack AB, Roland WD, Eiselt P, Mooney DJ, Halberstadt CR. Comparative study of seeding methods for three-dimensional polymeric scaffolds. *Journal of Biomedical Materials Research*. 2000;51(4):642–649.

144. Yeatts AB, Fisher JP. Bone tissue engineering bioreactors: Dynamic culture and the influence of shear stress. *Bone*. 2011;48(2):171–181.

145. Preibisch S, Saalfeld S, Tomancak P. Globally optimal stitching of tiled 3D microscopic image acquisitions. *Bioinformatics*. 2009;25(11):1463–1465.

146. van Wachem PB, Stronck JWS, Koers-Zuideveld R, Dijk F, Wildevuur CRH. Vacuum cell seeding: a new method for the fast application of an evenly distributed cell layer on porous vascular grafts. *Biomaterials*. 1990;11(8):602–606.

147. Noishiki Y, Yamane Y, Tomizawa Y, Okoshi T, Satoh S, Wildevuur CRH, Suzuki K. Rapid endothelialization of vascular prostheses by seeding autologous venous tissue fragments. *The Journal of Thoracic and Cardiovascular Surgery*. 1992;104(3):770–778.

148. Engbers-Buijtenhuijs P, Buttafoco L, Poot AA, Dijkstra PJ, De Vos RAI, Sterk LMT, Geelkerken RH, Vermes I, Feijen J. Biological characterisation of vascular grafts cultured in a bioreactor.

Biomaterials. 2006;27(11):2390–2397.

149. Nieponice A, Soletti L, Guan J, Deasy BM, Huard J, Wagner WR, Vorp D a. Development of a tissue engineered vascular graft combining a biodegradable scaffold, muscle-derived stem cells and a rotational vacuum seeding technique. *Biomaterials*. 2008;29(7):825–833.

150. Marasco S. Total Arterial Revascularization. *Operative Techniques in Thoracic and Cardiovascular Surgery*. 2016;21(1):20–30.

151. Diodato M, Chedrawy EG. Coronary Artery Bypass Graft Surgery: The Past, Present, and Future of Myocardial Revascularisation. *Surgery Research and Practice*. 2014;2014:1–6.

152. Ng KW, Leong DTW, Hutmacher DW. The challenge to measure cell proliferation in two and three dimensions. *Tissue Engineering*. 2005;11(1–2):182–191.

153. Huang AH, Balestrini JL, Udelsman B V., Zhou KC, Zhao L, Ferruzzi J, Starcher BC, Levene MJ, Humphrey JD, Niklason LE. Biaxial Stretch Improves Elastic Fiber Maturation, Collagen Arrangement, and Mechanical Properties in Engineered Arteries. *Tissue Engineering - Part C: Methods*. 2016;22(6):524–533.

154. Mironov V, Kasyanov V, Xiao ZS, Eisenberg C, Eisenberg L, Gonda S, Trusk T, Markwald RR, Prestwich GD. Fabrication of tubular tissue constructs by centrifugal casting of cells suspended in an in situ crosslinkable hyaluronan-gelatin hydrogel. *Biomaterials*. 2005;26(36):7628–7635.

155. Zaucha MT, Raykin J, Wan W, Gauvin R, Auger FA, Germain L, Michaels TE, Gleason RLJ. A Novel Cylindrical Biaxial Computer-Controlled Bioreactor and Biomechanical Testing Device. *Tissue engineering. Part A*. 2009;15(11):3331–3340.

156. Martinon F, Mayor A, Tschopp J. The inflammasomes: Guardians of the body. *Annual Review of Immunology*. 2009;27(1):229–265.

157. Zilla P, Bezuidenhout D, Human P. Prosthetic vascular grafts: Wrong models, wrong questions

and no healing. *Biomaterials*. 2007;28(34):5009–5027.

158.   Boehler RM, Graham JG, Shea LD. Tissue engineering tools for modulation of the immune

response. *BioTechniques*. 2011;51(4):239–254.

159.   Szafron JM, Khosravi R, Reinhardt J, Best CA, Bersi MR, Yi T, Breuer CK, Humphrey JD.

Immuno-driven and Mechano-mediated Neotissue Formation in Tissue Engineered Vascular

Grafts. *Annals of Biomedical Engineering*. 2018;46(11):1938–1950.

160.   Geelhoed WJ, Moroni L, Rotmans JI. Utilizing the Foreign Body Response to Grow Tissue

Engineered Blood Vessels in Vivo. *Journal of Cardiovascular Translational Research*.

2017;10(2):167–179.

Appendix

Developed Protocols

2mm Scaffold Electrospinning

1) First, wrap the 2mm mandrel in aluminum foil.
   a. Cut a 1cm thick strip of foil by following the edge of a straight ruler with a razor blade. Cut to the appropriate length (~ 13 cm) and proceed to wrap carefully around the mandrel. Tighten by rolling a second time with a piece of paper.
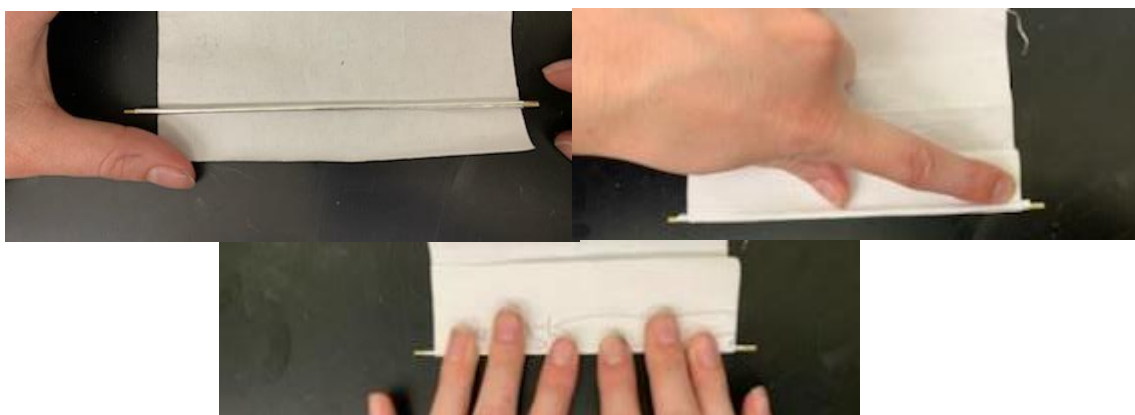

2) Insert the wrapped mandrel in a chuck. With one hand, hold the mandrel in the center of the chuck and with the other rotate the base to tighten the chuck. Repeat with the top mandrel. Make sure that the mandrel does not lean in any one direction. If it does, adjust it until it is as straight as possible. Make sure there is 12 cm of mandrel between chucks.
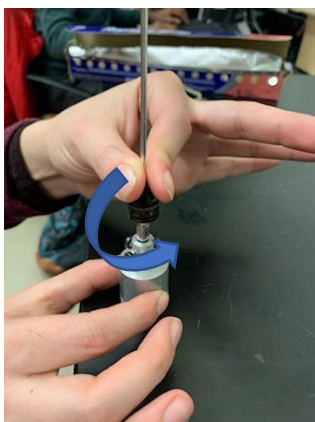
3) Insert mounted mandrel into the stage. Slide the golden end into the rotational motor, then fix the opposite side with the jointed mechanism. Tighten and fix with an Allen wrench.

4) Once the mandrel is mounted test the rotation by flicking the switch of the rotational transformer. If it wobbles then you need to reposition the mandrel, it was probably not straight. If the mandrel does not wobble too much then you can proceed. Gently cleanse the aluminum surface with a kimwipe and some acetone.

5) Turn on the small power supply next to the computer and boot up the computer. Open the IMC for CM/SCX. Make sure that the window that comes on reads COM3 and 9600. Go to program editor, sequence directory, and run the Scratch program. This starts your translational motion.
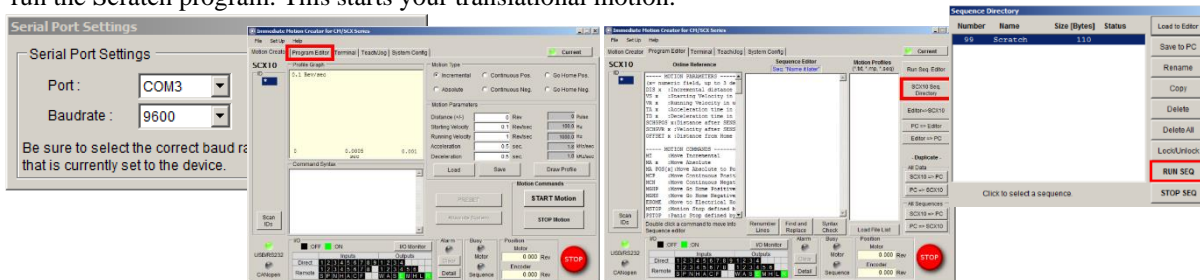
*always stop the motion at the point which it is closest to the edge of the bench. If you do not, when you restart the motion it will view wherever you stopped as the new starting point. The translational motion can only go so far and if you start too far down you will hurt the mechanism. To reset go to the first window, change the distance to -0.5 and press start motion until it is back at the correct starting point.

6) Take a 1ml syringe out of its packaging and collect 1.2 ml of the polymer solution with it. Attach a 27-gauge needle to the syringe and fill the needle with solution until a small amount comes out of the end.

Insert into the syringe pump and secure with the holder. Move plate until it is touching the end of the plunger. Check that the infusion rate is set at your desired level.

1.2 ml/hr

7) Attach the gator clip hooked to the main power generator on the far side of the enclosure to the needle. Slide a small washer over needle tip to help direct the flow.

8) Ensure that tip of needle is desired distance away from mandrel, 18 cm. Make sure both sides are parallel to the needle by measuring the distance of the stage from the wall and the far and near ends. Make sure that the needle is aimed initially at 5cm from the motor.

9) Set a timer to 40 minutes. Take note of the temperature and humidity in the enclosure and what time you are beginning your spin.

10) Start the process in this order: Lamp in the enclosure, rotational motor, translational program, infusion, then start the power and timer at the same time.

The lamp allows you to see the fibers more clearly as you are spinning. Keep an eye on the set up for the duration of the spin to make sure nothing goes wrong and you are there when the timer ends.

11) When time is up, stop the current. Then stop the syringe pump, rotational motor and translational motor. Take note of the amount of solution deposited and any general observations you can make on the quality of the scaffold based on visual inspection.

Turn off the power first when the timer goes off. Do not touch the cord or needle while the power is on or you will get shocked and it will hurt. Record your spin in the Production Log under scaffold files in the research folder. See 2mm Scaffold Processing for further instruction.

2mm Scaffold Processing

1) Label the scaffold on the motor side with its spin number, then remove the foil + scaffold from the mandrel.

2) Starting on the user end, cut away 1 cm of material starting at the inner end of the coffee filter section. Then cut another 1 cm section and store in a test tube with the spin number and date labeled on it. Next cut a 4cm section from the same end of the scaffold. This is your usable scaffold for experiments. Finally cut one more 1cm section. Put all sections in the test tube. These sections will be labeled 10, Graft Scaffold, and 5 respectively.

3) Remove the foil from the 10 and 5 pieces with tweezers. These will be used to test the thickness and SEM of the scaffold.

4) Remove foil from the Graft Scaffold by gently using tweezers. Use the tweezers to reduce the circumference of the foil within the scaffold by grabbing the inner lip and rolling on both sides, then gently pull on the aluminum sleeve so it slides out of the scaffold.

5) Measure the mass (mg) and length(mm) of the graft scaffold as well as the thickness (µm) of piece 5 and record it in the 2mm Scaffold Data Log along with any interesting notes (i.e. Delamination, beading, interuptions in the spin process, ect.)

Quality Control

*Every 10th scaffold is used for quality control purposes.

1) For these scaffolds, you take the total length of the scaffold (12 cm) and cut off the last 1 cm of both sides. KEEP TRACK OF WHICH SIDE WAS WHICH.

2) The remaining 10 cm shall be cut into 10 1cm long pieces labeled 1 through 10. Piece 1 corresponds to the side closest to the motor end and piece 10 corresponds to the operator side.

3) Each piece will have its mass and length measured as well as thickness. This will be recorded in the Quality Control Sheet of the 2mm Scaffold Data Log.

4) Add this data to the graphs on the sheet to determine if you are within the acceptable range of measurements and your scaffolds are usable for experiments.

Scaffold Mounting

Supplies:
4 scaffolds
8 3.5cm cannulas
8 collet chuck sets ->
2 Brackets
2 mounting rods
4 sets of nuts and washers
Needle nose tweezers
Wrench

Taper   Collet   Inner Sleeve

This protocol takes place in the cell culture hood to maintain sterility before seeding. Autoclave/sterilize everything before entering the hood. Inside the hood have a small container of 70% ethanol to keep parts in as you assemble the bioreactor, rinse interior of bioreactor box with 70% ethanol and allow to dry before setting scaffold assembly inside.

1) Secure one bracket in the far end of the mounting table frame, set the two support tables next to it.
2) Take one of your scaffolds and confirm that it is 4 cm long. Stretch .5 cm of the ends such that they will fit over the cannulas.
3) Once the scaffold is .5cm over the cannula, take a small piece of parafilm and use it to secure the scaffold to the cannula with a leak proof seal. Repeat for the first side of all 4 scaffolds.
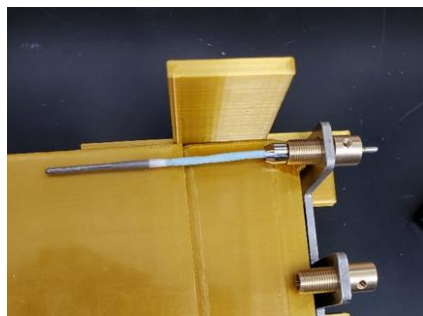

4) Carefully repeat the process with the other side of all four scaffolds, being careful to not twist the scaffolds while doing so.
5) One at a time, slip a collet over the cannula/scaffold connection with the end of the cannula flush with the face of the collet. Set aside.
6) Fasten each of the 8 inner sleeves into the brackets, as far as they will go. Afterwards, set one of the brackets into the first slot of the mounting table and position the support tables next to it, as pictured.

7) Carefully slip each collet

from your scaffold/cannulas/collet

assembly into the inner sleeves of the first bracket. Secure the cannula in place with the stainless steel setscrews on the base of the inner sleeve. Secure the scaffold collet with the tapers.

8) For the next side, slide the remaining tapers over the partially mounted scaffolds. (the narrow ends of the tapers should be facing eachother). Then slide the remaining collets into their correct position on the remaining cannulas.

9) Carefully remove support table A and slide the second bracket into its slot on the mounting table. Slide the cannula/collet connections into the inner sleeves. Before securing with setscrews, confirm that the exposed section of scaffold is as close to 3 cm long as possible. Secure set crews and tighten the taper.

10) Carefully slide support Table B out from between the brackets. Secure the two brackets together with stainless steel rods, wasters and nuts. Preserve the set space of 3cm between scaffold ends, with slight tension.
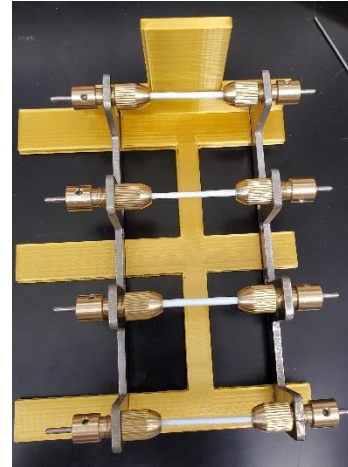

11) Set the assembly into the main bioreactor box, attach designated polypropylene tubes to their cannulas, and if necessary secure brackets to the bioreactor box and remove static rods. Sterilize by running 70% ETOH through the scaffolds in seeding mode for 30 min. Rinse 3 times with PBS and wet with cell media 24 hrs prior to seeding.

Calculating cell coverage with ImageJ

1) The examined scaffolds are cut vertically into five samples and each sample is SEM imaged in a 3x3 grid at 300x.

2) The images are processed with DiameterJ Segment for thresholding.Images that show the most accurate representation of cell coverage are manually chosen, then placed into the "Best Segmentation" folder created by the diameter program. (The segmented image should remain open on ImageJ and should have the cell coverage appearing in black, if not invert the image.)

3) Then, go to Process > Binary > Watershed, and to Analyze > Analyze Particles to measure the amount of cell coverage (black space) present from the segmented images.
(A command window will appear, for the "Size" parameter. In the experiment, it was concluded that images, primarily in drip seeding and counterpart, were best represented with a pixel size of 800 inch^2. The images with little to no surface coverage were best analyzed with the selection tool brush to manually select the cell coverage. For images that are entirely covered with cells, mainly dynamic seeding, it was best to use a pixel size of 60 inch^2. The smaller size ensures that the cells with little surface area are being included in the overall area percentage.)

4) Once the accurate pixel size is chosen, the "Show" option will have a drop-down arrow and "Overlay Masks" will be selected. This ensures that the highlighted surface coverage image appears. Also, the "Pixel units" and "Summarize" options should be checked. Once all the parameters are chosen, click OK. An output of the percent area and a highlighted image of the counted patches will pop up.
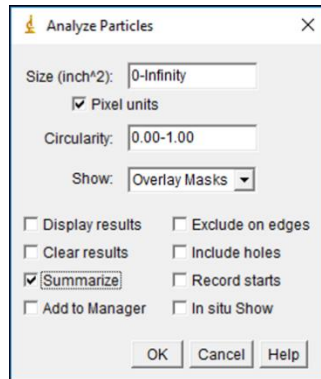
5) The area percentages can be saved as an excel file, once the results of all nine images are saved into the same spreadsheet, they are placed into a separate excel spreadsheet named "% Area Coverage". In that spreadsheet, the surface area is placed in cells corresponding to their location on the scaffold. Once the entire scaffold is processed, the excel spreadsheet (% Area Coverage) will display a visual representation of the cell coverage for each of the seeding mechanisms.

Vita

Sarah Kaye Saunders was born on February 13, 1995, in Roanoke, Virginia. She graduated with honors from Lord Botetourt High School, Daleville, Virginia in 2013. She received her Bachelor of Science in Biomedical Engineering from Virginia Commonwealth University (VCU) in May 2017 with minors in Physics, Mathematics and Mechanical Engineering. The following semester she proceeded to pursue her doctoral degree under the guidance of Dr. Joao Soares, Ph.D., a newly hired professor in the department of Mechanical and Nuclear Engineering at VCU. Following 2 years of doctoral study, Sarah received the American Heart Association Predoctoral fellowship in 2019 for her proposal titled "Modulation of Foreign Body Response to ETVGs via Manipulation of Dual Axial Mechanical Conditioning in vitro.", award number: 20PRE35210730. The award totaled $62,032 and funded her research from 2020-2021. She also became a Koerner Family Foundation Fellow in January 2022. Sarah was an active member of her community in the college of engineering and the graduate school at large. In her role as President of the Graduate Student Association she helped to secure health insurance for graduate and professional students, was instrumental in creating the VCU Graduate & Professional Student Climate Survey and facilitated collaboration between VA R1 universities including George Mason University and Virginia Tech in response to the Covid19 pandemic. Following her graduation, Sarah is excited to start employment June 27, 2022 as a Process Development Engineer for Humacyte, a tissue engineering company based in Research Triangle Park, North Carolina.